Adrian Peder Malum Danielsen
Andreas Grodås Jørs

Cold storage for an adsorption-based refrigeration cycle in Africa

Master's thesis

NTNU
Norwegian University of
Science and Technology

Adrian Peder Malum Danielsen
Andreas Grodås Jørs

Cold storage for an adsorption-based refrigeration cycle in Africa

NTNU
Norwegian University of
Science and Technology

Abstract

Harnessing solar energy is an essential strategy for electrifying rural areas of Africa, with solar panels being the common choice for electricity provision. This thesis, however, investigates the potential of solar energy in powering adsorption-based cooling technology, another promising solution to the region's cooling needs. The research centers on the development of a temperature-controlled ice storage system, aimed to improve food preservation in warm climates, particularly in Tanzania. This system, designed and tested at the Norwegian University of Science and Technology, utilizes an activated carbon/methanol adsorption pair, chosen for its suitable working temperature range and cost-effectiveness. Critical challenges is uncovered with this pairing, including high sensitivity to pressure changes and complexities in matching operational cycles with solar irradiation patterns due to extended desorption and adsorption times. Given these findings, the study proposes alternative strategies for improving the system's efficiency, including considering the use of other adsorption pairs due to their stability under varying pressures. It also suggests structural modifications to the system design, such as a more efficient heat collector configuration, aimed at enhancing heat transfer efficiency and reducing cycle durations. These proposed enhancements are critical for furthering the implementation and effectiveness of solar-driven adsorption-based cooling systems for sustainable food preservation in warmer climates.

Sammendrag

Å utnytte solenergi er en sentral strategi for å elektrifisere landlige regioner i Afrika, der solcellepaneler vanligvis er det foretrukne valget for strømforsyning. Denne masteroppgaven undersøker imidlertid potensialet for bruk av solenergi til å drive adsorpsjonsbaserte kjølesystemer, som er et alternativt og lovende svar på regionens kjølebehov. Forskningen fokuserer på utvikling av et temperaturkontrollert islagringssystem, med mål om å forbedre matkonservering i varmt klima, spesielt i Tanzania. Dette systemet, som er utviklet og testet ved Norges teknisk-naturvitenskapelige universitet, benytter et aktivt karbon-metanol adsorpsjonspar, valgt for dens passende arbeidstemperaturområde og kostnadseffektivitet. Det blir avdekket kritiske utfordringer med dette paret, inkludert høy følsomhet for trykkvariasjoner og kompleksiteten i å synkronisere driftssykluser med solbestrålingsmønstre på grunn av utvidede desorpsjons- og adsorpsjonstider. I lys av disse funnene foreslår studien alternative strategier for å forbedre systemets effektivitet, som inkluderer vurdering av andre adsorpsjonspar på grunn av bedre stabilitet under varierende trykkforhold. Den foreslår også strukturelle modifikasjoner i systemdesignet, som en mer effektiv varmesamlerkonfigurasjon, rettet mot å forbedre effektiviteten av varmeoverføring og redusere syklustider. Disse foreslåtte forbedringene er avgjørende for å fremme implementeringen og effektiviteten av solenergidrevne adsorpsjonsbaserte kjølesystemer for bærekraftig matkonservering i varmere klima.

Preface

This master thesis is completed on behalf of the Norwegian University of Science and Technology during the spring semester of 2023. Its written in connection with the final education of our masters programme in Energy and Environmental engineering. The thesis consists of a literature review as well as design and experimental assessment of an adsorption refrigeration cycle operating with solar energy to provide cold storage. Our deepest gratitude is extended to our supervisor, Trygve Magne Eikevik, and co-supervisor, Ole Jørgen Nydal, for their unwavering support and valuable guidance throughout this journey. We also wish to acknowledge the significant contributions of our laboratory technicians, Reidar Tellebon and Inge Håvard Rekstad, for their invaluable advice and assistance in the laboratory during the construction and testing phases of our project.

Certain segments of this thesis are an extension of the project assignment (TEP4521) undertaken in the Autumn semester of 2022. It should be noted that all uncited figures and tables are original and have been made by us.

Lastly, we express our heartfelt appreciation to our fellow students for enriching our academic journey with stimulating discussions and relentless motivation. These years at the university have been truly memorable, and we are grateful for the experience.

Trondheim, june 2023

Adrian Peder Malum Danielsen

Andreas Grodås Jørs

Table of Contents

List of Figures

List of Tables

1 Introduction

For many countries around the globe but in particular the countries situated on the African continent, Solar radiation is extremely high with long days at elevated temperatures. This has significant implications for local agricultural practices, particularly for those who depend on cultivating their own produce. Self-sufficiency in vegetable cultivation, while economically beneficial, presents challenges due to the region's climate conditions and limitations in preserving harvested food. In these areas, the longevity of stored products is threatened by not only the sweltering climate but also the scarcity of effective refrigeration systems. Consequently, this often results in significant food waste. For many smallholder farmers in Africa, their daily sustenance and a substantial portion of their income are derived from vegetable cultivation. The preservation of this produce is therefore critical to both their livelihoods and food security.

In particularly hot countries like Tanzania, these challenges are exacerbated, especially in districts where power outages are common. Operating conventional refrigeration equipment without a reliable electricity supply is challenging, and even when possible, the resultant emissions contribute to environmental degradation. However, advancements in refrigeration technology present a potential solution. Adsorption-based refrigeration cycles, driven by solar energy, can exploit the region's plentiful warmth. Such systems offer an environmentally friendly alternative to traditional refrigeration, providing a sustainable means to prolong the shelf life of locally grown produce. This approach could significantly reduce food wastage, offering a sustainable way forward in response to climate change and its effects on food preservation.

1.1 Dedication and Purpose

The aim of this task is to develop and design an adsorption-based cooling system that can operate with solar energy. This process will help to create a thermal cold storage in the form of an ice bath. The adsorption cycle is very robust, which means it is a stationary system with a naturally slow circulation. A normal cycle would last 24 hours with desorption during the day using solar heat, and an adsorption cycle at night producing cooling for a cooling chamber. The system mainly focuses on the cold part of the system, where the goal is too achieve a temperature controlled storage to provide a constant temperature over a long period of time. However, evaluating the system requires consideration of numerous elements beyond just the cold aspect, as a result the hot side also necessitates scrutiny. A system that isn't reliant on electricity and guarantees constant availability will facilitate proper food temperature, thereby contributing to waste reduction. This is particularly useful to residents living in the rural parts of Africa, where electricity is not an option.

1.2 Scope and limitations

The thesis has been carried out at the Department of Energy and Process Engineering at the Norwegian University of Science and Technology. The system has been designed and constructed at "Varmetekniske" laboratories where the following tests has been carried out. The budget is within a minimum in terms of money spent. This has made it sufficiently difficult during the design and construction phase. All of the materials used are found at the lab. Therefore, some of the components are made with materials that are not suitable for the given function, especially when it comes to conductivity and heat transfer. Since there has been no solar collector system available, a heating cable has been used as the heat supply. To be able to heat the collector sufficiently with a heating cable, the geometry is chosen to be circular. The main focus has been to develop a functional system, which could later be built in Tanzania. The procedure has been to develop a prototype design to learn from its functions and limitations, followed by an adsorption pair test to see how the adsorption uptake is between methanol and activated carbon. lastly, final changes are implemented to the prototype design to develop a functional cooling system.

1.3   Research objectives

In order to facilitate the development of a functional system, a thorough litterateur review has been done as a preliminary step. While a significant part of the review was conducted during the project work, additional research was also carried out to supplement the knowledge. The discovered insights has contributed towards the design phase, especially in relation to the calculations of components and appropriate sizing. There has been a practical system development in the lab, where the complete design of the system is constructed and brought into operation. The following tasks are to be considered:

1. Literature review of heat driven refrigeration cycles

2. Investigate solution for constant temperature in the refrigerated chamber

3. Make a system design of the integrated refrigeration system

4. Plan the test rig and the instrumentation

5. Build and test the system rig

6. Investigate the adsorption uptake for the chosen adsorption pair and produce simulation data

7. Document the system performance and limitations

8. Make proposal for further work

2 Cold chains in Africa

The term cold chain refers to the sequential refrigerated stages involved in the transportation and storage of perishable product, extending from the initial harvest phase to the ultimate consumption by end consumers. Following the harvest of vegetable or fruits, the process of decay commences. The primary objective of the cold chain is to mitigate this decay process, thereby prolonging the shelf life of the products. A well functioning cold chain endeavors to extend the duration of preservation as much as possible. It is crucial to acknowledge that different products, whether food or vaccines, exhibit distinct requirements in terms of optimal storage temperature and relative humidity. Consequently, storing dissimilar products within the same environment for an extended period of time is inadvisable. The cold chain can be classified into two main segments. Primary cooling, involving the extraction of heat from the products, and secondary cooling, encompassing the mechanisms employed to sustain optimal temperature conditions throughout the storage or transportation processes. [1]

2.1 Current status

One of the most important activities for the population in Tanzania, are the smallholder farmers and their vegetable production. It is a big source of their household income and their daily food consume. Unfortunately, such goods have a poor shelf life, especially in hot temperatures, which is also a big problem in a country like Tanzania with very high humidity and hot temperatures. When vegetables and food in general are exposed to high temperatures for a long period of time, quality will decrease drastically unless they are kept in a cool environment. In industrialized countries, this problem is solved with the help of a refrigerator with access to electricity continuously. In Tanzania, especially in areas with villages and less densely populated areas, power supply is very variable. Large parts of Tanzania have problems with the electricity supply, as power cuts occur very often. The time without power varies extremely. In these off-grid periods, refrigerators will not have the ability to operate hence no cooling of food will take place. The market for off-grid operating refrigerators is therefore very relevant for most parts of Tanzania, but also for other countries in Africa. [2]

At present, the state of the cold chain infrastructure in Africa continues to pose significant challenges. One of the primary concerns is the inconsistent power supply, which greatly impedes effective cold chain management across the continent. The unreliable electricity supply constitutes a considerable obstacle in maintaining the integrity of the cold chain. Furthermore, the limited infrastructure is another issue, as numerous African nations grapple with inadequate cold chain facilities, resulting in substantial postharvest losses. In order to preserve the quality of perishable products, it is important to address the lack of sufficient cold storage facilities and properly maintained equipment. An additional issue confronting the cold chain in Africa is the inadequacy of investments towards infrastructure. Relative to other regions globally, African nations often lack the requisite financial resources to allocate towards the establishment and upkeep of an efficient cold chain system. This predicament is further aggravated by the limited availability of cost-effective financing alternatives for small and medium-sized enterprises operating within the cold chain industry. [3]

Moreover, the scarcity of proficient personnel and training, coupled with a disjointed supply chain, presents formidable challenges. A limited number of institutions offer training in cold chain management within Africa. This dearth of experienced individuals hinders the recruitment and education of new personnel, ultimately contributing to suboptimal storage practices. Additionally, the involvement of numerous small-scale farmers and distributors in the handling of perishable goods leads to a fragmented supply chain. Collectively, these factors contribute to heightened waste and diminished product quality. [4]

2.2 Implications of insufficient cold chain management

Tanzania's horticulture sector has experienced a significant surge in growth over the past years, with an annual growth rate between 9-13%. This makes it the most rapidly expanding segment within the country's agricultural sector. The horticulture sub-sector was responsible for 38% of the total foreign income generated by the agricultural sector during 2019. The majority of the industry is made up of smallholder farmers, with women representing most of this demographic. These farmers, who typically own less than 2 hectares of land, contribute to 70% of the nation's exports of fruits and vegetables. The horticulture subsector is characterized by a diverse range of fruits and vegetables, including carrots, beans, potatoes and other important sources of nutrition. [2]

Despite these positive aspects, the sector is grappling with substantial food loss issues. Domestic market losses are estimated at 40%, while export market losses are less than 10%. Approximately a quarter of all vegetables produced at each harvest are wasted due to the absence of efficient postharvest facilities. Certain highly perishable fruits are underutilized, particularly in production areas, due to the lack of affordable cold storage facilities. Existing cold storage facilities are costly and out of reach for small-scale farmers. There is also a shortage of affordable off-grid cooling methods for fresh produce. Current passive evaporative coolers have several limitations, including shorter storage times, limited cooling chamber size, and challenges in temperature control and management, making them more suitable for precooling rather than bulk storage. Therefore, there is a pressing need for more sustainable precooling and bulk storage solutions. Furthermore, initiatives to build capacity, such as the creation of a center of excellence for sustainable cooling and cold chain, and improvements in market infrastructure, like enhancing road conditions in potential farming areas, are necessary. These measures will help increase the availability of fresh fruits and vegetables, reduce damage to fresh produce, boost farmers' incomes and prevent the decay process. [2]

2.3 Technology improvements and utilization

Significant potential exists in nations characterized by temperate climates and abundant sunlight. Presently, numerous technological solutions do not necessitate an electrical supply. One of the primary challenges is the maintenance of optimal temperatures for the storage of perishable commodities, such as fruits and vegetables. By capitalizing on existing technology and favorable meteorological conditions, solar energy can be harnessed as a viable power source. An exemplification of such an innovation is the adsorption cooling systems. These leverage an adsorption-based refrigeration cycle, capable of harnessing solar energy, offers a sustainable solution for cold storage, including ice production. This system can derive power directly from solar radiation or indirectly via integration with a solar thermal storage system. The inherent robustness of the adsorption cycle, characterized by its lack of moving components and reliance on natural circulation, enhances its reliability and durability.

Nonetheless, to ensure consistent cold storage temperature, a temperature-regulated storage mechanism on the cold side is necessary. This setup enables the cold storage to consistently maintain a uniform temperature within the refrigeration chamber. One plausible approach entails the construction of a natural circulation loop linking the cold storage to the refrigerated chamber. Moreover, a thermostat solution, previously developed for thermal storage systems, could potentially be adapted for the cold storage cycle to achieve consistent temperatures within the refrigerated chamber. Alternatively, a simplistic approach could involve a separate water-ice storage system maintained at zero degrees Celsius. There are various approaches for the application of this technology. Its pertinence for regions in Africa is primarily due to its ability to function without reliance on electrical supply. With only the need for solar energy as a heat source, an adsorption pair can be used for cooling. This technology possesses the potential to substantially augment the cold chain infrastructure.

3 Adsorption

The following chapters dealing with literature, i.e. chapters 3-5, have several segments from the project work. This is therefore a continuation of this work with added and altered contents.

Due to its simple and cheap construction, and high adaptability, the most common refrigeration technology today is the use of heat pumps. It consists of mainly four components; Compressor, condenser, expansion valve and evaporator, where the compressor is the driving force of the system. With its possibility to run in both cooling and heating modes, the heat pump can cover both the seasonal demands of winter and summer. However, due to electricity powering the system, it is not available in off-grid areas. Adsorption refrigeration technology shares some similarities with heat pumps, in that it consists of a condenser and an evaporator. Yet, the main driving force in the system does not come from a compressor but rather a pressure difference by virtue of adsorption and desorption processes within an adsorption bed. It is powered by solar heat and thus independent from the electricity grid. The system can practically run with only three components; an Adsorption bed, condenser, and evaporator. Where the adsorption bed consists of an adsorption pair known as adsorbent and adsorbate.

3.1 Principle of adsorption

There are typically three types of adsorption pair phenomena to be used: Physical, chemical and composite adsorption. The main difference sits in the type of bonding used, where physical adsorption is bound by weak Van Der Waals forces and chemical adsorption uses strong chemical bonding. It is therefore two different types of interactions in that physical adsorption uses a refrigerant on a solid porous structure, whereas Chemical adsorption is mainly a hydration/dehydration reaction of salt hydrates. Composite adsorption is on the other hand a combination of both, where physical porous structures are impregnated with chlorides to raise heat transfer performance and permeability. For example silica gel and chlorides/methanol. A further overview of properties containing the two primary types is given in Table 3.1 and Figure 3.1. [5][6]

Table 3.1: Physical vs chemical adsorption [7]

Physical	Chemical
Van der waals forces between adsorbate and adsorbent	Chemical forces of bonding type between adsorbate and adsorbent
Reversible process where adsorption decrease with increasing temperature and increase with increasing pressure	Irreversible process where adsorption increase with increasing temperature and pressure has no effect
Low heat of adsorption at about 40 Kj mol^{-1}	High heat of adsorption at about 400 Kj mol^{-1}
The adsorption is a multilayered process	The adsorption is a single layered process
Does not need activation energy	Needs activation energy
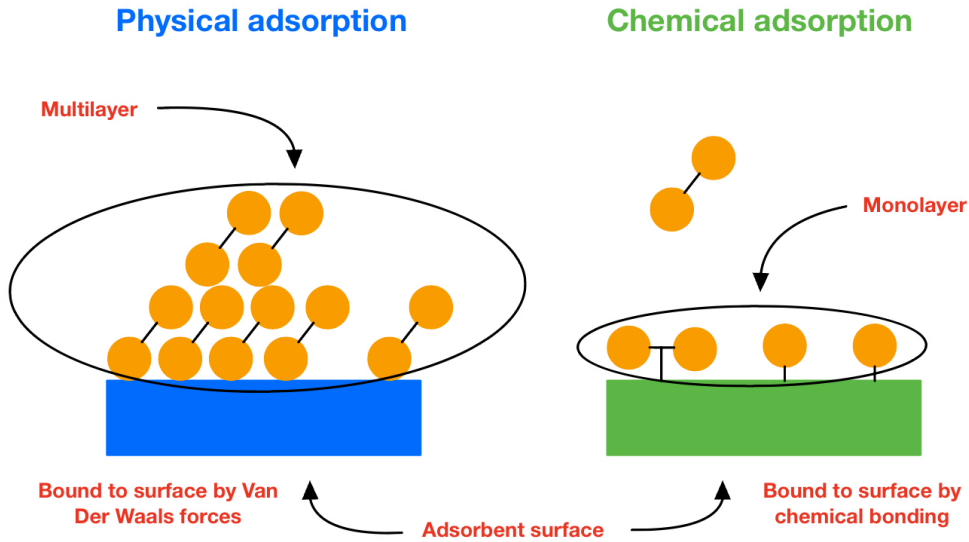
Figure 3.1: Physical vs chemical adsorption

For physical adsorption, the adsorption pair consists of an adsorbent and adsorbate, where the first is the solid material used to adsorb and the latter is the fluid being adsorbed. Putting together an adsorption pair is based on the intended use, where for cooling purposes the area of use is typically divided into three fields of operation. Namely air conditioning, chilling and freezing. For this project, the area of interest is mainly freezing but certain aspects of the others are discussed. In addition to application purposes, the system can be categorised as high or low-pressure systems and high or low-temperature systems.

The theory behind how the Van Der Walls forces in physical adsorption work. Is that a temporary shift in atom structure, creates a non-permanent dipole in the atom. This will in turn make it susceptible to connect with other atoms. This is displayed in Figure 3.2 [8][9]

For use in refrigeration technology, the most promising adsorption types are physical and composite adsorption. In chemical adsorption the thermal conductivity as well as heat and mass transfer is poor. Although it gives some benefits like low driving temperatures and dissociation pressures, it would be more preferable to use it as a composite for higher efficiencies and prevent salt agglomeration and swelling. [5][6]
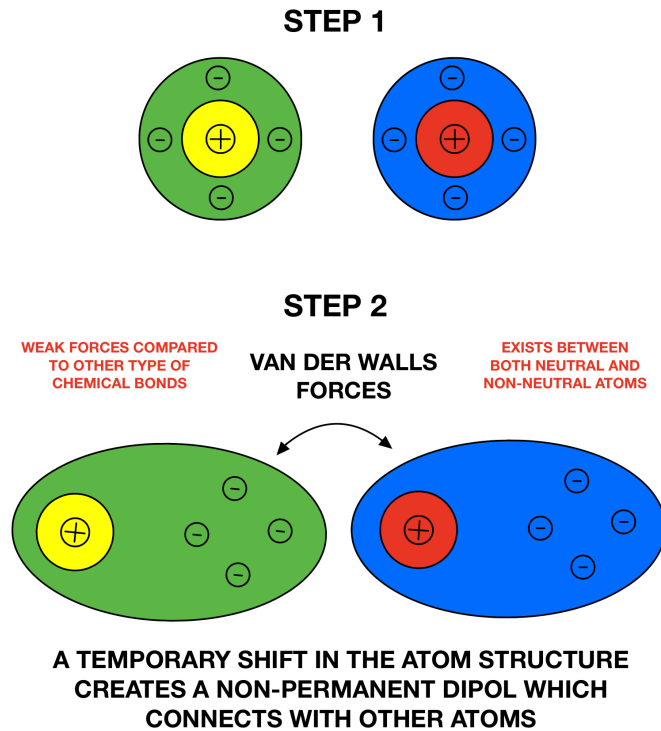
Figure 3.2: Physical adsorption

The type of adsorption cycle can be divided into intermittent and continuous systems. For a single-bed construction, cooling can only be provided during the cooling stage of the cycle. Meaning there is no supply of cooling during the other half of the cycle. This is known as an intermittent system. For a simple solar-driven adsorption cycle, the system is heated during day time and cooled during the night, thus following the cycle of the sun. When two or more beds are connected together, one adsorption bed can be heated while the other is cooled and vice versa. Hence, the system can run continuously. Having a continuous system has several advantages over an intermittent system. The possibility to run interrupted can be combined with heat and mass recovery and thus increase the COP and cooling power.

In Figure 3.3 a conventional single-bed adsorption cycle can be seen. It is made up of three components; 1: Adsorption bed, 2: condenser, 3: evaporator. The evaporator is shown within an isolated water bath. A corresponding p-T-x diagram is given in Figure 3.4. The cycle can be divided into 4 steps, Two for heating and two for cooling.

Step 1

The first step starts with heating the adsorption bed from solar radiation and thus increasing the temperature of the system. At the start of this stage, the bed is at its lowest temperature after being cooled in the previous adsorption process. As the temperature is increasing, the vapour expands, causing a corresponding pressure increase in the adsorber. The temperature increase stops when the refrigerant reaches the saturated pressure for the condensing temperature. In the p-T-x diagram the temperature increases from T_{a2} to T_{d1}, while the pressure rises from evaporator pressure p_e to condenser pressure p_c. The pressure difference that occurs between the adsorber and condenser is what drives the system.

Step 2

When the adsorption bed has reached the condensing pressure the adsorbate starts to desorb from the adsorption bed. At this point, the fluid moves from the bed to the condenser. A continuing

temperature increase from T_{d1} to T_{d2} maintains the desorption of fluid, which is condensed at the same rate as desorption. The condenser is cooled by natural convection as it is put in ambient temperature and thus exposed to daily temperature fluctuations. After heat is rejected in the condenser, the fluid is collected in the evaporator by gravity. Alternatively, it can be collected in a liquid receiver before the evaporator.

Step 3

As there is little to no solar energy being delivered to the adsorber, it will slowly start to cool. With the temperature decreasing from T_{d2} to T_{a1}, the pressure is declining from p_c until it reaches the evaporation pressure for the saturated evaporation temperature p_e. Marking the start of the adsorption process.

Step 4

In the final step of the cycle, the refrigerant is throttled from condensing pressure to evaporation pressure while the adsorbent continues to cool. Thus reducing the temperature of the fluid to evaporation temperature, enabling the cooling of the water container. The fluid will at this stage be evaporated in the evaporator, turning the liquid/gas mixture into gas. Moreover, the gas is then adsorbed by the adsorbent. Once the refrigerant is fully adsorbed the cycle can start over again.
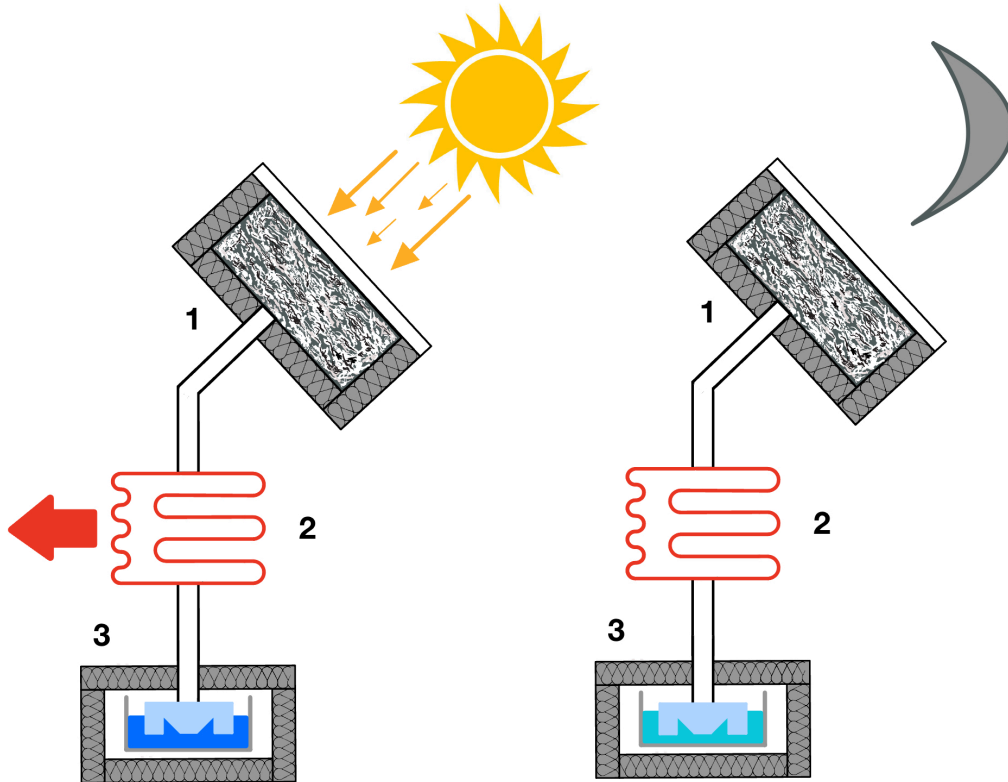
Figure 3.3: Simple adsorption cycle
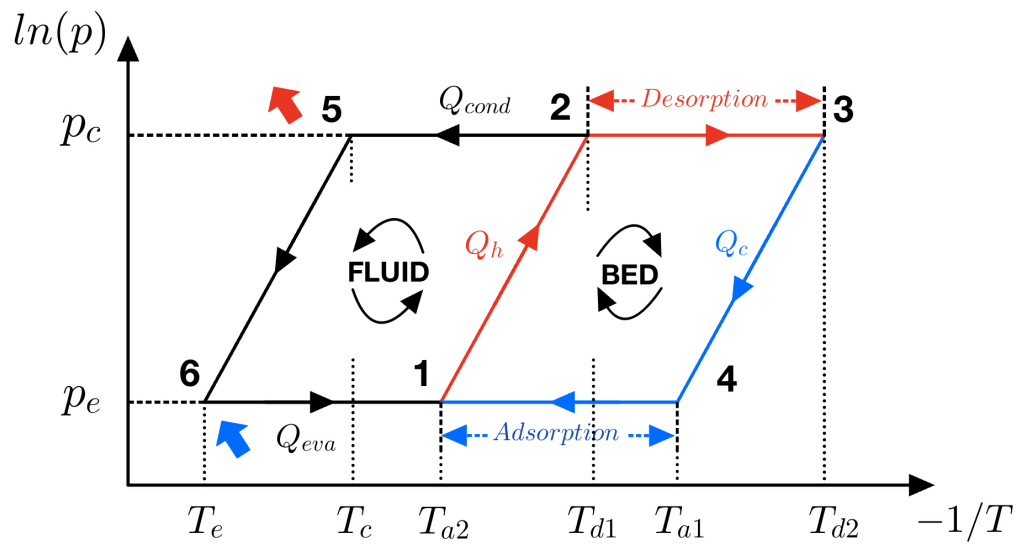
Figure 3.4: p-T-x diagram of adsorption refrigeration cycle

4 Adsorption pair

When choosing adsorption pair for the ice maker, certain properties are important to possess. For the adsorbent these can be listed as [10]:

- Adsorption of a large amount of the adsorbate under low-temperature conditions to yield good COP

- Desorption of most of the adsorbate when exposed to thermal energy

- Possession of high latent heat of adsorption compared to sensible heat

- No deterioration with age or use

- Non-toxic and non-corrosive

For adsorbate these can be:

- Evaporation temperature below 0°C

- Small molecular size to enable it to be adsorbed into the adsorbent

- High latent heat of vaporization and low specific volume.

- Thermally stable with the adsorbent at the cycle operating temperature ranges

- Non-toxic, non-corrosive and non-flammable

- Low saturation pressures (slightly above atmospheric) at normal operating temperature

Getting an adsorption pair that satisfies all of the above is difficult if not impossible as one usually excludes the other. In addition to the properties mentioned above, a low regeneration (desorption) temperature and high thermal conductivity are advantageous when designing the solar collector. [5] For the ability to produce ice from the setup, the evaporation temperature should be at least -5°C. It is therefore important to have an absorbate with the possibility to go below 0°C. This automatically excludes adsorption pairs with the use of water, such as silica gel/water and Zeolite/water.

In addition there are certain important properties to consider:

- Heat of adsorption.

- Adsorption quantity

- COP

- SCP

- Evaporation temperature

- Driving temperature

The heat of adsorption describes the energy released and captured during adsorption. While the adsorption quantity displays the amount of adsorbate captured by the adsorbent expressed in mass/mass. Combined, these two parameters give a good indicator of the strength of the adsorption pairs when compared. Although, by itself, it cannot describe abilities relevant to its intended use. It is therefore important to include the COP, SCP, evaporation temperature, and driving temperature to find the adsorption pair best suited for an adsorption-based solar ice maker.

4.1 Activated carbon

As an adsorbent, the surface area of activated carbon makes it a particularly suitable agent. One gram alone can have a surface area above 3000 m^2. It is made by pyrolyzing organic materials such as coconut shells and wood charcoal. Although all kinds of organic materials can be used, the type of material decides the structure of the finished product. For example, hard shells and bones form small pores, while coal forms a wide range of pores. [11] Activated carbon can be divided into several subcategories depending on the form. Some of which are powder, fibre, granule, solid, and monolithic. Although many more exist. Carbon in general is mainly used for air and water filtration but can also have multiple other purposes, among other refrigeration. The powdered form is generally between 15-25 μm and is used for liquids, while the granular is 0.8-3.0 mm diameter granules used for gas. The activated carbon fibre has fibres of 7-15 μm and can be used for both water and gas. [12]

4.1.1 Activated carbon/Methanol

One of the most common adsorption pairs currently in use is activated carbon/methanol. This is due to its large adsorption quantity and lower adsorption heat but also because of its ability to be used for freezing purposes as opposed to water-based pairs. [6] The low adsorption heat at 1800-2000 kJ/kg is beneficial for the coefficient of performance (COP). Low desorption temperature also enables the use of solar energy as the temperature needed is no more than 100 °C. It should although be used with caution as the methanol will start to decompose into other compounds at 140 °C. There has even been reported degradation at temperatures as low as 120 °C. When using methanol, aluminium alloys were found to have a stronger catalytic effect on the decomposition and should therefore be avoided [13]. The activated carbon/methanol pair also has the disadvantage of operating under sub-atmospheric conditions. Meaning there needs to be a vacuum within the system, making the manufacturing and operation more complex. Seeing that the system can be compromised with rather small air leakages. [14]

A simple adsorption cooling device was in 1986 experimented by Pons & Guilleminot containing activated carbon/Methanol. The device had no concentration, no valve and no rectifying column. Making it a good baseline for other experiments. The COP of the system reached 0.12 (0.43 cycle COP) with a regeneration temperature of 95 °C, evaporator temperature of -5 °C and condenser temperature of 25-30 °C. [15]

El-sharkawy et al. published in 2009 a study of methanol on carbon-based adsorbents. The results depicted great results for the Maxsorb III compared to activated charcoal and traditional activated carbon (AC-35). Although, the differences are largest for higher evaporation temperatures. The uptake and cycle performance for the system is decreasing with decreasing evaporation temperatures. Adsorption systems for freezing purposes therefore have substantially lower performances compared to chilling. An evaporator temperature of 15 °C is shown to have an uptake of 1 kg/kg compared to a temperature of -5 °C and 0.247 kg/kg. For the objective of this task, the evaporation temperatures below 0 °C is what's relevant. In Table 4.1 results from methanol on carbon with adsorption temperature of 30 °C and evaporation temperature of -5°C are shown with varying regeneration temperature. It clearly shows that a higher regeneration temperature is preferable for good SCE and COP and that it is especially important at low evaporation temperatures where the cooling effect is low. The table also shows how the differences between standard and high-performance carbon diminish at preferable temperatures. Albeit, the SCE of Maxsorb III has a 26% increase from activated charcoal making it a substantially better option [16]

Table 4.1: Adsorption of methanol on carbon adsorbent with adsorption temperature at 30°C and evaporator temperature of -5°C [16]

Regeneration temperature [°C]	Properties	Maxsorb III	Activated charcoal	LH	DEG	AC-35
80	Wmax [kJ/kg]	0.247	0.211	0.190	0.171	0.200
	Wmin [kJ/kg]	0.127	0.128	0.137	0.135	0.158
	SCE [kJ/kg]	137	94	61	40	48
	COP [–]	0.60	0.54	0.45	0.36	0.39
90	Wmax [kJ/kg]	0.247	0.211	0.190	0.171	0.200
	Wmin [kJ/kg]	0.047	0.061	0.090	0.100	0.110
	SCE [kJ/kg]	228	170	116	81	103
	COP [–]	0.67	0.64	0.56	0.48	0.53
100	Wmax [kJ/kg]	0.247	0.211	0.190	0.171	0.200
	Wmin [kJ/kg]	0.015	0.026	0.057	0.072	0.071
	SCE [kJ/kg]	265	211	153	112	147
	COP [–]	0.68	0.66	0.59	0.53	0.58
110	Wmax [kJ/kg]	0.247	0.211	0.190	0.171	0.200
	Wmin [kJ/kg]	0.004	0.010	0.035	0.052	0.043
	SCE [kJ/kg]	277	229	177	135	179
	COP [–]	0.67	0.66	0.60	0.55	0.60

A more recent review by Younes et al. based on the results from El-Sharkawy shows the superiority of Maxsorb compared to other carbon constituents given in Figure 4.1. Both uptake and specific cooling effect for the Maxsorb carbon is almost twice that of activated carbon fibre.
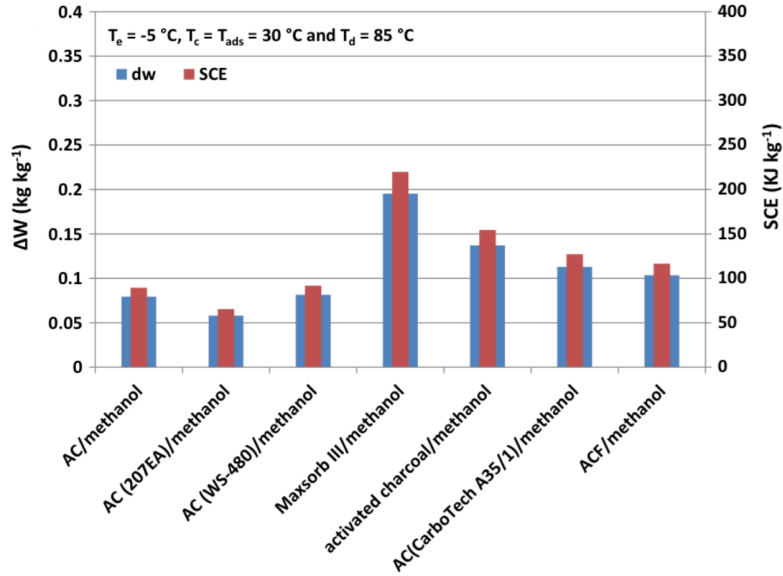
Figure 4.1: Comparison between the highest ΔW and SCE for the presented adsorbent/adsorbate pairs using methanol for refrigeration application [17]

Wang et al. studied the difference between granular and solidified activated carbon. The experiments showed higher heat transfer performances for solidified beds compared to granular with heat transfer coefficients of 99 and 25 W/(m^2 °C). Leading to better SCP and COP for the system. regarding heat transfer, the design of gas flow channels also played an important role in the performance of the adsorbers. This was especially important for solidified beds. [18]

4.1.2 Activated carbon/Ethanol

Using ethanol as a refrigerant has several benefits but the main reasons are being environmentally friendly and non-toxic. It also has a high vapour pressure at low temperatures. Ethanol is therefore suitable for low-temperature systems such as waste heat between 60-95 °C. The applicability of activated carbon/ethanol is mainly directed against chilling and not freezing purposes.

In 2004 Li et al. investigated the differences between methanol and ethanol in a simple activated carbon-driven solar ice maker. At the same conditions, ethanol was not able to produce ice as opposed to methanol. For the activated carbon/methanol working pair, the amount of desorbed and adsorbed refrigerant was stable under desorbing and adsorbing conditions. The working pair was also directly dependent on the energy supplied to the system. However, this was not the case for the activated carbon/ethanol working pair, as the amount of desorbed and adsorbed refrigerant fluctuated significantly. The performance was about 3-4 times higher when using methanol as adsorbate compared to ethanol. The study therefore pictured activated carbon/methanol as the most suitable working pair for solar ice makers by far. [19]

A two-bed activated carbon fibre (ACF)/ethanol adsorption chiller was theoretically investigated by Saha et al. in 2007, creating a transient model to use for low-temperature waste heat sources. The simulation results displayed high performance for the system, surpassing that of silica-gel/water. [20][21] The same adsorption pair was experimentally investigated by El-Sharkawy et al. to find the adsorption characteristics for cooling applications. [22] [23]

El-Sharkaway et al. published in 2008 experimental results on activated carbon/ethanol pair for cooling using Maxsorb III as an adsorbent. The experiment showed the uptake of ethanol as high as 1.2 kg per kilogram of adsorbent due to its high surface area of over 3000 m^2/g. However, realistic uptake is substantially lower when adjusting to relevant temperatures and pressures. At an evaporation temperature of 7 °C, heat source temperature of 80 °C, and 30 °C adsorption temperature the uptake varies between 0.29 to 0.78 kg/kg from start to end. In addition, for freezing systems the evaporation temperature is around -5 to -10 °C which further decreases the uptake. The results for Maxsorb are still far greater than for active carbon fibre (A-20), where concentration limits for the same parameters are between 0.24 to 0.58 kg/kg. The concentration range is therefore about 44 % better. Furthermore, the adsorption rate of ACF/ethanol is much faster than Maxsorb/ethanol, making it more suitable for solar adsorption cooling where cycle times are relatively long. The isosteric heat of adsorption for the Maxsorb/ethanol is found to be 1026 kJ/kg. And from Figure 4.2 the SCE can be seen as somewhere between 300-600 kJ/kg, depending on the evaporation temperature. For a freezing system, this will be even lower. From figure 4.3 a comparison of Maxsorb against other adsorption pairs is shown. It clearly shows that Maxsorb provides a higher SCE than the rest. [24]
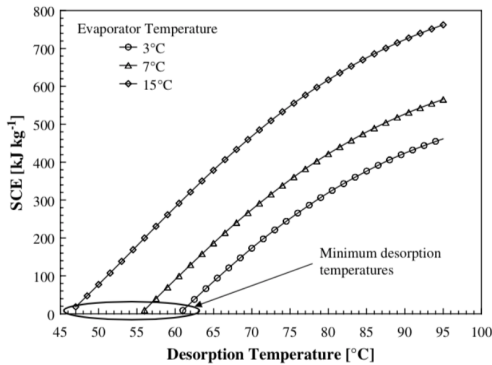
Figure 4.2: Effect of desorption temperature on specific cooling effect for different evaporating temperatures [24]
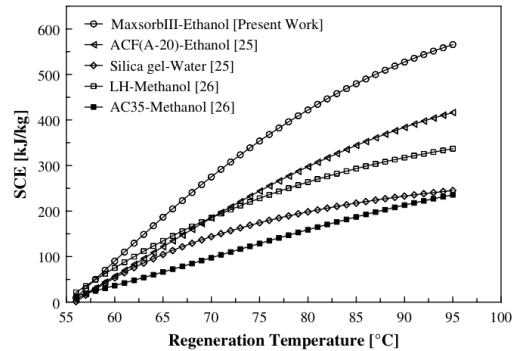
Figure 4.3: Effect of desorption temperature on specific cooling effect for five different pairs.

A graphic representation of other types of activated carbon with ethanol is shown in Figure 4.4. In addition to carbon based adsorbents, there is also shown synthetic polymers known as phenol resin in combination with ethanol which has recently been developed. In this example, the resin has been treated with potassium hydroxide. As such, it is more advanced and costly than activated carbon. Yet, the Maxsorb is not far from in performance.
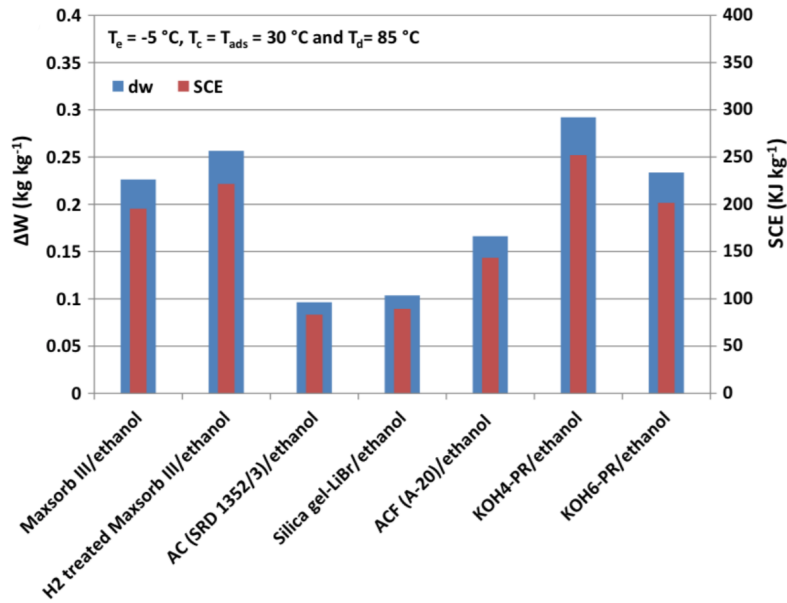
Figure 4.4: Comparison between the highest ΔW and SCE for the presented adsorbent/adsorbate pairs using ethanol for refrigeration application [17]

4.1.3 Activated carbon/Ammonia

Critoph investigated in 1989 the use of methanol and ammonia in activated carbon refrigeration. With a simple system containing only one adsorber bed, valve, and no thermal storage, a cycle COP of approximately 0.5 for methanol and 0.4 for ammonia was reached. But although methanol seemed to be the better choice, low system pressures and possible chemical instability did not make the use of methanol an obvious choice compared to ammonia [25]

In 1993 Critoph studied the use of forced convection in adsorption cycles to enhance heat transfer, in which the results appeared to offer better power densities. The study was performed for a heat pump cycle but is still applicable to general adsorption technology.[26] The work continued in 1998 where thermal storage is the keyword. By using inert beds to store heat, the ammonia can be heated outside of the standard cycle rather than heating the beds directly. In this way, efficiency increases. The setup consisted of two adsorption beds and two inert beds, such as the cycle could run continuously. [27]

Table 4.2 examined by Tamainot-Telto et al. in 2009, is showcasing a model simulation of ammonia on different activated carbon materials. The carbon types included monolithic, granular, carbon fibre, carbon powder, and compacted carbon. The carbon contents are mainly from coconut shells, coal, and some polymers. Within each category of activated carbon, the performances are rather substantial, as the best samples have in some cases more than 100% better COP than the worst. Still, the variation between the top sample in each category is comparatively small. With the right sample of activated carbon, the distinction between granular, powder, fibre etc is arguably insignificant when looking at COP. However, the specific cooling production was vastly different. [28]

Table 4.2: Best performance of ammonia on carbon based adsorbents with two-bed configuration at driving temperature of 100 °C [28]

Samples	q_c (MJ/m^3)	COP
KOH-AC (monolithic)	66	0.45
SRD1352/2 (granular)	36	0.48
FM10/700 (fibre)	27	0.48
C-2132 (powder)	31	0.46
SRD1352/2 (compacted)	43	0.48

4.1.4 Activated carbon/Synthetic refrigerants

The use of synthetic refrigerants was previously very common as it outperformed natural refrigerants. Although, from the 80's, the use of ozone-depleting substances gradually decreased on the basis of the Montreal protocol in 1987 and the Kyoto protocol in 1997. The protocol obliges the member countries to reduce emissions which are damaging to the ozone layer. Since then, the adoption of natural refrigerants has been researched extensively. Natural refrigerants are not a new medium as it was the main used refrigerants up until the 30's when HFC and CFC entered the market. Many of the disadvantages of natural refrigerants have however been resolved with modern technology. As the focus of modern research is directed towards renewable technology, synthetic refrigerants such as R22 and R134a have not been reviewed for this paper. It is though worth noting that synthetic materials are continuously being developed and could later prove to be both environmentally friendly, more economical and yield superior performance.

4.2 Silica gel/water

Silica gel/water is an adsorption pair with a lot of research. Unfortunately, it is not an option for ice production as the evaporation temperature needs to be lower than 0 °C. Sakoda & Suzuki investigated already in 1984 the use of silica gel/water as adsorption pair for cooling by the use of simulation. [29] The adsorption pair was also examined experimentally by Boelman et al. [30] and analytically by Saha et al. [31] in 1995. Further work on the same pair, implementing a multi-stage system [32] and multi-bed system [33] was performed respectively in 1997 and 2003 by Saha et al. A two-bed system was also investigated analytically by Chua et al. in 1999. [34] In addition, the performance of a multi-bed regenerative adsorption chiller was solved numerically by Chua et al. in 2001. [35]

4.3 Zeolite/water

Another water-based adsorption pair which have been researched widely is Zeolite/water. Alike silica-gel/water, the use is limited to refrigeration purposes with an evaporation temperature above 0 °C. Zeolite is a collective term for alumina silicate crystals composed of alkali or alkali soil. In total there are over 40 types of natural zeolites but because natural zeolites are difficult to obtain in many countries, the use of synthetic zeolites is therefore commonly used. In total there are over 150 types of synthetic zeolites grouped as type A, type X, type Y and type ZSM. The current main types of synthetics are 4A, 5A, 10x and 13x. [6]

Zeolite as an adsorbent first started in the late 1970s with the work of Tchernev, where zeolite was discovered to adsorb and desorb large amounts of water vapour. Later work included the commercialisation of a refrigerator with zeolite/water as the operating element at a COP of 0.15. [36]

Solmus et al. investigated the adsorption properties of natural-zeolite/water to use in cooling cycles and compared them against other relevant adsorption pairs. The results depicted zeolite/water as the least dependent on evaporator and condenser temperatures but also the most dependent on high regeneration temperatures. Whereas activated carbon/methanol and silica-gel/water exhibited a minimal increase in cyclic adsorption capacity swings above 140 °C, the zeolite/water experienced a significant gain. For all given conditions the activated carbon/methanol got the highest cyclic adsorption capacity swings and therefore proves to be the strongest option, especially for low-temperature systems. [37]

4.4   Comparison of adsorption pairs

A comparison of the discussed adsorption pairs are presented in Table 4.3.

Table 4.3: Comparison of various working pairs [38]

Working pair	Operating temperature (°C)	Working pressure (Bar)	Adsorption heat (kJ/kg)	Application
Silica gel/water	Below 90 °C	0.01-0.3 [Vacum conditionn]	1000-1500	Air conditioning
Activated carbon/methanol	Below 120 °C	0.01-0.35	1800-2000	Ice making
Activated carbon/ammonia	Up to 150 °C	3-10.4	2000-2700	Refrigeration/ice making
Zeolite/water	Up to 200 °C	3.4-8.5	3300-4200	Air conditioning
Zeolite/ammonia	150-200 °C	3.5-7	4000-6000	Refrigeration/ice making

In a recent review by Younes et al, physical adsorbent-adsorbate pairs have been analyzed and compared by using adsorption isotherm models and employing an ideal adsorption cycle to find the adsorption uptake and specific cooling capacity. Both cooling and refrigeration purposes have been investigated in addition to reporting SCP and COP of selected systems. For the solar-powered ice maker, only the refrigeration result is of interest where the evaporation temperature is kept at -5 °C. An excerpt from the highest uptake of ΔW (kg/kg) and SCP (kJ/kg) is given in Figure 4.5. It is worth noting that the driving temperature is in this setting set at 85 °C and is thus lower than necessary. A driving temperature of 100 °C would yield better results, especially for methanol where the optimal temperature range is around 95-120 °C.
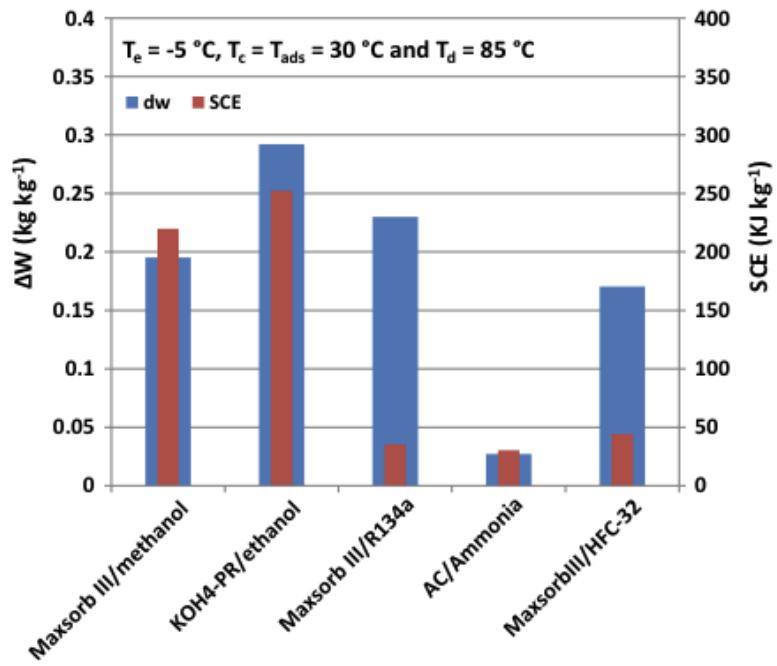
Figure 4.5: Adsorption pair comparison [17]

5 Performance improvements

Since the start of adsorption technology in the 70's, many improvements have been done to boost performance. Some are more advanced than others. These include among others, multiple beds, valve control, heat and mass recovery, thermal wave cycles, and cascading systems. The spectrum of adsorption technology is broad as it can be used for many different purposes. Solar-powered adsorption cooling is one of the simplest forms of adsorption cooling technology but the process can also be powered by fuel and waste heat. The principle of adsorption is not a new phenomenon and is mostly used for air and water purification. The different types of adsorption refrigeration cycles are shown in Figure 5.1 and the most relevant performance improvements are mentioned in the following chapter.
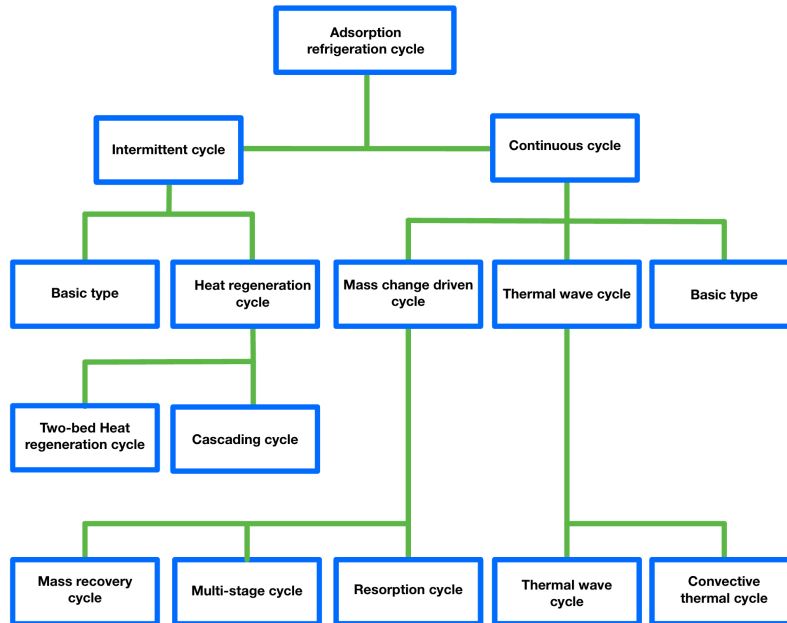
Figure 5.1: Classification of adsorption cycles [38]

5.1 Single and multi-bed

When using a system configuration with only one available bed, there can only be one cycle running at a time. Thus limiting the efficiency of the system. For solar-driven adsorption systems, this is mostly synonymous with one cooling cycle per day. Therefore, in order to increase cooling production, a larger system is needed. This will in turn increase the capital cost of the investment. A possibility to boost the efficiency of the system is accordingly to increase the number of beds for the device. By utilizing a double-bed or multi-bed technology, the number of simultaneous cooling cycles increases linearly. For a double-bed system, one cycle will be cooling while the other is regenerating and vice versa. Hence, the system efficiency and cooling production increase. In theory, increasing the number of beds increases the efficiency accordingly. However, adding more beds will also result in a more complex system. For a single-bed arrangement, valves and other components can be excluded. Whereas with more beds, control systems in addition to valves, storage etc is needed. Consequently, the robustness drops, considering electrical components and moving parts have a shorter life expectancy. Electricity or a solar panel is also necessary to power the electrical components. For rural areas in Africa, this could impose an issue seeing as access to repairs and spare components are limited. The extra cost will nevertheless pay off with elevated cooling capacity, and more predictable operation.

In a given standard two-bed system pictured as a schematic in Figure 5.2 there is one condenser, one evaporator, two adsorbers and four valves. The adsorbers work opposite of each other such that when adsorber 1 is heating, adsorber 2 is cooling. In this situation valve 2 and valve 4 is open. This allows the heated adsorber 1 to be connected to the condenser, while the cooled adsorber 2 to be connected to the evaporator. In the opposite case where adsorber 1 is cooling and adsorber 2 is heating, valve 1 and valve 3 are open while the others are closed. The corresponding p-T-x diagram is given in Figure 5.3.
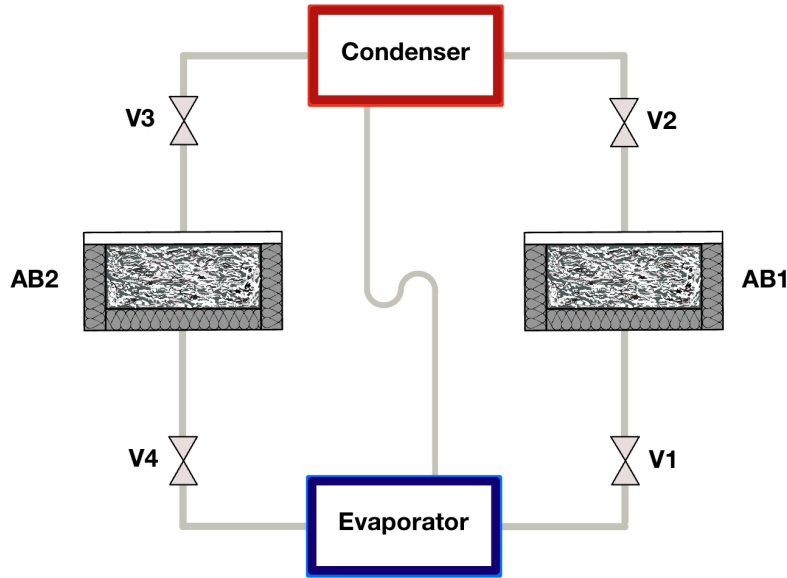
Figure 5.2: Adsorption cycle schematics
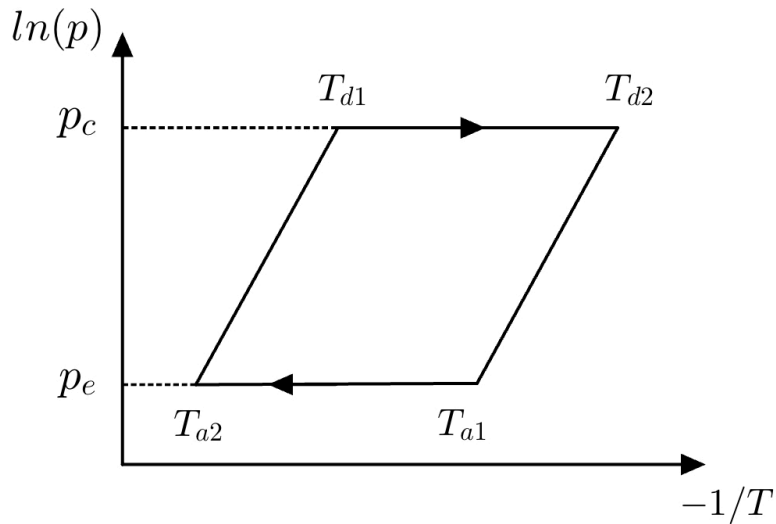
Figure 5.3: Simple p-T-x diagram of adsorption refrigeration cycle

A model simulation of ammonia on different activated carbon materials was examined by Tamainot-Telto et al. The carbon types included monolithic, granular, carbon fibre, carbon powder, and compacted carbon. From their results, there is a distinct difference between single and double-bed construction. At a temperature of 100 °C, the highest COP for a single bed is 0.4, whereas for a double bed it´s 0.48. A summary of their results is given in Table 5.1. [28]

Table 5.1: Carbon/ammonia Best performance with single and two-bed configuration at driving temperature of 100 °C [28]

Samples	$\mathbf{COP}_S$	$\boldsymbol{q_c}$ $(\mathbf{MJ}/\boldsymbol{m^3})_D$	$\mathbf{COP}_D$
KOH-AC (monolithic)	0.34	66	0.45
SRD1352/2 (granular)	0.38	36	0.48
FM10/700 (fibre)	0.35	27	0.48
C-2132 (powder)	0.4	31	0.46
SRD1352/2 (compacted)	0.37	43	0.48

5.2 Heat and mass recovery

In a simple adsorption cycle, the adsorption bed is heated by the sun to start the desorption process. The heat from the working fluid is then rejected in the condenser. To start the cooling process, heat must also be removed from the bed. This can be done by air venting or water cooling. In total there is a lot of heat being removed from the system to the surrounding, which could be stored and used instead. By storing rejected heat for the next cycle, the total cycle time can be reduced. Since the heating and desorption stage of the cycle requires a substantial amount of heat, it will be rewarding both for cycle times and predictability to store the excess heat. Thus, the efficiency will also increase as shorter cycles give higher cooling capacities. Using heat recovery is especially beneficial but most common in adsorption systems with multiple beds. In such cases, the excess heat from one adsorption bed can heat the other. The only downside is the extra components and therefore added complexity and cost.

5.2.1 Heat recovery

Heat recovery between two beds is typically performed at each half cycle when one adsorption bed is at T_{a2} and the other is at T_{d2}. At this point, the temperature difference is at its highest and thus heat can easily be recovered. A thermal fluid like water or oil is then circulated between the beds to transfer heat until both beds reach the same temperature. This is shown as points e and e' in Figure 5.4. In this manner, the thermal load can decrease by about 30% of the total heat input [39]. For a solar-driven adsorption system, both the cooling and heating process speeds up. Hence increasing the efficiency of the system. The decrease in thermal load can be expressed in Equation 1.

$$Q_{decrease} = Q_{a2} - d_1 - e \tag{1}$$
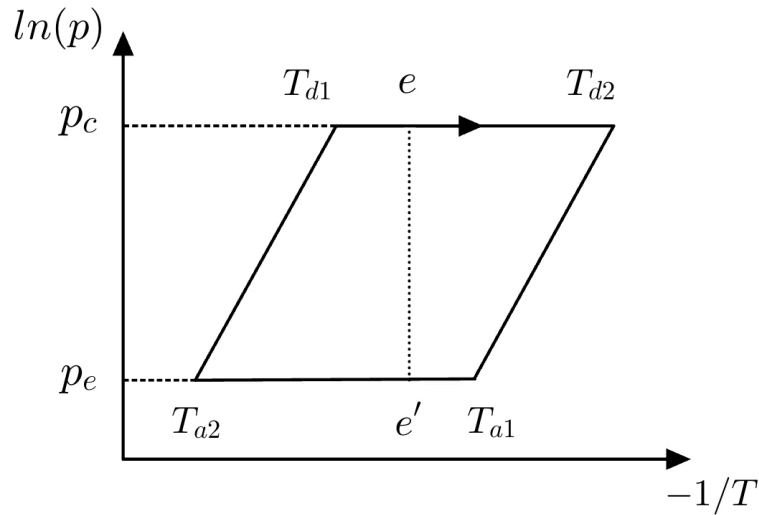
Figure 5.4: Heat recovery diagram of simple two-bed cycle

A simple schematic of a heat recovery implementation is given in Figure 5.5. In this system, there is no water cooling of the adsorption beds, only air. Thus, making it a fairly basic system. The piping between adsorption beds 1 and 2 together with Valve 5 and 6 makes up the heat recovery branch. A pump is also installed to circulate the thermal fluid between the beds. When heat recovery mode is activated, valve 1-4 is closed while 5 and 6 are opened.
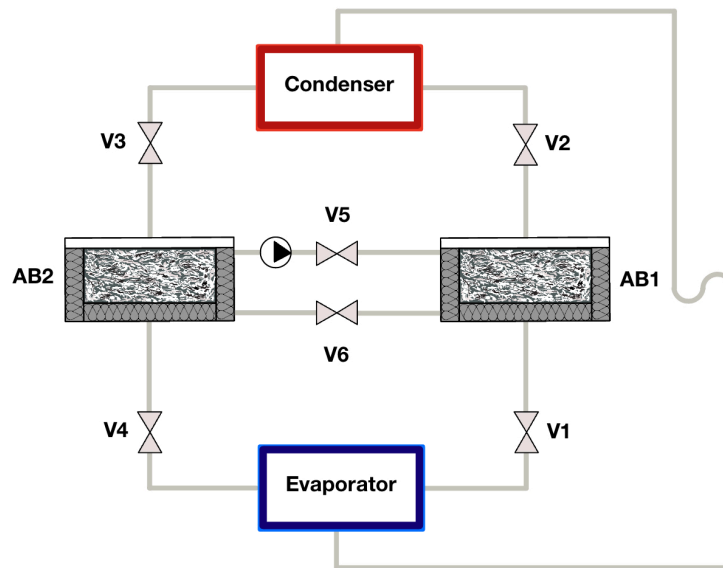
Figure 5.5: Heat recovery schematic of simple two-bed cycle

By using heat recovery between adsorption beds the COP can according to Wang increase by 25% [40] compared to a basic one adsorber intermittent system. The experiment was executed with activated carbon/methanol as adsorption pair. Wang also found the heat capacity of the metallic adsorber and thermal fluid to have a great influence on the COP. An increase in heat capacity ratio R will likewise significantly decrease system COP. When using water as a thermal fluid (R=2.9), the COP is reduced by 25-30% compared to oil (R=1.85). In another study by wang et al. using activated carbon/methanol, the impact of replacing water as thermal fluid with oil was found to be a 20% increase in COP [41].

Chekirou et al. investigated heat recovery for an AC-35/methanol cooling machine. The optimum regenerating temperature was found to be 125 °C and 105 °C with and without heat recovery. The performance coefficient was also found to increase from 0.483 for a single adsorber to 0.682 when employing heat recovery between two adsorbers. A total increase of 41%. The conditions for maximum efficiency included an evaporator temperature T_e of 0 °C, condenser temperature T_c of 30 °C and adsorption temperature T_a of 25 °C. Recovered energy for the implementation was also found to be 29% of the total necessary heat input. [42]

A layout of a two-bed heat recovery system with fluid cooling is pictured in Figure 5.6. The system works in three different modes; Cooling of adsorber 1 and heating of adsorber 2, heating of adsorber 1 and cooling of adsorber 2, and heat recovery between the adsorber. The system layout is made up of six three-way valves, one closing valve, and two pumps. Black lines represent the active piping for each system mode, whereas grey lines are not in use. There are two main separate loops running within the setup. One with the adsorbate e.g methanol running between the condenser, evaporator, and adsorption beds, and one for the thermal fluid e.g oil flowing between the adsorption beds and cooler. There is in addition a third loop marked in blue, ensuring low temperatures to the cooler. This is typically supplied with water. Figure 5.6 shows the case where adsorber 1 is cooling and adsorber 2 is heating. Once each half cycle of adsorption/desorption is completed, the system changes into heat recovery mode pictured in Figure 5.7. When the temperature difference between the adsorbers is equalized, the heat recovery mode is stopped and the cycle is reversed to provide adsorber 1 with heat and adsorber 2 with cooling. This change is illustrated in Figure 5.8. For a heat pump cycle, the adsorber would in addition to the cooler be connected to a heating system. In this scenario, the heater would be linked to the loop in which the thermal fluid is flowing. Thus one adsorber is connected to the heater and the other to the cooler for each half cycle.
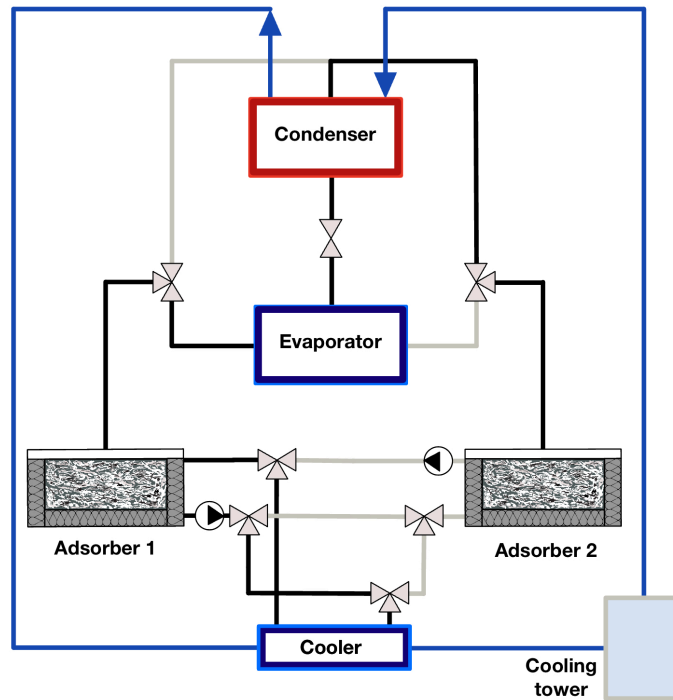
Figure 5.6: Heat recovery of a simple two-bed cycle with thermal fluid cooling. Adsorber 1 is connected to the evaporator, thus providing cooling in adsorption phase, while adsorber 2 is connected to the condenser in desorption phase [40]
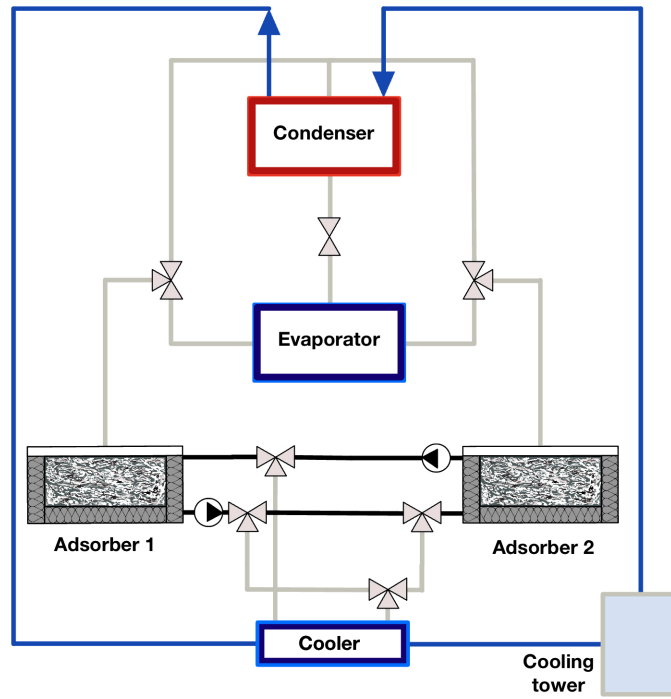
Figure 5.7: Heat recovery of a simple two-bed cycle with thermal fluid cooling, running in heat recovery mode between the half cycles [40]
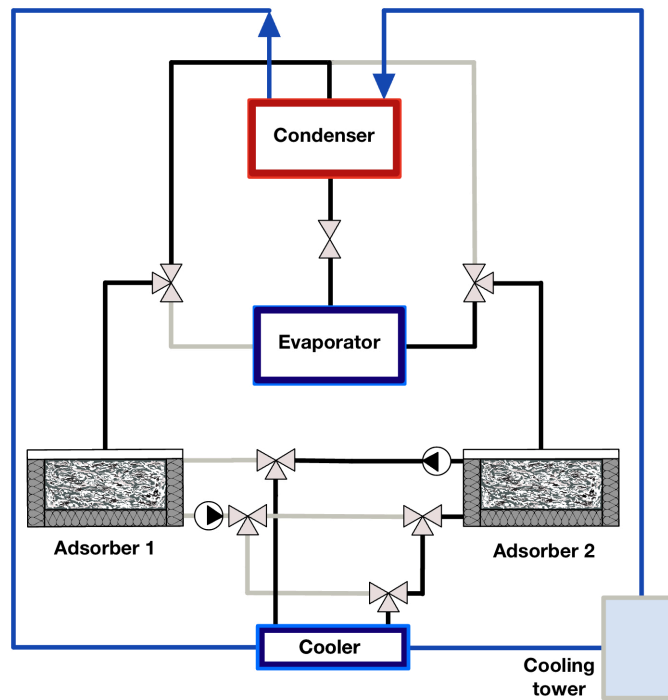
Figure 5.8: Heat recovery of a simple two-bed cycle with thermal fluid cooling. Adsorber 2 is connected to the evaporator, thus providing cooling in adsorption phase, while adsorber 1 is connected to the condenser in desorption phase [40]

5.2.2 Mass recovery

In addition to heat recovery, there is also the possibility to recover mass. This is usually done in combination with heat recovery. When mass recovery is installed in the circuit, a fifth valve is installed and connected between adsorbers 1 and 2 as depicted in Figure 5.9. In this case valve 5 is opened when the system switches between adsorption and desorption. This allows refrigerant vapour to transfer from the hot adsorber to the cold adsorber. [43]
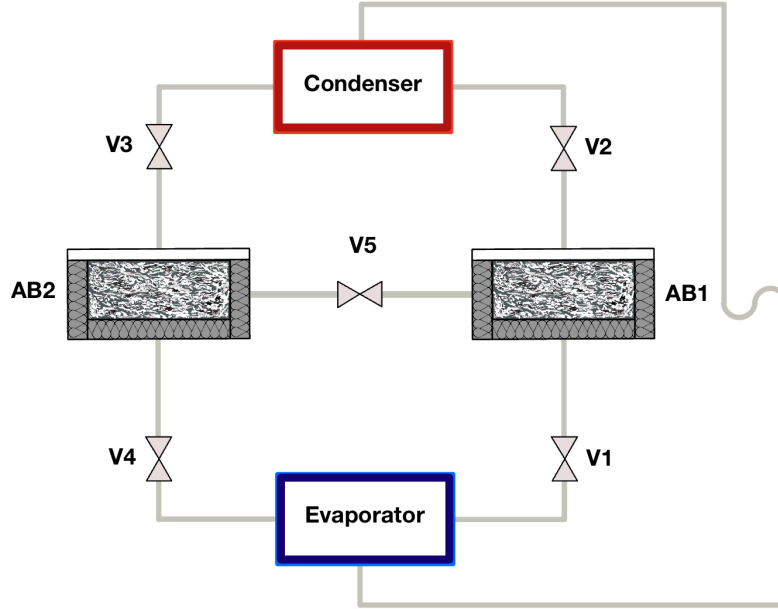
Figure 5.9: Mass recovery schematic of simple two-bed cycle

Mass recovery is used at the end of each half cycle similar to heat recovery but functions fundamentally differently. In heat recovery, the adsorbers are indirectly connected through heat exchange. The thermal fluid transfers heat without being in contact with the adsorption pair and stops when the temperature difference is equalised. Hence, pressure is altered as a consequence of the temperature change but not directly affected. For mass recovery, the adsorbent beds are interconnected directly such that the high-pressure vapour comes in contact with the low-pressure vapour. This process is driven by the pressure difference between the adsorbers and thus continues until the pressure is equalized. In this case, the pressure within the desorbed bed p_c decreases, while the pressure within the adsorbed bed p_e increases until they meet at an equilibrium pressure p_m. [39] [44] By incorporating mass recovery the adsorption and desorption phase is extended and cycle mass is increased. Meaning the cyclic adsorption capacity, and correspondingly SCP is improved. This is shown in Figure 5.10 where T_{a1} is replaced with T'_{a1} and T_{d1} is replaced with T'_{d1}. In addition, there is added two new points, T_{a3} and T_{d3} at the equilibrium pressure[45]. The mass recovery part of the cycle is from T_{d2} to T_{d3} and T_{a2} to T_{a3}. Once the adsorption beds have reached equilibrium pressure, the normal cycle continues.
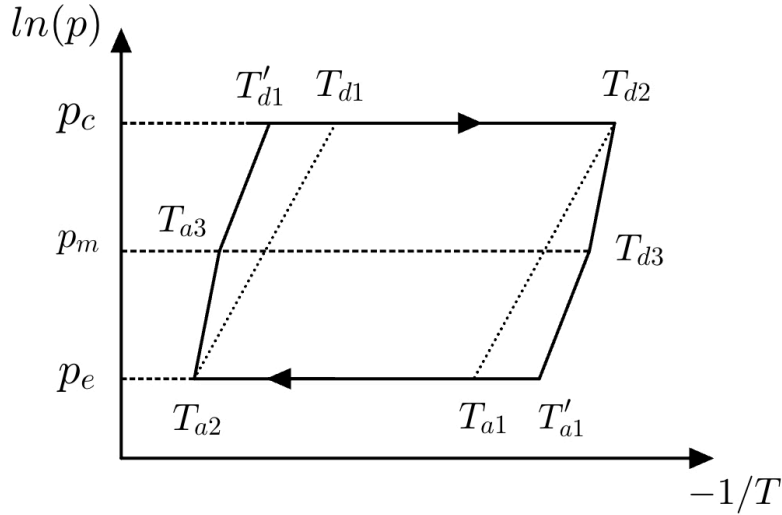
Figure 5.10: Mass recovery diagram of simple two-bed cycle

Wang et al. studied the use of heat and mass recovery for solidified activated carbon. The results presented an increase of cooling power between 7-11% for a two-bed system with mass recovery installed. In addition, the needed heating power decreased by 20-30% when using heat recovery. Thus giving the ice maker an optimal COP of 0.125 and an SCP of 16.8 W/kg at 30 °C evaporation temperature. The study also predicts a strong increase in performance by adding more beds, as a three-bed system is predicted to yield a COP of 0.239 and SCP of 22 W/kg. Giving a SCP and COP improvement of 32% and 92%. [46]

Akahira et al. performed in 2004 cycle simulations with mass recovery of a silica-gel/water system. The mass recovery structure utilizes the pressure difference between the adsorber and desorber to increase mass flow. Results from the simulation show that a system with mass recovery gives superior cooling capacity compared to conventional systems, with a 9.4% increase in cooling capacity compared to a conventional cycle. However, mass recovery is most effective for low regeneration temperatures [47]. The simulation results were later investigated by experimental prototypes to verify the results. [48]

A three-bed adsorption chiller using silica gel/water together with mass recovery was investigated by Zajaczkowski in 2016 using a new cycle time allocation (CTA). The COP of the analyzed chiller increased by 7% for the new CTA without mass recovery but the system increased a total of 35% when implementing mass recovery at a driving temperature of 65 °C. At 85 °C the COP improvement was only at 2% and 15% without and with mass recovery. Thus showing the effects of mass recovery is strongest at lower driving temperatures. [49]

5.2.3 Heat and mass recovery

When combining heat and mass recovery in the same system, the typical way of operating is having mass recovery followed by heat recovery. A diagram for such cases is given in Figure 5.11. At the switch of adsorption/desorption, mass recovery starts and runs until pressure balance is achieved at T_{d3} and T_{a3}. Heat recovery is then initiated and operated until the temperature balance has been met at points e and e'.

Qu et al, studied heat and mass recovery for an activated carbon/methanol system. From the results, mass recovery alone enhanced the cooling capacity by 20%. Although, COP did not necessarily increase as it was dependent on operating conditions. When employing both heat and mass recovery within the same system, COP increased by 30% compared to the basic cycle. However, combined the COP was also 10% higher than a heat recovery cycle. It therefore shows that the combination works well together. [39]

Figure 5.11: Heat and mass recovery of simple two-bed cycle

A novel adsorption chiller using silica gel/water was investigated by Lu & Wang. in 2013. In their results, the cooling capacity and COP for the cycle increased from 14.6 kW and 0.47 to 15.8 kW and 0.53 when incorporating mass-heat recovery. The setup and cycle used are pictured in Figure 5.12. [50]

Figure 5.12: Heat and mass recovery of novel two-bed cycle

6 Formulas

In order to design the refrigeration system, it was imperative to carefully select appropriate and relevant applications. Calculations accounting for heat and mass performance were performed to ensure attainment of the desired temperature in the refrigerator. Furthermore, determination of the cooling chamber dimensions and associated cooling loads, as well as the requisite quantities of refrigerant and adsorbent, were based on these calculations. The selection of appropriate sizing for both the cooling chamber and constituent system components was a critical factor in achieving the targeted temperature. The following system design and formulas is based on the research of Ramaswamy and the previous work of Michael John. [51]

6.1 Cooling Load

The total refrigeration cooling load represents the quantity of thermal energy that must be removed from the refrigeration system to attain the target temperature level. This metric encapsulates the thermal load introduced to the refrigerated compartment as a result of the heat generated by the stored items as well as the heat transfer occurring through the walls. To determine the appropriate amounts of refrigerant and adsorbent required, the total cooling load must first be computed. Based on Ramaswamy research, this metric comprises four distinct components: the product load, wall gain load, miscellaneous load, and air change load. By accurately estimating each of these individual loads, the total cooling load can be calculated to inform the selection and amount of refrigerant and adsorbent.[52]

6.1.1 Product Load

The term "product load" refers to the heat energy that must be removed from a refrigerated product in order to maintain the desired temperature level. This involves the process of product cooling, which entails the extraction of sensible heat at a suitable cooling rate. Furthermore, it is important to note that heat input resulting from the respiration of the pre-cooled and stored products also contributes to the product load. If the product has not undergone pre-cooling prior to storage, it is imperative that the resulting heat input from respiration be factored into the design of the cold-storage system. The amount of heat that must be extracted from the product Q_{pr} can be calculated utilizing Equation 2.

$$Q_{pr} = m_w C_{p_w} \Delta T \tag{2}$$

Where m_w is the mass of water in the refrigeration chamber, C_{pw} is the specific heat capacity of water and ΔT is the assumption of temperature change of water before and after the adsorption process.

6.1.2 Product Load Ice Bath

An additional product load is determined for the ice bath. The ice bath volume $V_{icebath}$ is the volume of the ice bath cylinder minus the volume of refrigeration chamber cylinder as shown in Equation 3. Where D_{ice} and H_{ice} is the ice bath cylinder diameter and height respectively. d_{ref} and h_{ref} is the refrigeration chamber diameter and height.

$$V_{icebath} = \frac{\pi D_{ice}^2 H_{ice}}{4} - \frac{\pi d_{ref}^2 h_{ref}}{4} \tag{3}$$

Since the highest specific heat capacity of the products stored in the refrigerator is water, Equation 4 is used to determine the product load of the ice bath $Q_{pr_{ice}}$ with respect to the water conditions and the temperature change of water and ice.

$$Q_{pr_{ice}} = m_w C_{p_w} \Delta T \tag{4}$$

6.1.3 Wall Gain Load

This term refers to the heat loss through the walls of the system. In this case, it happens as a result of conduction heat transfer. The degree of thermal conductivity witnessed in a system is subjected to significant variance based on the particular materials utilized in its construction. This system employs steel for the fabrication of the refrigerator wall, a material characterized by a relatively low degree of thermal conductivity. This implies that the transmission of thermal energy across the wall poses a challenge. The heat loss Q_w through the walls can be expressed by Equation 5.

$$\dot{Q}_w = \frac{k}{x} A_s \Delta T \tag{5}$$

Where k is the thermal conductivity, A_s is the ice bath cylinder surface area, x is the insulation thickness and ΔT is the temperature change of water before and after the adsorption process.. The surface area is determined by Equation 6.

$$A_s = \frac{\pi D^2}{2} + \pi D H \tag{6}$$

D represents the ice batch cylinder diameter and H is the cylinder height . The heat loss can be used to calculate the wall gain load Q_w for the system, as shown in Equation 7. It is found by multiplying the heat loss with the amount of seconds during a day.

$$Q_w = 24 \cdot 3600 \cdot \dot{Q}_w \tag{7}$$

6.1.4 Air Exchange Load

The load of air exchange is influenced by the opening of doors and ventilation. The act of opening a cold storage room results in gaining heat from the outside environment. One can quantify this process through the use of equivalent air exchange estimates by taking into account the amount of heat gained per unit volume and the volume of the room. Equation 8 considers the amount of air change, the refrigerator volume and the temperature change. The present analysis operates with the assumption of a refrigerator consistently occupied of a capacity of 50% of its original storage.

$$Q_{air} = \frac{n_{air}}{2} m_{air} C_{p_a} \Delta T \tag{8}$$

Where n_{air} is the amount of air changes, m_{air} is the mass of air, C_{p_a} is the air specific heat capacity and ΔT is the temperature change between the ambient and refrigerator.

6.1.5 Miscellaneous Heat Load

Heat input from other sources such as fans, lights and additional work constitute the miscellaneous heat load. While such inputs are typically incorporated into calculations based on provided data, the current investigation will only be occupied by the intended products. In light of the system characteristics , it was assumed that the miscellaneous heat load is negligible and equal to zero.

6.1.6 Total Cooling Load

The total refrigeration cooling load for the system is comprised of the aggregate sum of all individual loads above. The product loads, wall gain load and air exchange load makes up the total refrigeration load in Equation 9.

$$Q_{tot} = Q_{pr} + Q_{pr_{ice}} + Q_w + Q_{air} \tag{9}$$

With the determination of the overall cooling load, and assuming certain conditions, it becomes feasible to estimate the required quantities of refrigerant and adsorbent within the system. This estimation serves as a guide for the design and adjustment of the system's components, aligning them with the quantities necessary to attain the desired cooling effect.

6.2 Amount of refrigerant

The amount of refrigerant m_{ref} required for the system is given in Equation 10.

$$m_{ref} = \frac{Q_{tot}}{L_{tme} \cdot N_c} \tag{10}$$

Where L_{tme} is the latent heat of evaporation of methanol for the desired evaporator temperature and N_c is the amount of cycles per day. To be able to achieve the desired amount of cooling which is applicable, it is necessary to run more than one cycle per day at the startup session. For each cycle, an additional wall gain load needs to be added into the above equation. The desired amount of refrigerant is most applicable for a three day cycle to achieve the set point temperature, however, this is for the system startup only. After day three, the system will only operate with one cycle per day. The amount of refrigerant needed is given in Equation 11.

$$m_{ref} = \frac{Q_{tot} + (Q_w \cdot (N_c - 1))}{L_{tme} \cdot N_c} \tag{11}$$

Where Q_{tot} is the total cooling load and Q_w is the additional wall gain load.

6.3 Amount of adsorbent

The amount of adsorbent m_{ads} has a connection with the refrigerant. Activated carbon has different adsorption uptakes when it comes to the type of product and supplier. Granular activated carbon bought from Klartvann, originally from Calcgoncarbon is used for this experiment. Since there is no information of the adsorption uptake of this type, other research articles based on the same process has been investigated. Equation 12 can be used to determine the desired carboun amount.

$$m_{ads} = \frac{m_{ref}}{\Delta m} \tag{12}$$

Where Δm is the mass specific loading of adsorbate per gram of dry adsorbent mass $[g\ g^{-1}]$, also known as the accessible adsorption uptake during adsorption.

6.4 Evaporator Coil

In the evaporator of an adsorption cooling system, the primary function of the evaporator coil is to extract heat from water during the adsorption cycle, to make ice. The design of the coil is a spiral configuration, which necessitates careful sizing to ensure efficient utilization of the cooling effect without causing excessive freezing of the water.

Utilizing a material with high thermal conductivity is crucial for optimizing heat transfer within the evaporator coil, thereby minimizing unwanted heat losses. Additionally, proper insulation is essential for preserving the integrity of the system and further mitigating heat loss. The length of the evaporator coil l_{tot} is determined from Equation 13 where the amount of volume V_{ref} is shown in Equation 14.

$$l_{tot} = \frac{V_{ref}}{\pi r^2} \tag{13}$$

$$V_{ref} = \frac{m_{ref}}{\rho_{ref}} \tag{14}$$

Where ρ_{ref} is the refrigerant density and r is the evaporator coil radius. To select the optimal sizing, it´s also important to determine the height of the evaporator coil. The coil configuration is divided into two parts, so that you have an upper coil and a lower one. This is for the methanol to distribute as effective as possible around the refrigeration chamber. When the length is known, the height h_{coil} can be found from Equation 15, where the circumference O_{coil} is found from Equation 16.

$$h_{coil} = \frac{l_{tot}}{O_{coil}} \cdot pitch \tag{15}$$

$$O_{coil} = \pi d_{rc} \tag{16}$$

Where the pitch is the distance from center to center of the upper and bottom coil and d_r is the refrigeration chamber diameter.

6.5 Collector Sizing

The collector sizing, also known as an adsorber bed is designed based on the amount of refrigerant and adsorbent in the system. The required length $l_{Collector}$ is given in Equation 17, where V_{tot} is the total volume of both methanol and activated carbon and r is the radius difference between outer steel pipe and inner copper pipe.

$$l_{Collector} = \frac{V_{tot}}{\pi r^2} \tag{17}$$

The total volume V_{tot} is the combined volume of refrigerant and activated carbon. The adsorbent volume V_{ac} is given in Equation 18, where m_{ac} and ρ_{ac} is the amount and density of carbon.

$$V_{ac} = \frac{m_{ac}}{\rho_{ac}} \tag{18}$$

6.6 Condenser Sizing

In an adsorption cooling system, the refrigerant dissipates heat and undergoes condensation within the condenser. The condenser is strategically positioned at a lower elevation relative to the collector to maintain the desired temperature gradient. This arrangement is essential in ensuring that the condenser operates at a temperature near ambient conditions while minimizing any influence from the heating element. Additionally, the condenser is designed with a slope orientation to facilitate the flow of the working fluid into it, to achieve as efficient heat exchange and condensation processes as possible.

A key parameter of interest is the amount of heat generated and subsequently removed. Within this configuration ,the amount of heat generation can be derived from Equation 19.

$$Q_c = m_{ref}Cp_{ref_g} \cdot (T_i - T_b) + m_{ref}L_{ref} + m_{ref}Cp_{ref_{liq}} \cdot (T_b - T_f) \tag{19}$$

The condenser heat load, denoted as Q_c is influenced by several factors, such as the latent heat of evaporation of the refrigerant at condenser temperature L_{ref}, the specific heat capacity Cp_{ref} of the refrigerant for both vapor and liquid states, and the change in refrigerant temperature. The temperature change consists of the boiling point of methanol T_b, the collector T_i and condenser T_f temperatures.

The mass of cooling water and the logarithmic mean temperature is obtained from Equation 20 and Equation 21 respectively.

$$m_w = \frac{Q_c}{Cp_w \Delta T_w} \tag{20}$$

$$\Delta T_m = \frac{\Delta T_1 - \Delta T_2}{ln\frac{\Delta T_1}{\Delta T_2}} \tag{21}$$

Where Cp_w is the specific heat capacity of water and ΔT_w is the allowable increase in water temperature when methanol enters the condenser. The log mean temperature difference ΔT_m is the temperature differences for both the refrigerant and water.

The overall heat transfer coefficient U is presented in Equation 22. This coefficient is a measure of the heat flow that occurs in the condenser.

$$\frac{1}{U} = \frac{1}{h_o} + \frac{x}{k} + \frac{1}{h_i} + R_o + R_i \tag{22}$$

Where h_o and h_i is the convective heat transfer coefficient of water and methanol, k is the thermal conductivity of steel, x is the wall thickness of the condenser, as well as R_o and R_i which is the fouling factor of water and methanol respectively.

The rate of heat removed $Q_{c_{removed}}$ from the condenser is shown in Equation 23. Here, Q_c is the heat generation and t_{des} is the assumed desorption time of the system.

$$Q_{c_{removed}} = \frac{Q_c}{t_{des}} \tag{23}$$

In order to achieve the length of the condenser, the area is needed. This value is obtained from Equation 24 where the previous values of the overall heat transfer coefficient and log mean temperature is used.

The final length of the condenser is made up of Equation 25, where d is the diameter of the copper pipe containing methanol.

$$A_c = \frac{Q_{c_{removed}}}{U \Delta T_m} \tag{24}$$

$$l_{Condenser} = \frac{A_c}{\pi d} \tag{25}$$

6.7 Dubinin-Radushkevitch (D-R) characterisation curves

To get a better understanding of the current system there is used simulations of the Dubinin-Radushkevitch (D-R) isotherm in order to get valuable insight into the characteristics of the activated carbon/ methanol pair. The equation is given in Equation 26 where W is the adsorption capacity of the adsorbent, W_0 is the maximum adsorption capacity, P_s is the saturation pressure, P is the pressure and D is the exponential constant. The background data used in the equation is based on experimental data.

$$W = W_0 exp[-D(Tln(\frac{P_s}{P}))^2] \tag{26}$$

7 Design

In determining the architecture of an adsorption system, a multitude of considerations warrant attention, including lessons learned from past experiences. The design considerations are not limited to internal functionalities but also extend to external factors. Importantly, the system with the highest functionality is not always synonymous with the most suitable solution. This perspective becomes salient when evaluating the environmental footprint of potential solutions and the intended demographic of users. This chapter explores various aspects that contribute to the decision-making process, ultimately leading to the final design of the adsorption system.

7.1 Development of adsorption cooling

Since the start of adsorption cooling systems in the late 1970s, there has been an unceasing pursuit of research within this domain. Initial explorations primarily focused on single-bed systems, incorporating refrigerants that were chiefly constituted of Hydrofluorocarbons (HFCs) and Chlorofluorocarbons (CFCs). This landscape underwent a significant transformation post the Montreal and Kyoto protocols, which mandated the cessation of ozone-depleting substances. Subsequent to these conventions, there was an increased incorporation of natural refrigerants such as methanol, carbon dioxide (CO_2), water, and ammonia, effectively replacing the prior reliance on high-performance synthetic refrigerants. This shift catalyzed a new trajectory of research, directed towards discovering environmentally friendly adsorption pair combinations.

The first generation of these systems was confronted with significant challenges, including suboptimal efficiency and cooling capacity, attributable largely to inadequate heat transfer within the system and inferior adsorbate uptake. However, a number of these limitations have been improved through the development of continuous cooling systems furnished with heat and mass recovery mechanisms, and the integration of water-cooled adsorption beds. Moreover, coordinated research endeavours focusing on adsorption pairs have culminated in significant improvements in the system's adsorption uptake. Experimental investigations with various carbon materials have led to an increased adsorption capacity of activated carbon materials over time. Similar advancements have been noted with zeolites.

In addition, there is a growing amount of research concerning novel composite adsorbents, with the potential to augment the proficiency of physical and chemical adsorbents. Design innovations, particularly in the architecture of the adsorption beds, have also contributed to the enhancement of heat transfer, with various tubular and rectangular setups undergoing testing. Finally, finding the optimal temperature and temporal ranges for various adsorption pairs is of pivotal importance in achieving desirable levels of efficiency and cooling capacities. This aspect continues to be a vital focus of ongoing research.

7.2 Literature study design obstacles

Upon comparing empirical studies to ascertain the most favourable design, several complexities become apparent. The prevalent parameters for comparison are naturally the Coefficient of Performance (COP) and the Specific Cooling Power (SCP) as they represent the efficiency and capacity of the system. A higher COP tends to correspond to a heightened SCP, as increased efficiency translates to more cooling per cycle. However, this correlation is not consistently observed in adsorption systems where the cycle durations vary. A maximum COP is frequently reliant on extended cycle times, as the COP amplifies over time to allow more gas to adsorb/desorb until a convergence point is reached. Conversely, the SCP increases with shorter cycle durations. Hence, the selection of optimal parameters represents a trade-off between efficiency and cooling power. This equilibrium becomes crucial in adsorption systems powered by fossil fuels or waste heat to ensure system profitability. However, in a solar-powered system, this trade-off is of lesser importance.

For single-bed systems powered by solar energy and without valves, a cycle conventionally spans one day, with desorption occurring during the day and adsorption at night. Consequently, the cooling power is relatively low compared to adsorption systems performing multiple cycles daily. Advanced systems powered by fuel or waste heat can execute a cycle within hours, minutes, or even seconds, a feature unattainable in rudimentary solar-powered systems. Regeneration temperatures can be higher when fuel is used, as it can readily attain temperatures of 200 °C. Elevated regeneration temperatures yield superior outcomes. Furthermore, fuel usage and waste heat offers better heat transfer and consistency compared to solar power. The desired regeneration temperatures are typically above 100 °C, achievable in warmer climates during mid-day when solar radiation is at its highest. As a result, heating the adsorption beds is confined to only a part of the day, creating an intermittent system incapable of continuous cooling. Alternatively, a type of heat storage must be employed to supply heat during the night. In such a scenario, the thermal fluid should ideally be oil or other fluids with high heat capacity and boiling points. The utilization of water is likely to be inefficient due to its low boiling point. For instance, in the case of the activated-carbon methanol adsorption pair, the ideal regeneration temperatures are between 90-120 °C. Maintaining sufficient temperatures with water as a thermal fluid is thus challenging. For low-temperature systems using silica gel/water, however, water as a thermal fluid can be more appropriate since regeneration temperatures typically lie between 60-95 °C.

Efficiency and cooling power-based comparisons may not yield an accurate representation when different bed configurations are present. Increasing the number of beds enhances performance as more cycles can concurrently operate. The most significant improvement is naturally from single- to double-bed configuration, where one bed can operate in opposition to the other. Thermal storage also notably bolsters the system. By harnessing excess heat from the desorption process, the subsequent cycle experiences a reduced time frame. The surplus heat warms the adsorption bed faster than solar radiation as it primarily uses convection instead of radiation. This can be particularly advantageous in a multi-bed configuration, where the heat gain from one bed is utilized for the other. Heat storage can also empower solar-powered systems to operate outside of peak radiation hours, creating a more continuous cycle and thereby increasing COP and SCP. The type of cooling applied to the adsorption bed exerts a considerable influence on the results. Predominantly, there are two types of cooling; air and thermal fluid. While air cooling is a simpler and cheaper method, it is less time-efficient for bed cooling. A thermal fluid, on the other hand, has superior thermal properties and thus offers rapid cooling. However, it necessitates higher initial investment and complex system arrangements. When employing a thermal fluid for cooling, typically water, additional infrastructure such as piping, valves, storage tanks, and heat exchangers are required.

Determining the most appropriate adsorption pair, given the preceding arguments, poses a significant challenge. When comparing adsorption pairs, finding results with similar setups is difficult. Even if the number of beds, thermal storage, etc. is comparable, the total system is still comprised of different materials, component configurations and so forth. For instance, a system with a granular activated carbon/methanol pair can have differing structural configurations, fin arrangements, pipe sizes, heat exchanger designs, and much more. Consequently, there are diverse outcomes for similar experiments. Comparing data therefore poses a challenge. Moreover, the performance of an adsorption system can vary substantially with the type of adsorbent/adsorbate. Therefore, every system is custom fitted for each type of adsorption pair. Assessing parameters such as adsorbent uptake (kg/kg) is therefore equally significant as COP and SCP when deciding on an adsorption pair.

The final design should be optimally tailored to suit the needs of rural regions in Africa. Identifying and selecting the best option is thus not exclusively reliant on system parameters, but also on cost and material accessibility. Additionally, the proposed solution must be simple to operate with a long lifespan and a low likelihood of failure. The preferred setup is a trade-off between cost, efficiency, and simplicity. Incorporating enhancements such as thermal storage, water cooling, and multi-bed construction must consequently be balanced against these constraints. Despite this research field undergoing considerable advancements over the past four decades, it has yet to be commercialized. As a result, the cost of constructing such a system remains high. This raises the question of whether solar adsorption systems are a viable option given the recent advancements and cost reductions in solar cell technology. This technology is continually becoming cheaper and

more efficient and would have no problem supplying an electrically driven refrigeration system. Therefore, the implementation of solar adsorption cooling must be evaluated in relation to solar cells.

7.3 System design discussion

When designing a system for use in rural villages in Africa, simplicity and cost are weighted higher than system output. The ideal system is therefore one that is cheap, accessible and has little to no maintenance. For a solar-powered system, the cooling output is less than for a fuel-powered or waste heat powered cycle. It is therefore even more essential to utilize the energy potential. However, a simple and cheap system is mostly in line with 1.generation systems where there is only one adsorber and no valves. Thus yielding low performance. New research within the field of adsorption has mainly been towards optimizing cooling machines for commercial use, by implementing several beds, cascading systems, heat and mass recovery and so forth. It is therefore difficult to picture that the outcome of creating a simple solar-powered ice-making cycle would be significantly better than it was 40 years ago. However new types of adsorbents such as Maxsorb III activated carbon is proven to be substantially better than their predecessors. Nonetheless, such simple systems will not be able to compete with new and advanced systems but nor is that the objective. Providing cooling to rural villages is likely to be supplied by humanitarian organizations as the price itself is too steep for locals. The purpose of the cooling is mainly critical products like vaccines, which do not require a lot of ice production. It would however be neat to also have enough ice to cool food products. For instance fish and other meat. As this will substantially increase the standard of living.

As previously mentioned, the main competitor for adsorption cooling is solar panels that generate electricity. Said system only needs a panel, battery, and wiring. It is therefore easy to install, and simple to maintain. On average Forbes estimates the cost of solar panels to be between 1$ to 1.5$ per watt for monocrystalline panel systems for home use or 0.9$ to 1$ for polycrystalline. Meaning a 1 KW system will have a total cost of around 1000$ [53]. Yet, fitting an entire house with solar panels is more extensive work than powering a simple fridge. A fridge can typically use between 50-500 W depending on the age, size and type. The average watt is somewhat lower as the compressor only runs part-time. One solar panel of 100-300 W is therefore likely enough to power a small fridge, where the price for the panel alone is e.g 180$ for 280 W [54]. The major advantage solar panels possess in comparison to adsorption cooling is regardless not the cost but the flexibility. The possibility to not only power cooling units but also light, appliances, and other electricity-consuming processes. The price of solar panels should therefore be viewed against the multipurpose it possesses and not only for cooling.

If advanced solar-powered adsorption cycles are the preferred choice in areas without electricity, there might be a need for an additional power supply to the system. When multiple valves are needed to operate the cycle, so are extra control systems. Some valves can be controlled by pressure and temperature, or other self-regulating mechanisms but in advanced systems, the valves need to communicate with each other. Hence a control unit must be connected to the valves. The amount of electricity needed to run the aforesaid is very little and technically possible with only a small battery. Yet, the batteries will need charging or changing at some point. Thus a small solar panel is a natural choice to power the unit and valves. If the system is comprised of several closing valves, the simplest form of control is timer adjusted cycle. In this case, the valves are opened and closed at specific time intervals, which are optimized for the highest efficiency and cooling power. One issue with this simple form of control is the variations in regeneration temperature. On days with lower radiation the desorption and adsorption process takes more time, hence the cycle will switch before the adsorbate is fully adsorbed. Using pressure, temperature, and mass flow sensors is also a possibility. The ideal form of control is a combination of multiple sensors, e.g temperature and mass flow which are then programmed to open and close the valves at different operating points. Still, more sensors and complexity mean added cost.

During the design phase, three primary alternatives emerge for the adsorption bed configuration: a single-bed system, a double-bed system with mass recovery, and a double-bed system with both heat and mass recovery. Each setup offers the possibility of employing water cooling and thermal

storage. The single-bed system represents the most cost-effective and simplest construction, yet it also offers the least effective performance. Conversely, the double-bed system with both heat and mass recovery is posited as the most advanced system, when excluding multi-bed and cascading systems from consideration. In a traditional solar-powered ice maker, the adsorption cycle mirrors the solar cycle, yielding a singular cooling period per day. However, the application of water cooling to the adsorber should, in theory, allow for the execution of multiple cycles per day, particularly enabling at least two desorption periods during daylight hours. Given that no heating, and thus no desorption, can occur during the evening and night hours, the system's potential is not fully exploited.

Should a double-bed system with mass recovery be selected, the system's efficiency could see substantial improvement. However, in the absence of water cooling, the question remains whether the system can run multiple cycles a day to maximize the potential of a two-bed construction. A similar issue arises with the double-bed system featuring both heat and mass recovery when the adsorption beds are exposed to sunlight. To overcome this problem, the installation of thermal storage is likely required. Consequently, a solar collector could supply heat during the day to a thermal storage system comprised of oil or another fluid. The oil could then be redirected to the adsorber during the desorption phase, enabling the adsorber to be positioned in the shade. This arrangement would also permit the ice machine to operate during the night, as heat from the storage tank can be employed in the absence of solar radiation. A proposed design for heat storage, applicable to all three setups, is depicted in Figure 7.1.
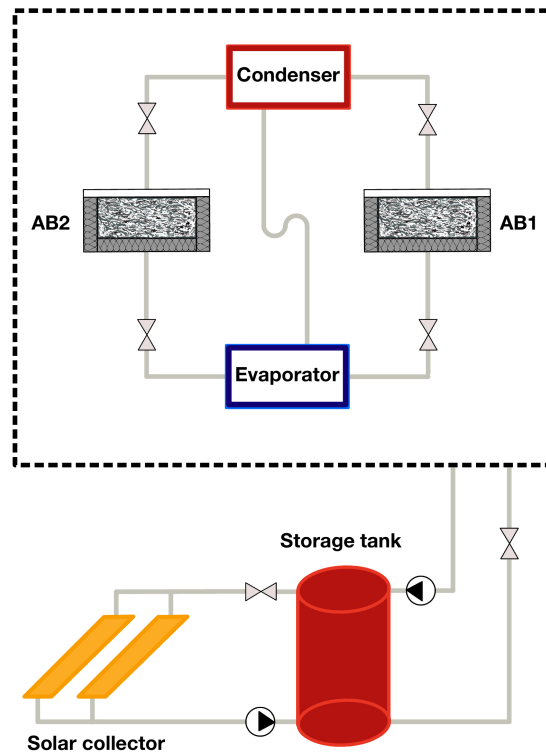
Figure 7.1: Heat storage

7.4 Final design

Based on the preceding information the ice maker should use activated carbon/methanol as adsorption pair due to its ability to operate below 0 °C. Its low adsorption heat and desorption temperature makes it an optimal choice for a solar-powered system operating in hot climates where regeneration temperatures are expected to reach temperatures of 100-110 °C. Methanol as an adsorbate has also proven itself to be superior to ethanol and ammonia at the given operating conditions. For COP and cooling power, the evaporation and regeneration temperature has proven

to be pivotal parameters. While a lower evaporation temperature is positive for freezing within the ice-maker, it reduces the efficiency and cooling power greatly. In the case of Maxsorb/methanol, adsorbent uptake decreased by 75% when evaporation temperature was reduced from 15 °C to -5 °C. Air-conditioning systems therefore have significantly better performance than ice-makers. An evaporation temperature is therefore currently set at -5 °C instead of -10 °C to make sure the water freezes while still maintaining performance. A highest possible regenerating temperature is beneficial as long as it does not exceed 120 °C for the methanol to avoid decomposing. The condensing temperature for the system will vary with the outdoor temperature. As a consequence, the temperature gradient can be considerable between night and day. During sun hours the condensing temperature is likely around 30 °C. It is important to keep the condenser in a shaded area to get the lowest possible condensing temperatures. The condenser could ideally be water-cooled on the same circuit as the adsorber for higher efficiencies but as of now, water cooling is avoided

For the adsorption bed design, heat transfer is very important. A tubular design is therefore likely to provide the best result. However, the cost and simplicity also increase. A rectangular design can as a result be a viable option instead by mounting metal fins in the casing to increase heat transfer and thus lowering the cost of the construct. A cost analysis should be performed to find the total savings before deciding. For the materials of the adsorber, aluminium alloys were found to have a stronger catalytic effect on the decomposition of methanol than copper and should therefore be avoided. Copper is therefore a better alternative. still, the methanol also showed decomposition within the copper over time, meaning that none of them are ideal alternatives. Iron alloys such as steel are therefore more applicable when considering decomposition.

While multi-bed systems with water cooling and recovery systems may seem attractive, the complexity and cost associated with constructing and maintaining such a system are problematic. Such a system would likely only be justifiable in commercial cooling systems using waste heat capable of operating 24-hour cycles. Applying water cooling and heat storage to a system that should fundamentally be simple and cost-effective does not align with the intended usage. Without these system components, the utilisation of a double bed construction loses its benefit as the key advantage of having multiple beds is the use of heat and mass recovery in addition to establishing a continuous rather than intermittent system. With these considerations in mind, the proposed system comprises a single bed without heat storage or recovery systems. This proposed system is depicted in Figure 7.2. It consists of a collector, condenser, and evaporator, along with other regulatory mechanisms primarily used for testing purposes. Considering the experiment is to be performed in a lab, the collector employs a tubular design to facilitate the use of a heating cable to simulate the thermal heat gain. Further detailed descriptions of the system components are given in Section 8.2.
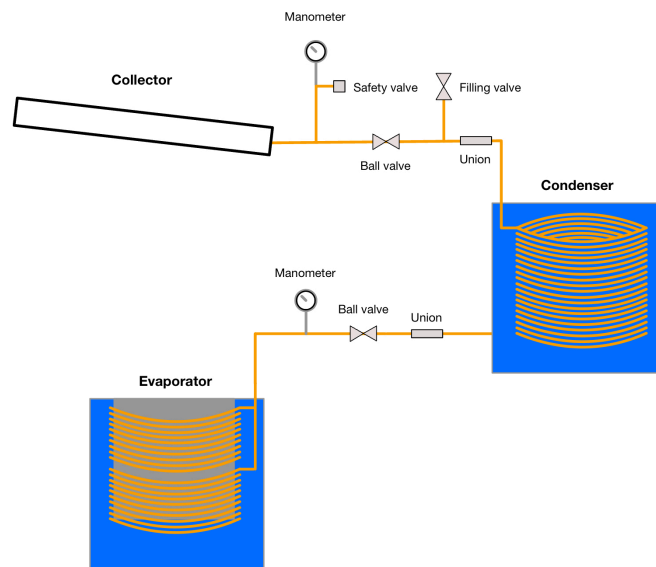
Figure 7.2: Experimental setup

8 Methodology and experimental Setup

This section details the methodologies adopted for the execution of the research study. It explicates the significant computations leading to the final design of the experimental procedure. Further, it encompasses an overview of the system components employed, the operation of the system, potential sources of error, as well as the inherent limitations of the system. The principal intent of this chapter is to furnish a comprehensive depiction of the construction phase, followed by the operation of the system. The manner in which this information is presented aims to facilitate the replication of the experiment.

8.1 Calculations

The ensuing computations are tailored to ascertain the realistic quantities of methanol and carbon required to attain an operational system under specified conditions. All of these were formerly elucidated in Section 6. An efficacious cooling process necessitates the precision in the components' dimensions, with particular emphasis on the evaporator, housing the refrigerator. The choice of materials, their inherent properties, the cooling chamber's dimensions, and the refrigerator's size form the groundwork for the calculations. Furthermore, the quantities of methanol and carbon are computed to ensure the collector's appropriate size. The condenser size is ascertained considering the required water volume for methanol cooling and the quantum of heat that must be evacuated from it to achieve the desired methanol temperature upon exiting the condenser. The sizing of the evaporator coils is determined based on the methanol volume required for the adsorption process to achieve the target temperature.

8.1.1 Total Cooling Load

For calculating the amount of adsorbent and adsorbate, and further sizing of the system components, the first step is to determine the product load of the system. By using the equation from Equation 2 with the assumptions given in Table 8.1, it is possible to determine the product load of the interior wares. In these assumptions, water is selected as the product.

Table 8.1: Product load assumptions for cooling chamber

Assumptions	Value	Unit
T_o (outside temperature)	30	$°C$
T_i (Inside temperature)	2	$°C$
C_{p_w} (Spesific heat capacity water)	4.187	kJ/kgK
ρ_w (density water)	1000	kg/m^3
V (Volume chamber)	20	L

$$Q_{pr} = m_w C_W (T_o - T_i) = 10 \cdot 4.187 \cdot (30 - 2) = \underline{1172.36} \quad [kJ]$$

To obtain the desired temperature level, the product load, known as the amount of heat energy removed from the refrigerated product is equal to 1172.36 kJ. An additional product load for the ice bath is calculated using Equation 3 and Equation 4 from chapter 5.1, with the assumptions presented in Table 8.2.

Table 8.2: Product load ice bath assumptions for cooling chamber

Assumptions	Value	Unit
$m_{w_{ice}}$ (Mass of Ice Bath)	44.46	kg
D_{ice} (Ice Bath Cylinder Radius)	40.6	cm^2
d_{ref} (Refrigeration Chamber radius)	25.4	cm^2
H_{ice} (Ice Bath Cylinder Height)	50	cm
h_{ref} (Refrigeration Chamber Height)	40	cm

$$V_{icebath} = \frac{\pi D_{ice}^2 H_{ice}}{4} - \frac{\pi d_{ref}^2 h_{ref}}{4} = \frac{\pi \cdot 40.6^2 \cdot 50}{4} - \frac{\pi \cdot 25.4^2 \cdot 40}{4} = \underline{44462.65} \quad [cm^3]$$

$$Q_{pr_{ice}} = m_{w_{ice}} C_W (T_o - T_i) = 44.46 \cdot 4.187 \cdot (30 - 2) = \underline{5584.95} \quad [kJ]$$

This approach resulted in an ice bath product load of initially 5584.95 kJ.

The heat loss through the walls of the system and the overall wall gain load is determined from Equation 5 and Equation 7 with the following properties presented in Table 8.3.

Table 8.3: Wall Gain Load assumptions

Assumptions	Value	Unit
k (Thermal Conductivity Armaflex)	0.033	W/mK
x (Insulation Thickness)	0.1	m
D_{ice} (Ice Bath Cylinder Radius)	40.6	cm^2
H_{ice} (Ice Bath Cylinder Height)	50	cm
T_{amb} (Temperature Ambient)	30	$°C$
T_{in} (Temperature Inside Refrigerator)	0	$°C$

$$\dot{Q}_w = \frac{k}{x} A_s \Delta T = \frac{0.033}{0.1} \cdot 0.896667 \cdot (30 - 0) = \underline{8.8770033} \quad [J/s]$$

$$A_s = \frac{\pi D^2}{2} + \pi D H = \frac{\pi \cdot 40.6^2}{2} + \pi \cdot 40.6 \cdot 50 = \underline{0.896667} \quad [m^2]$$

$$Q_w = 24 \cdot 3600 \cdot \dot{Q}_w = 24 \cdot 3600 \cdot 8.8770033 = \underline{766.97} \quad [kJ]$$

To be able to achieve the result in kJ, one can convert the obtained value of $\dot{Q}_w$ in J/s by considering and multiplying the total amount of seconds during a day. This implementation gives a wall gain load of 766.97 kJ.

The systems air exchange occurs upon opening the refrigerator, influencing the thermal balance by gaining heat from outside. It is assumed that the refrigerator lid is lifted on and off 20 times during a 24 hour cycle. During this cycle, it is assumed that the air at room temperature will replace all of the air inside the refrigerator. Another assumptions is that the refrigerator will contain a quantity of food that makes up 50% of the total volume. Even though the air exchange load does not constitute to much in terms of the total cooling load, it is yet included to achieve a more accurate assessment. The air exchange load is determined from Equation 8 based on the assumptions from Table 8.4.

Table 8.4: Air Exchange Load assumptions

Assumptions	Value	Unit
n_{air} (Number of lid openings)	20	–
ρ_{air} (Mass Density)	1.164	kg/m^3
V_{ice} (Refrigerator Volume)	0.02	m^3
$C_{p_{air}}$ (Specific Heat Capacity (30°C))	1.006	$kJ/kg \cdot K$
T_{amb} (Temperature Ambient)	30	°C
T_{in} (Temperature Refrigerator)	2	°C

$$Q_{air} = \frac{n_{air}}{2} m_{air} C_{p_a} \Delta T = \frac{20}{2} \cdot 1.164 \cdot 0.02 \cdot 1.006 \cdot (30 - 2) = \underline{6.56} \quad [kJ]$$

The calculated air exchange load for the system has been determined to be 6.56 kJ, offering a valuable assessment based on the assumptions mentioned.

The total refrigeration cooling load includes all loads in Table 8.5 and is used for Equation 9.

Table 8.5: Total Cooling Load for the refrigerator

S/N	Cooling Load	Value	
1	Product Load	1172.36	$[kJ]$
2	Product Load Ice Bath	5584.95	$[kJ]$
3	Wall Gain Load	766.97	$[kJ]$
4	Air Exchange Load	6.56	$[kJ]$
5	Miscellaneous Heat Load	0	$[kJ]$
	Total Cooling Load	7530.84	$[kJ]$

$$Q_{Tot} = (Q_1 + Q_2 + Q_3 + Q_4 + Q_5) = 1172.36 + 5584.95 + 766.97 + 6.56 + 0 = \underline{7530.84} \quad [kJ]$$

The total cooling load for the refrigeration system is calculated to be 7530.84 kJ, which is a critical parameter for ascertaining the amount of refrigerant and adsorbent in the system.

8.1.2 Refrigerant and Adsorbent amount

The system is designed to operate with an adsorbent pair of methanol and activated carbon. In section 5.2, the amount of refrigerant and adsorbent required for the system is presented. The desired amount of refrigerant is applicable for a number of three cycles from the startup session. With this assumption the temperature within the evaporator is expected to reach its designated temperature zone within three consecutive cycles. The refrigerant amount is found by using Equation 11. The amount of adsorbent is obtained from Equation 12. The properties used is shown in Table 8.6.

Table 8.6: Amount of refrigerant and adsorbent properties

Assumptions	Value	Unit
Q_{tot} (Total Cooling Load)	7530.84	kJ
Q_w (Wall Gain Load)	766.97	kJ
N_c (Number of cycles)	3	$-$
L_{tme} (Latent Heat of Evaporation)	1180.25	kJ/kg
Δm (Accessible volume (adsorption))	0.25	gg^{-1}

$$m_{ref} = \frac{Q_{tot} + (Q_w \cdot (N_c - 1))}{L_{tme} \cdot N_c} = \frac{7530.84 + (766.97 \cdot 2)}{(1180.25 \cdot 3)} = \underline{2.5601} \quad [kg] \approx \underline{3.23} \quad [L]$$

$$m_{ads} = \frac{m_{ref}}{\Delta m} = \frac{2.5601}{0.25} = \underline{10.2404} \quad [kg]$$

Since the system is operating with liquid methanol, converting kg to liter is practical. A total of 3.23 L methanol and 10.24 kg of activated carbon is required for the system to be functional.

8.1.3   Evaporator Coil

The length of the evaporator coil is determined such that the extraction of heat from water is enough to produce ice. Table 8.7 shows the following properties needed for the evaporator design. The total length is found by utilizing Equation 13 and the refrigerant volume by Equation 14. A volume of 3.23 L results in a total evaporator coil length of 18.36 m.

Table 8.7: Evaporator Coil properties

Assumptions	Value	Unit
ρ_{ref} (Mass Density Methanol)	0.791	g/m^2
r (Radius coil)	0.00749	m
d_{cp} (Diameter Copper Pipe)	0.25749	m
$pitch$ (pitch Length)	0.01898	m

$$V_{ref} = \frac{m_{ref}}{\rho_{ref}} = \frac{2.5601}{0.791} = \underline{3.23} \quad [L]$$

$$l_{tot} = \frac{V_{ref}}{\pi r^2} = \frac{0.003236}{\pi \cdot 0.00749^2} = \underline{18.36} \quad [m]$$

Its essential to determine the proper height as well, since the evaporator coils design is of spiral configuration. Equation 15 is used to determine the height of the coil. With a circumference of 0.8089 m which is found from Equation 16, the height of the evaporator coil is determined to be 0.4309 m.

$$O_{coil} = \pi d_{cp} = \pi \cdot 0.25749 = \underline{0.8089} = \quad [m]$$

$$h_{coil} = \frac{l_{tot}}{O_{coil}} \cdot pitch = \frac{18.36}{0.8089} \cdot 0.01898 = \underline{0.4309} \quad [m]$$

As delineated in Section 6.4, achieving optimal and efficient methanol distribution within the coil is a desirable condition. In pursuit of this objective a bifurcated structure, a T-connection is implemented at the entry point to the evaporator, thereby facilitating the connection of two discrete coils.

8.1.4 Collector

The condenser length is found based on the previous calculated values of the refrigerant and adsorbent amount. It is sufficient to design the collector, where the reaction between the adsorption pair takes place, with enough storage for the amount of methanol and activated carbon to react. The total volume is the combined volume of methanol and activated carbon, where the latter volume is calculated using Equation 18. With the properties from Table 8.8, a total volume of 23.4077 L will give a collector length of 1.33 m based on Equation 17.

Table 8.8: Collector properties

Assumptions	Value	Unit
V_{tot} (Total Volume)	23.4077	L
r (Radius coil)	0.00749	m
d_{cp} (Diameter Copper Pipe)	0.25749	m
$pitch$ (pitch Length)	0.01898	m

$$l_{Collector} = \frac{V_{tot}}{\pi r^2} = \frac{23.4077}{\pi \cdot (0.74 - 0.14)^2} = \underline{1.33} \quad [m]$$

$$V_{ac} = \frac{m_{ac}}{\rho_{ac}} = \frac{10.2404}{0.54} = \underline{18.96} \quad [L]$$

This sufficient length will ensure adequate desorption of methanol within the system. Moreover, the dimensions of the collector have been calculated to accommodate the maximum possible quantity of activated carbon. This effective utilisation of space eradicates the potential existence of air gaps between the refrigerant and the adsorbent.

8.1.5 Condenser

Equation 23 is used to define the condenser heat load , which is a measure of the generated heat. This amounts a quantity of 3627.14 kJ. The equation is calculated with the properties of Table 8.9.

Table 8.9: Condenser properties for heat generation

Assumptions	Value	Unit
m_{ref} (Mass methanol)	2.5601	kg
Cp_{ref_g} (Specific Heat Capacity) [vapor]	3.62	kJ/kgK
$Cp_{ref_{liq}}$ (Specific Heat Capacity) [liquid]	2.53	kJ/kgK
T_i (Inlet Temperature)	110	$°C$
T_b (Boiling Temperature)	64.7	$°C$
T_f (Condenser Temperature)	30	$°C$
L_{ref} (Latent Heat of Evaporation)	1165	kJ/kg

$$
\begin{aligned}
Q_c &= m_{ref}Cp_{ref_g} \cdot (T_i - T_b) + m_{ref}L_{ref} + m_{ref}Cp_{ref_{liq}} \cdot (T_b - T_f) \\
&= 2.5601(\cdot 3.62 \cdot (110 - 64.7) + 1165 + 2.53 \cdot (64.7 - 30)) \\
&= \underline{3627.14} \quad [kJ]
\end{aligned}
$$

Utilizing Equation 20 and incorporating the properties derived from the product load assumptions presented in Table 8.1, the required volume of water in the condenser has been measured to be 86.7 L. The log mean temperature difference (LMTD) is obtained using Equation 21, which is applicable when the temperature differences for both the refrigerant and water are known. This results in an LMTD equal to 19.53 K.

$$
m_w = \frac{Q_c}{Cp_w \Delta T_w} = \frac{3627.14}{4.182 \cdot 10} = \underline{86.7} \quad [L]
$$

$$
\Delta T_m = \frac{\Delta T_1 - \Delta T_2}{ln\frac{\Delta T_1}{\Delta T_2}} = \underline{19.53} \quad [K]
$$

Moreover, the overall heat transfer coefficient has been determined through the application of Equation 22. In this measurement, various properties have been considered, such as the heat transfer coefficients for both methanol and the water bath, the wall thickness and thermal conductivity of the pipe, and the fouling factors of water and methanol in terms of the condenser material that is used. Along with the properties from Table 8.10, the overall heat transfer coefficient is determined to be 29.8 W/m^2K.

Table 8.10: Overall Heat transfer coefficient properties

Assumptions	Value	Unit
x (Wall thickness pipe)	$0.89 \cdot 10^{-3}$	m
h_o (Convective heat transfer coefficient water bath)	43.25	$W/m^2 K$
h_i (Convective heat transfer coefficient methanol)	100	$W/m^2 K$
k (Thermal conductivity pipe)	390	W/mK
R_o (Fouling factor water and steel pipe)	0.0001	$m^2 {}^\circ C/W$
R_i (Fouling factor methanol and steel pipe)	0.0003	$m^2 {}^\circ C/W$

$$\frac{1}{U} = \frac{1}{h_o} + \frac{x}{k} + \frac{1}{h_i} + R_o + R_i = \frac{1}{43.25} + \frac{0.89 \cdot 10^{-3}}{390} + \frac{1}{100} + 0.0001 + 0.0003$$
$$U = \underline{29.8} \quad [W/m^2 K]$$

The removal of heat generated from the condenser can be determined using Equation 23. However, predicting the desorption time in a newly configured system has proven to be a challenging task, primarily due to uncertainties surrounding how activated carbon properties will interact with the present methanol. As a result, an assumption of a 2-hour desorption time has been adopted based on available literature. To accurately predicting the desorption time, it is necessary to investigate the adsorption uptake for the current adsorption pair. Such an experiment has been done and examined in more detail in Chapter 8.6.

$$Q_{c_{removed}} = \frac{Q_c}{t_{des}} = \frac{3627.14}{2 \cdot 3600} = \underline{503.77} \quad [W]$$

To complete the design of the condenser, it is necessary to determine the appropriate length of the condenser coil. This is achieved by using Equation 24 to calculate the area of the condenser coil, based on the previous obtained values for the removed heat generation, overall heat transfer coefficient and log mean temperature difference. Once the area has been determined, Equation 25 is used to calculate the length of the condenser coil, based on the area of 0.86559 m^2 and the coil diameter. The resulting length of the condenser coil is found to be 18.39 [m].

$$A_c = \frac{Q_{c_{removed}}}{U \Delta T_m} = \frac{503.77}{29.8 \cdot \Delta 19.53} = \underline{0.86559} \quad [m^2]$$

$$l_{Condenser} = \frac{A_c}{\pi d} = \frac{0.86559}{\pi \cdot 14.98 \cdot 10^{-3}} = \underline{18.39} \quad [m]$$

8.2 System components

The experimental setup consists of three main components. Namely, the collector holding the carbon, the water-cooled condenser, and the ice bath evaporator. In addition, there are several other smaller components such as valves, manometers, connections, and sensors. An overview of the system is given in Figure 8.1.

Figure 8.1: Experimental setup

8.2.1 Collector

In order to adsorb methanol from the system, the collector contains a substantial quantity of activated carbon. The collector is composed of two pipes, as depicted in Figure 8.3. The inner pipe, made of copper pictured in Figure 8.2, acts as a distributor, evenly dispensing the methanol throughout the surrounding carbon. The outer pipe, on the other hand, is made of stainless steel and serves as a housing for the activated carbon. The serrations on the inner pipe, combined with a mesh netting wrapped around it, ensure that the methanol can flow freely in and out of the carbon while preventing the carbon from falling through.

Figure 8.2: Inner pipe of collector
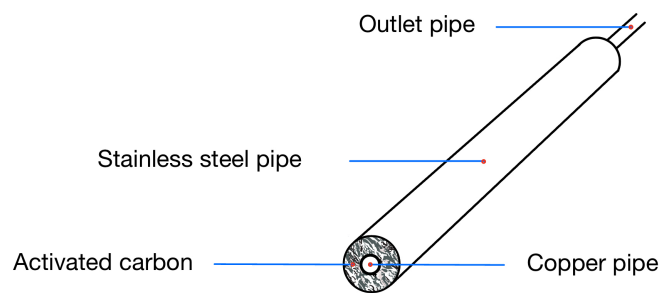
Figure 8.3: Collector

The current method being employed for applying heat to the system involves the utilization of a heating cable wrapped around the stainless steel pipe to increase the temperature of methanol during a process of regeneration or desorption. The primary objective of this approach is to simulate the use of solar power in a simple manner, as the project primarily focuses on the cold side. Furthermore, implementing a heating cable wrapped around the exterior of the pipe facilitates uniform heat distribution, which is advantageous in this application.

8.2.2 Condenser

To cool down and condense the warm methanol flowing from the collector, it is critical to have a sufficient surface area to transfer heat to the ambient. In addition, the choice of cooling medium is a key factor to consider. A water-cooled condenser is therefore implemented as it has a higher heat transfer rate than air. Further more, copper pipes are selected due to its high thermal conductivity. The layout of the condenser can be pictured in Figure 8.4 where a spiral coil is submerged in an open water container.

Figure 8.4: Condenser

8.2.3 Evaporator

The primary objective of the adsorption project is to create a solution for maintaining low temperatures within a cold chamber for extended periods without cooling production. The isolation of the storage area is a critical component of this solution. However, given the prolonged exposure of the chamber to warm climates, isolation alone is insufficient. Consequently, an ice bath is employed to leverage the high thermal capacity of water. The design of the evaporator bears similarity to that of the condenser, with the exception that the spiral coil wraps around the cold chamber. Therefore, the evaporator comprises an inner chamber filled with the product load to be cooled and an outer chamber containing water. This concept is illustrated in Figure 8.5 and Figure 8.6.

Figure 8.5: Evaporator coil wrapped around the refrigerated chamber. The coil on top is the inlet from the condenser.

Figure 8.6: Casing to the evaporator coil which is to be filled with water. Styrofoam plates are placed at the bottom which can be removed to make the ice bath bigger.

During desorption, warm methanol gas is directed from the collector to the condenser unit where it is cooled to ambient temperature. As the methanol fluid exits the condenser it drops into the evaporator coil where it slowly fills the tube. When the adsorption process begins, the condensed methanol will start to evaporate back to the collector, producing refrigeration as it draws heat from the surrounding water. The aim is that this cold production will create ice formation on the cobber pipes, which in turn allows for longer cooling due to the latent heat of phase change for water. To ensure a more homogeneous layer of ice within the water, the evaporator coil is divided into two sections. One at the top half and one at the bottom half of the cold chamber.

Through the induction of temperatures below the freezing point, water can serve as an effective phase change material, facilitating a method of enthalpy "storage" within the resulting ice crystals. This phenomenon depends on the transition of water from its liquid state to a solid state, a process that liberates heat energy, commonly referred to as the latent heat of fusion. This energy is quantitatively equivalent to 334 $kJkg^1$. Intriguingly, the aforementioned energy amount must be reintroduced to facilitate the melting of the ice. The interplay of these thermodynamic principles can be observed in Figure 8.7. The ability of ice to maintain reduced temperatures over extended periods makes it an excellent agent for long-term temperature regulation.
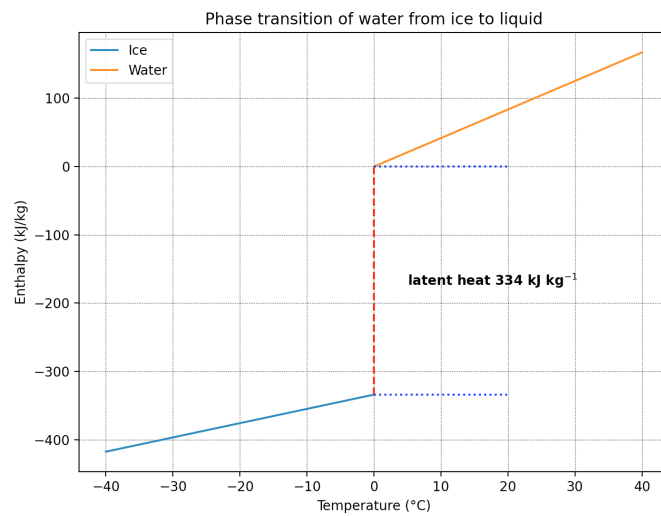
Figure 8.7: Latent heat

8.2.4   Loggers

To control the system environment and record the cycle changes, a total of 16 Type K thermocouple sensors have been placed around the different components. These are then connected to two separate Pico logging devices. As depicted in Figure 8.10, the collector has a total of three sensors. One at the outlet to measure the outgoing methanol, one at the outer steel pipe to control the temperature, and one under the heating cable to monitor the applied effect. For the condenser, a sensor is placed on the inlet and outlet pipe to find the heat removal through the condenser. In addition, there is one sensor in the water to monitor how much heat is extracted from the hot methanol. At the evaporator, there is a total of nine sensors located at several layers. Starting from the chamber there are three sensors; the bottom centre, wall mid, and wall top as depicted in Figure 8.8. These measures the refrigerated temperature to see if there is thermal stratification within the container. A further four sensors are placed on the evaporator coil, two at the top coil and two on the bottom coil as shown in Figure 8.9. The goal is to be able to see where in the coil the methanol is located during the adsorption process as the evaporation will move further down the coil for each part methanol being evaporated. Lastly, there are two logging points in the ice water located at the top and bottom of the container. Since ice floats there is reason to believe there will be a temperature difference with height.
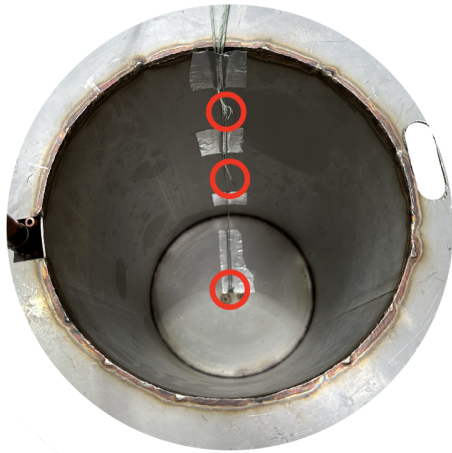
Figure 8.8: Sensor placement on the refrigerated chamber. Red circles indicate the sensors.
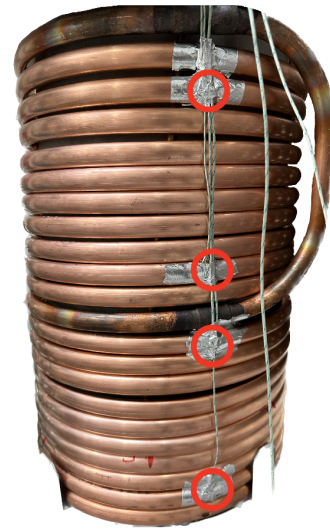
Figure 8.9: Sensor placements on the evaporator coil. Red circles indicate the sensors. A clear division of the upper and lower coil can also be pictured.
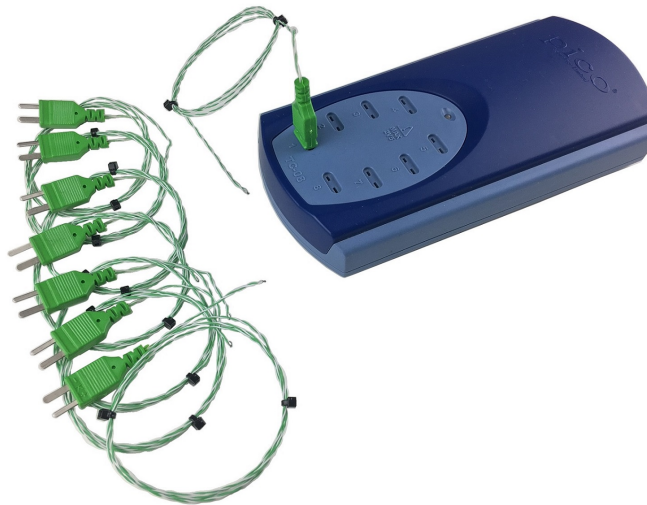
Figure 8.10: Pico logger

8.2.5   Control mechanisms

While temperature sensors are crucial to understand the operation of the system, there is also a need to monitor the pressure. Not only can pressure measurements detect leakages but also prevent too high pressures or faulty operation. Two manometers are therefore placed as depicted on the schematics of Figure 7.2. However, these manometers are analog such that readings must be performed manually. The reason for having two manometers is the possibility to close off parts of the system while still maintaining pressure readings. The manometers in use are shown in Figure 8.11.

In addition to manometers, there are also placed two corresponding closing valves in the system pictured in Figure 8.12 to divide the system into a heating side and a cooling side. In this manner, the evaporator can be closed off during heating to ensure proper cooling of the methanol before it enters the evaporator. There is also the possibility to disconnect the system part for part in case of modifications.

Figure 8.11: Manometer

Figure 8.12: Closing valve

8.3 Pressure Testing

To ensure the operability and safety of the system, a thorough pressure test was conducted on the system components. During the execution of these pressure tests, the system was observed to encounter a pressure decrement. However, after further testing, optimal operation was maintained from the ball valve down to the condenser and evaporator, localizing the source at the upper part of the system. Leak testing was conducted, and the results conclusively indicated small leakages in the collector connection. Nevertheless, a notable pressure decrease was still witnessed. Consequently, it was posited that the issue arose from a different source. After a more intensive testing period of longer duration, the supposed leakage was confirmed to be the carbon itself, which was experiencing adsorption of the nitrogen gas used during testing. By filling the system with nitrogen gas, the adsorption process could be witnessed. This process initially developed as a normal leakage with a constant decrease in pressure, before it declined and eventually stabilized at a constant pressure. Achieving the steady pressure took almost half a day, which made it hard to recognize. On the other hand, it provided a good indication of the system's adsorption time.

8.4 Operation

During the execution of the experimental setup, the operational procedure is largely dictated by real-time developments. Given the absence of prior results as benchmarks, it is imperative to observe the system dynamics firsthand before establishing any detailed procedures. The initial experimental plan designated a desorption time of six hours, supplemented by an adsorption period of 18 hours. However, to attain the desired outcomes, the desorption continued as long as mass transport was observed within the system. Under different temperatures, this typically indicated

varying desorption times. A similar approach was employed during adsorption. While this could potentially suggest the system operating within unrealistic timeframes, it was crucial to ascertain a baseline pertaining to the total time consumed for desorption and adsorption processes within the system.

Initially, the system was set at 110°C to identify the maximum uptake of methanol. Following this, the temperature was sequentially reduced in ten-degree increments down to 80°C to analyze the adsorption uptake under both maximal and minimal conditions. Throughout all experimental trials, the duration of operation was determined by mass transport. This implied that the regeneration process could be halted after five hours or continue for ten hours if methanol flow from the collector to the evaporator persisted. A similar guideline was followed for adsorption. Subsequently, the same operational procedure was replicated with valve regulation to assess whether more favourable results could be achieved. By intermittently opening and closing the valves, the system could be compartmentalized, thereby creating more favourable conditions and driving forces. Finally, the system was to emulate the solar trajectory of an average day in Tanzania, signifying a gradual increase in the heating effect until it reaches peak effect, coinciding with midday sun intensity, followed by a gradual decrease analogous to sunset. Despite a structured operational plan, the actual testing deviated due to unanticipated outcomes, rendering the execution of all parameters unnecessary before implementing system adjustments. As a result, the system primarily operated at maximum temperatures to circumvent the observed anomalies.

8.5   Adjusted setup

The outcomes from the initial experimental trials suggested that methanol underwent decomposition into dimethyl ether and other byproducts due to excessively elevated temperatures. Insufficient control over the core temperature may have resulted in the methanol surpassing 140°C, which represents the theoretical threshold at which methanol becomes unstable. The hypothesis of methanol degradation was founded on several observations. Firstly, a reduction in desorption was noted with each successive system operation, followed by a decrease in adsorption. Secondly, the temperature and pressure within the collector exhibited an escalation with each desorption cycle. The rising pressure, in particular, signals the existence of other compounds, as methanol decomposition initiates the production of additional gases occupying the voids. Specifically, dimethyl ether possesses higher saturation pressures, thereby contributing to an increased pressure within the collector.

The preliminary trials of the system unveiled multiple shortcomings in its design, necessitating several modifications to rectify the issues. The initial corrective measure involved the integration of a thermocouple into the carbon to facilitate more precise data acquisition. This was achieved by boring a hole into the flange of the collector. Subsequently, it was deemed essential to improve the methanol distribution and heat transfer within the activated carbon. To address this design challenge, the collector's mainframe remained unaltered to prevent a prolonged remodelling process. However, internal modifications were implemented. Capitalizing on the high thermal conductivity of copper, the incorporation of additional piping within the carbon facilitated enhanced heat distribution. A primary concern for the system was related to the collector core's ability to attain the desired heat, given its substantial diameter and compact packing. By affixing four supplementary copper pipes to the preexisting one, as illustrated in Figure 8.13, the theoretical heat and mass transfer within the system are expected to increase, consequently reducing desorption times.

Furthermore, the original dimensions of the evaporator were excessive, leading to a larger ice bath than required. Consequently, the water was removed to enhance the quality of the measurements within the evaporator. Additionally, the ratio between methanol and carbon has been found to be inordinate. Reference to the initial calculations for methanol and carbon quantity in Equation 11 was predicated on the assumption of executing three cycles per day, a premise that has proved challenging to realize in practical terms. Therefore, an increase in the carbon quantity is needed, although the current design of the collector does not permit additional space. Hence, a decision was made to extract the residual methanol in the evaporator and utilize only what has been desorbed into the carbon. This modification resulted in the removal of approximately 1.5 liters of methanol from the system. In Figure 8.14 and Figure 8.15, the new end and inside modifications of the collector is presented.

Figure 8.13: Methanol dispenser inside the collector. Extended capacity with four extra pipes to increase heat transfer and methanol dispersion.

Figure 8.14: End of collector before the flange is mounted.

Figure 8.15: Inside the collector with new modifications.

8.6   Experimental setup for simulation data

In conjunction with the primary refrigeration system, a supplementary adsorption apparatus has been devised to evaluate the adsorption capacity of the activated carbon. This system is relatively simplistic and comprises a limited number of components. The experiment was necessitated by the lack of data from the supplier and existing literature. The procured activated carbon is intended for water filtration applications, and as such, does not provide relevant information on methanol adsorption. Furthermore, no research literature on this specific carbon variety has been identified. Although samples with comparable surface areas are available, adsorption characteristics exhibit considerable variation. Consequently, accurate assumptions regarding adsorption capabilities can only be derived from empirical findings.

The arrangement incorporates two glass containers, one containing carbon and the other filled with methanol. A pipe connection is situated between the containers, facilitating vapour and condensation transfer during the adsorption and desorption processes. Additionally, a sensor is embedded in the carbon, and two sensors are placed in the methanol. To establish a vacuum within the system, a vacuum pump is connected to the activated carbon container. This configuration is depicted in Figure 8.16. At later stages this setup was altered to also have a closing valve and manometer between, to yield more accurate results. The final setup with manometer and closing valve installed is also the only configuration used in the presented results. A total of one 800 gram

of activated carbon is placed in the jar, occupying a volume of approximately 1600 ml, while 400 g of methanol, yielding 506 g, is used given that the adsorption is anticipated to be substantially below 0.5 kg/kg. Regarding the heating of activated carbon during regeneration, a challenge arose in terms of uniformly distributing heat to the container. The adopted solution entailed the use of a cooking pot filled with water, which was heated via a stove. To prevent direct contact between the pot and the container, several building blocks were utilized to elevate the bottle.

Figure 8.16: Experimental setup for simulation data

By acquiring adsorption properties through empirical observations, more precise computations can be generated, resulting in a superior optimization of the adsorption system. By recording pressures and adsorption quantities at varying regeneration temperatures, characterization curves can be formulated for the carbon utilizing the Dubinin-Astakhov equation. This enables a more comprehensive understanding of performance under diverse operating conditions and supplies more accurate simulation data. In conjunction with the primary system, these insights can be employed to develop more robust simulation codes, which serve as a foundation for predicting the consequences of alterations to the main system, as modifications will be necessary.

The simulation process was conducted using Python, with the initial phase involving the extraction of the experimental constants from the Dubinin-Radushkevich (D-R) equation. The specific constants in question are the exponential constant (D) and the maximum adsorption capacity $(W0)$. The procurement of these constants was facilitated by generating a linear relationship between $ln(W)$ and $[Tln(Ps/P)]^2$, thereby linearizing equation Equation 26. The analysis of adsorption was conducted under varying activated carbon temperatures while maintaining a constant methanol temperature, a condition that inherently keeps the saturation pressure unchanged. This approach results in distinctive equilibrium pressures given the constant saturation pressure and disparate adsorbent temperatures. These varying equilibrium pressures thus facilitate the plotting of a linear relationship between adsorption and temperature. The same method can be employed across different evaporation temperatures. The validation of the D-R equation was carried out through a linear fit of the Dubinin-Astakhov (D-A) equation. This involved the manipulation of the exponent n, set at 2 in this context, across different values to determine the most accurate linearization.

Following the determination and verification of the constants W_0 and D, the next steps involved the plotting of isobars and isotherms. The isobars serve to depict the influence of increased adsorbent temperature on the adsorption capacity, with the pressure held constant. Each isobar line corresponds to a specific evaporator temperature, allowing for a representation of how reducing the evaporator temperature impacts the adsorption capacity. Conversely, the isotherms demonstrate the effect of pressure increase on constant adsorbent temperatures, with each isotherm corresponding to a fixed adsorbent temperature. The resulting curves provide valuable insight into the determination of temperature zones and operational conditions for the proposed system, offering an indication of anticipated performance levels. To ensure the accuracy of the data, the Python scripts employed for simulation were corroborated against the experimental data and resulting graphs from El-Sharkawy et al.'s "Study on Adsorption of Methanol onto Carbon-based Adsorbents" [16], thereby confirming the replicability of the data with the same scripts.

8.7   Sources of error

When starting the initial testing, several concerns came to light. The main difficulty was because of inaccurate temperature readings. When building the system, the thermocouple inside the carbon was dropped to avoid further delays in the testing. It therefore proved challenging to regulate the carbon temperature as the only sensor was placed on the steel wall and collector outlet. Theoretically, when placing a sensor on the copper pipe at the outlet and isolating around, a fairly accurate reading on the desorbed methanol temperature is given. However, steel has very poor heat transfer characteristics. It was therefore an immense temperature difference between the steel wall and the collector outlet. As a result, the carbon situated on the outer edge of the pipe is expected to have a substantially higher temperature than the carbon situated in the centre. With methanol's high thermal sensitivity, this poses an issue. When going above 120 °C the methanol starts to decompose into compounds like dimethyl ether [13] which constricts the system's performance. The rate of decomposition increases with temperature.

An additional source of potential inaccuracies lies in the reliance on literature to determine the methanol adsorption values utilized for calculating the dimensions of the system. Given the time constraints associated with system fabrication, it was necessary to make assumptions concerning the adsorption pair. Consequently, the adsorption uptake could exhibit minor deviations from expectations. The resultant error may lead to a system in which the cooling capacity falls short of expectations, causing the water to fail to reach its intended temperature range. Under such circumstances, the cooling chamber may struggle to achieve or maintain its optimal temperature. Given that the surrounding water bath regulates the cooling chamber, appropriate dimensioning is crucial for system functionality. In instances where the system is underdimensioned, the cooling chamber may reach its ideal temperature but struggle to sustain it. Conversely, in overdimensioned scenarios, the water may never reach a sufficiently cool temperature.

When it comes to sizing the different components, a significant degree of uncertainty is embedded within the calculations due to the lack of known variables in the system. Apart from the maximum adsorption uptake, the system's mass flow characteristics remain largely unknown. This is linked to the rate of adsorption and associated desorption times, which are in turn directly influenced by factors such as temperature, materials, pressure, among others. Practically, this signifies that calculations are significantly swayed by assumptions. Determining the duration required for system desorption without adequate testing is challenging, as it is primarily reliant on the specific adsorption pair involved. Moreover, it also depends considerably on the collector's design. The heat transfer from the heating cable to the steel wall of the collector, and through the steel and activated carbon, is difficult to anticipate without complex simulations. The same holds true for the dispersion of methanol inside the activated carbon. The type of carbon, whether granular, fibrous, solid, or powdered, will exhibit varying gas and heat transfer characteristics, as well as adsorption capacities. Additionally, the size of the granules chosen and the density of their packing play a crucial role. Considering these multifaceted factors, a trial-and-error approach becomes necessary for the accurate design of a high-performance system.

8.8   Limitations

While carrying out calculations for the main setup, it becomes evident that a lack of data could potentially pose a challenge in achieving a well-designed system. Given the limited time for the task, the parameters of the system are determined based on literature research and logical assumptions. The decision for adsorption/desorption times is made based on comparable literature, while the use of mass transport in calculations is avoided due to its unpredictability. Ideally, these parameters should be explored in the secondary setup before doing calculations.

The chosen materials and sizes also present a limitation, being largely reliant on what's available in the lab. Therefore, some preferred materials are not available, limiting the system's performance. For example in the collector pipe and cooling chamber the preferred material is copper due to its superior thermal conductivity over steel. This limitation also extends to system components such as manometers, sensors, regulators, and so on. The available manometers are only analog, rendering them unsuitable for any automated recordings. In the context of a 24-hour cycle, this poses a challenge in gathering all the necessary data. Furthermore, the manometers are inaccurate and have overly broad intervals, making precise pressure readings on the vacuum difficult to achieve. There was initially also not the available parts to insert thermocouples into the carbon and copper core.

9 Results and discussion

This chapter delves into the experimental exploration of two different system configuration, with the first being the initial system and the latter being the altered collector. In addition, the adsorption uptake experiment with corresponding simulation data is presented. The results are thoroughly investigated with accompanying discussions, before the main challenges and findings are presented.

9.1 Prototype Design Analysis

The first experiment was carried out utilizing the system rig, where the primary design under investigation involved a single copper tube in the collector, surrounded by activated carbon. This collector configuration, however, did not make use of thermocouple sensors, thereby hindering the accurate measurement of the temperatures of both methanol and carbon. On the other hand, sensors were fitted on the exterior of the outer pipe to record the temperature of the carbon, and also at the collector's outlet to monitor the temperature of the methanol at those specific locations. Predictions related to the precise original temperatures of carbon and methanol based on these assumptions are tough to make prior to the actual experiment. The collector's exterior is composed of steel, a material known for its subpar heat transfer properties. Consequently, the temperatures inside and outside the pipe could vary significantly. Conversely, the copper pipe, through which methanol flows, possesses excellent thermal conductivity, enabling effective heat transfer. Therefore, it's reasonable to expect that the temperatures inside and outside this pipe would be more equal.

9.1.1 Initial startup

The initial evaluation of the system was conducted to determine whether it functioned as expected. With many assumptions regarding calculations and design, the performance of the system was rather uncertain. The first test was carried out when the system was placed in a vacuum and methanol was introduced into it. At this stage, the system was not externally heated and operated at room temperature. Immediately after the methanol was injected, the system responded with a rise in the collector's temperature and a subsequent decrease in the evaporator's temperature. It should be noted that because this was the first test, the evaporator's casing was not yet insulated, which negatively impacted its ability to retain the cooling effect. The increase in temperature from the collector is due to the adsorption reaction between methanol and the activated carbon. As the pressure descends below the vapour pressure of methanol, the liquid commences evaporation, thus extracting heat from its surroundings. This acquired heat is subsequently deposited in the carbon during adsorption, leading to a temperature decrease in the evaporator and a temperature increase in the collector. This phenomenon is visually illustrated in Figure 9.1. Because the reaction was stronger than anticipated, data recording was started after the reaction had already occurred. Hence, the curve begins when the temperature of the carbon started to decrease again. The highest temperature the carbon reached was almost 50 °C, which clearly indicates a strong adsorption process within the system.
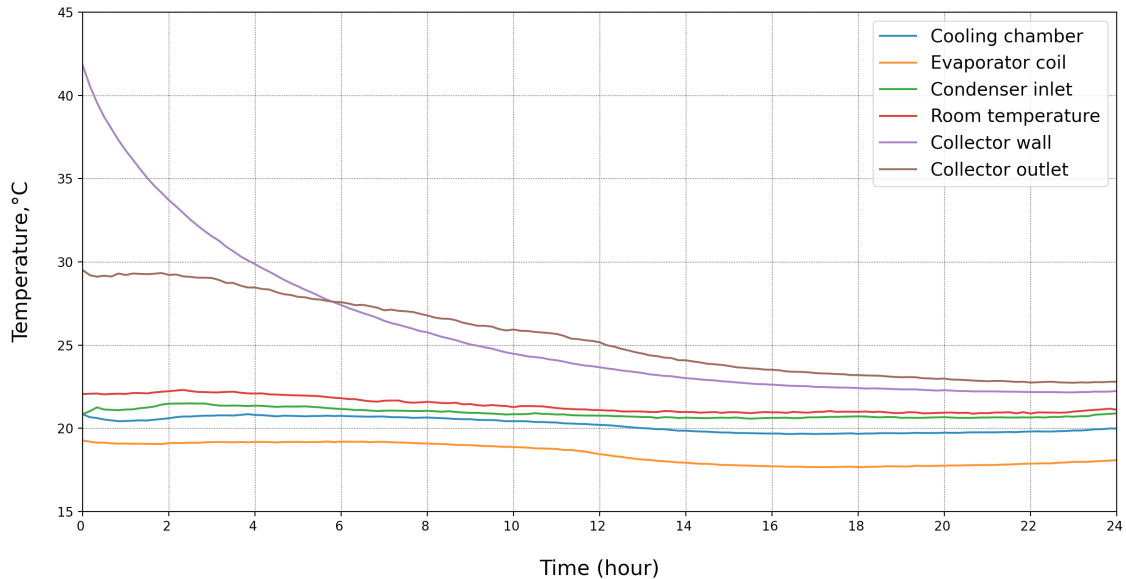
Figure 9.1: Adsorption curve for 24 hours of cooling

The graph shows that the temperature of the collector's wall (its outer surface) dropped from 42 °C but did not reach room temperature until a 24-hour cycle had completed. This could suggest a slow temperature change within the collector. It's also possible that the adsorption process was still ongoing, which continued to carry heat to the collector, albeit at a slower pace than heat was being removed from the system. The data showed that the most significant temperature decrease happened within the first five hours. Between the two parts of the collector, the outer wall experienced the greatest temperature decrease, while the temperature of the collector outlet decreased more gradually. After 12 hours, the cooling paths of both the collector wall and outlet began to align and levelled off around the 22-hour mark.

As for the evaporator coil, a gradual decline in temperature is observable at the beginning of the recording, which intensifies around the 11-hour mark. The sensor at the lowest part of the first evaporator coil is consistently selected for the graphs, as this is presumed to be the coldest point. Additional sensors are installed to log the temperatures at various coil heights and are depicted when there is a significant deviation among them. In this instance, the upper part of the coil, which is not depicted, is slightly cooler. Given that the adsorption at the lower part of the coil initiates later than at the top, the increased gradient at 11 hours can probably be attributed to this factor. Regarding the remaining lines on the graphs, the temperatures largely remain constant around ambient temperature. However, the cooling chamber exhibits a minor temperature decline, aligning with the trend of the evaporator coil.

9.1.2   Simulation one

In the initial test of the system, the temperature of the outer wall was kept at a maximum of 120 °C. This was based on the assumption that the internal activated carbon would maintain slightly lower temperatures. The collector outlet was used as a reference on the methanol temperature, as at this stage, no sensor was installed in the activated carbon or the collector core. The temperatures were therefore believed to be well within the limits of methanol degradation. During this initial trial, the collector was not insulated, and the heating period was deliberately kept short. To prevent any damage to the methanol, the heating process was terminated once the temperature attained 120 °C.

The empirical data from this test can be observed in Figure 9.2. The graph reveals a rapid rise in the steel wall's temperature to the desired range, taking approximately an hour before reaching a plateau at the given energy input. The collector outlet mirrors a similar trajectory, albeit at

lower temperatures. The condenser inlet's temperature began to rise when the collector wall reached approximately 105 °C, exhibiting a sudden and swift increase. The temperature rapidly equilibrates to nearly the same value as the collector outlet. As the collector outlet lacks insulation, the temperatures of the two parameters closely resemble each other, which is attributable to the mass flow of methanol. Upon desorption of methanol from the system, it commences its downward flow through the condenser and into the evaporator. Given the high temperature of the methanol, the condenser inlet temperature serves as an accurate indicator of mass transport. When the collector's heating is switched off, the mass flow of methanol halts abruptly, observable at the condenser inlet. The collector outlet undergoes a slightly longer cooling process due to its contact with the heated collector.

Concerning the evaporation temperatures, negligible fluctuations were noted following the desorption process. This can be ascribed to the brief heating period preceding the adsorption process. Furthermore, it may suggest an early indication of the evaporator being oversized relative to the water container. During the system's construction, the evaporator casing inadvertently exceeded the initially intended height, which was supposed to be corrected with styrofoam plates. Regrettably, the anchoring system failed, resulting in a final design where the casing contained more water than intended. This could potentially contribute to suboptimal evaporation temperatures. An important note is also the lack of insulation on the evaporator at this stage, something that would make the cooling escape fairly rapidly. However, some decline in temperatures was still expected to be viewed.
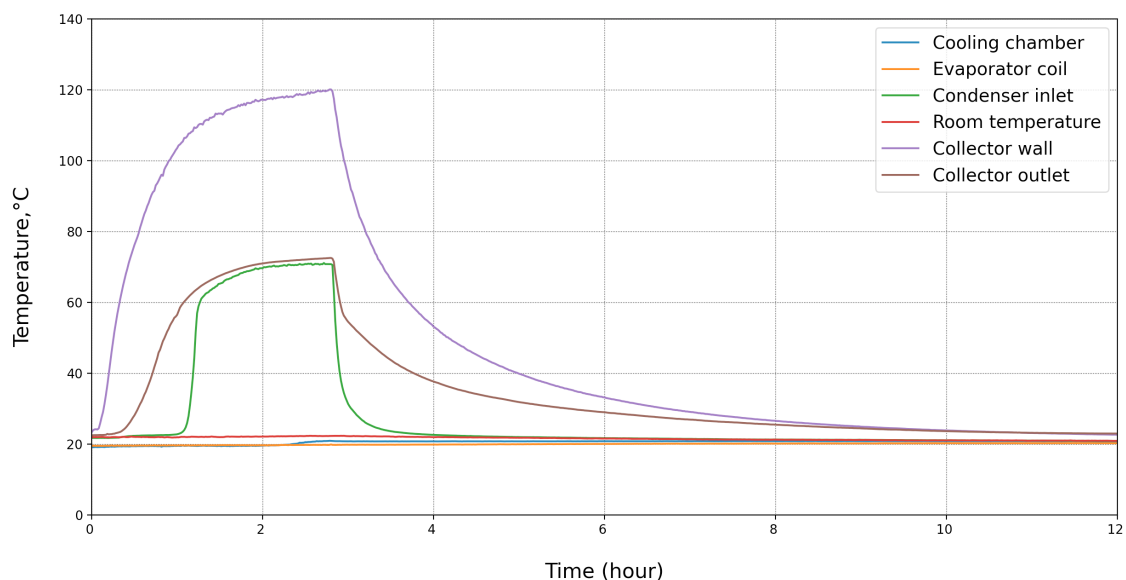
Figure 9.2: Simulation one. Heating at 120 °C

9.1.3 Simulation Two

In the subsequent simulation, the temperature applied to the collector pipe was considerably higher. This was primarily due to using the collector outlet temperature as a reference point for the temperature of the carbon. Between the first and second simulation, insulation was added to the collector using glava, enhancing its heat retention capability. This modification enabled the collector to achieve much higher temperatures than previously possible. A graph illustrating this simulation can be seen in Figure 9.3. The maximum temperature of the collector wall reached 267 °C, while the collector outlet reached just under 95 °C. The pressure recorded when the temperature achieved 267 °C was 1.55 bar, measured in absolute pressure. The condenser inlet temperature again mirrored that of the collector outlet, except for the final three hours. The graph also displayed variable temperatures, a result of experimental manipulation to gauge the system's response. It's worth noting that the mass flow, indicated at the condenser inlet, ceased as soon as the collector's heating was stopped, even with the collector wall's temperature well above 150 °C. The heating

was halted twice, with the mass flow ceasing almost immediately each time. In this simulation, heating persisted until the mass flow stopped, logging a total of five hours of flow.

Regarding evaporation, the results were less than satisfactory as temperatures barely budged below room temperature. Initial speculation attributed this issue to the collector. The inferior heat conductivity of steel and activated carbon could inhibit effective heating of the methanol in the core. Without sensors embedded in the collector, the temperatures were essentially a blind guess. In addition to poor heat transfer, the collector's internal design could be a limiting factor in the dispersion of the methanol.
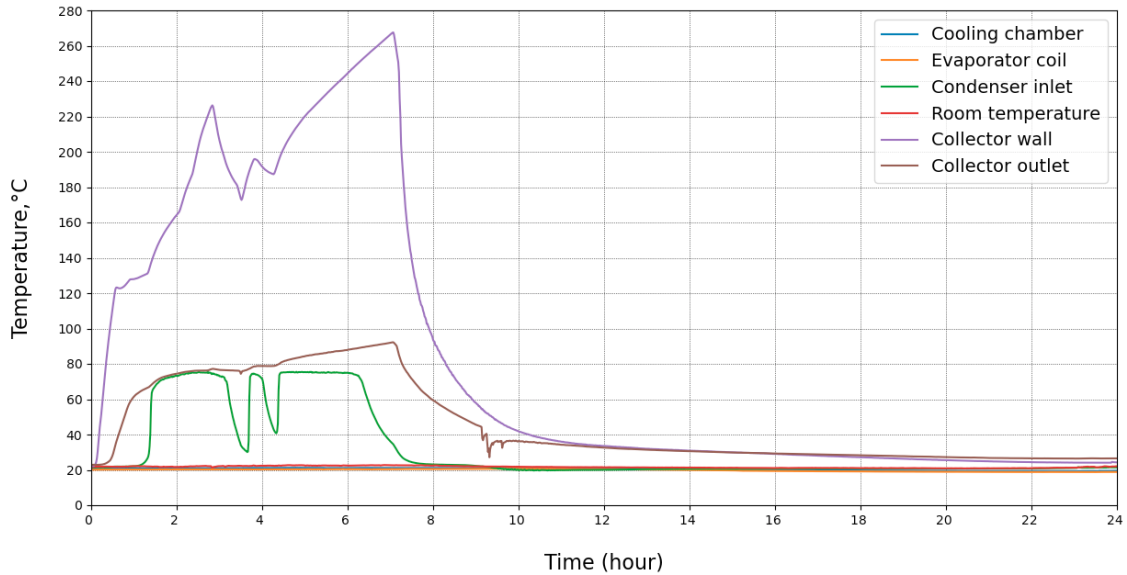
Figure 9.3: Simulation two. Higher temperatures with longer mass flow.

9.1.4 Simulation Three

For simulation number three the temperatures were once more held at a high temperature. The heating was sustained for an approximate duration of three and a half hours, subsequent to which the heating cable was deactivated. It is noteworthy that the external surface of the collector attained a maximal temperature of 260 °C. Simultaneously, the outlet temperature of the collector was measured at 116 °C, after which it began a downward trend. This can be pictured in Figure 9.4. During this simulation, the system's pressure peaked at 1.9 bar under maximum temperature at the start. Once again the mass flow of methanol can be seen tightly connected to the heating at the collector. To avoid the temperatures surpassing 260 °C, the applied heat was reduced under three circumstances, all of which stopped the mass flow.
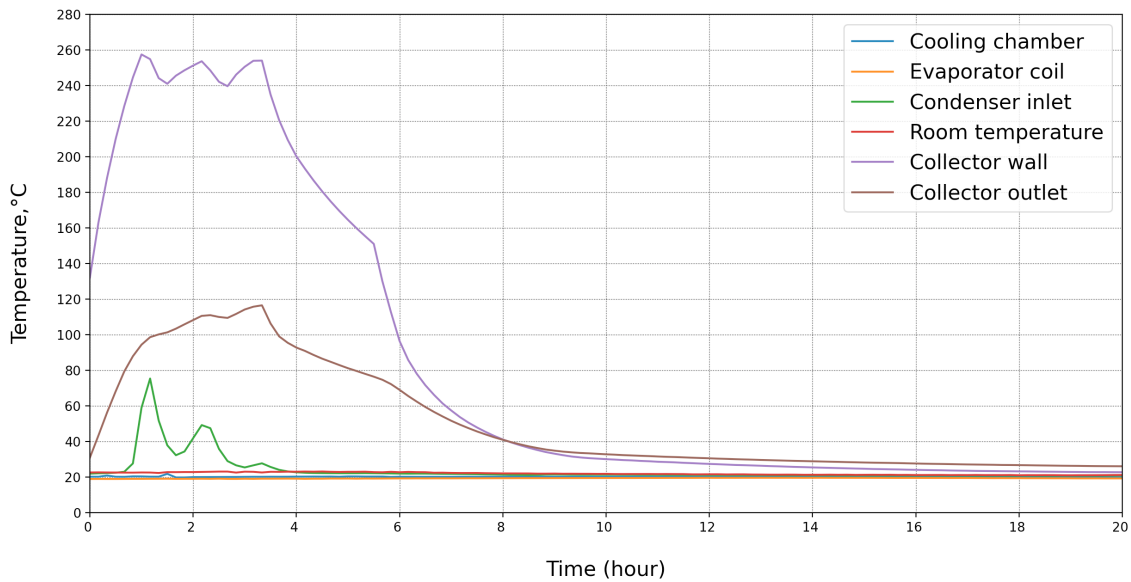
Figure 9.4: Simulation three. High temperatures with less mass flow

An in-depth examination of the evaporator during the adsorption phase is depicted in Figure 9.5. This figure presents data corresponding to the evaporator coil and the chamber which are the primary sites for cooling. Under this simulation, the evaporator was covered in insulation to prevent any loss in cooling potential. Still with a more effective container, the evaporation is more or less non-existent. The temperature of the cooling chamber and evaporator coil is only a fraction lower than the room temperature. In addition, a small decrease can only be seen after 14 hours. At this point, the collector has more or less returned to stable temperatures. Signalling the lack of adsorption, as the cooling process should commence much sooner.
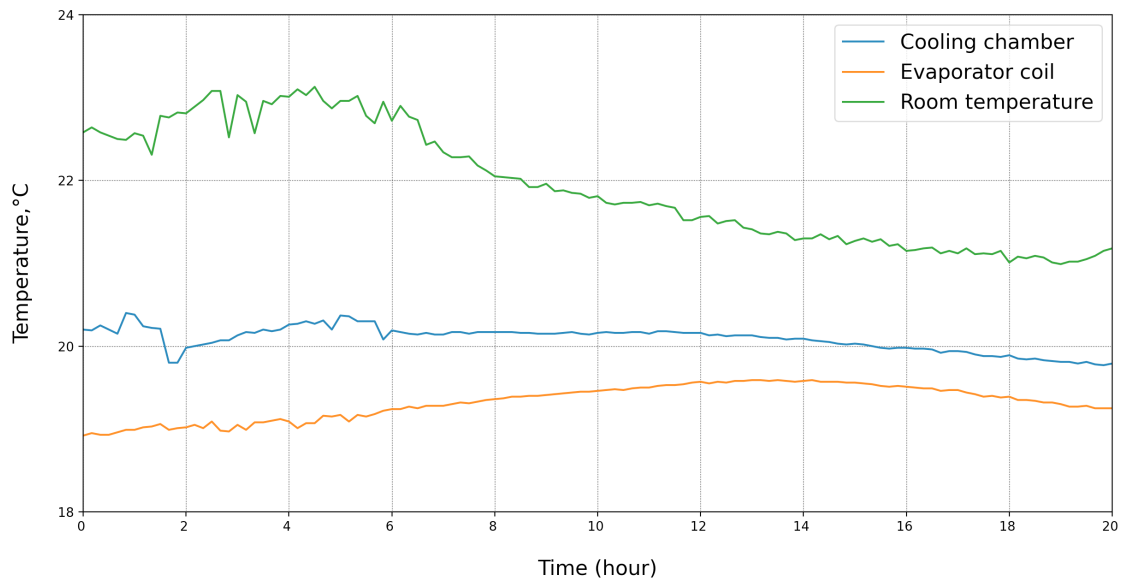
Figure 9.5: Adsorption curve for the evaporator during simulation three

9.1.5   Simulation four

The fourth experimental simulation, delineated in Figure 9.7, was conducted over a 24-hour cycle, during which the desorption phase was initiated at a collector wall temperature of 265 degrees. A

total of five hours were used during adsorption, at which the collector outlet reached a maximum temperature of 115°C with a corresponding pressure above 3 bar. An intriguing observation can be drawn from the graphical representation, where the outlet temperature does not commence its decline until the outer wall of the collector approaches a temperature proximate to that of the collector outlet. Further scrutiny of the graph reveals the collector outlet has a slower temperature decrease at the end of heating. This is attributed to added insulation as pictured in Figure 9.6. Regarding mass flow, the fourth day followed the same footsteps as previous simulations with shorter and shorter desorption processes.

Simulation number four exhibits similarities with the preceding tests, primarily the minimal cooling achieved. A closer analysis of the cooling process reveals that the temperatures in both the evaporator coil and the corresponding cooling chamber have remained constant, indicating no discernible cooling. Despite adhering to an identical procedural methodology for this test, a clear trend of decreasing cooling efficiency can be observed with each successive test run.

Figure 9.6: Added insulation around the collector outlet for increased recording accuracy, and reduced heat loss
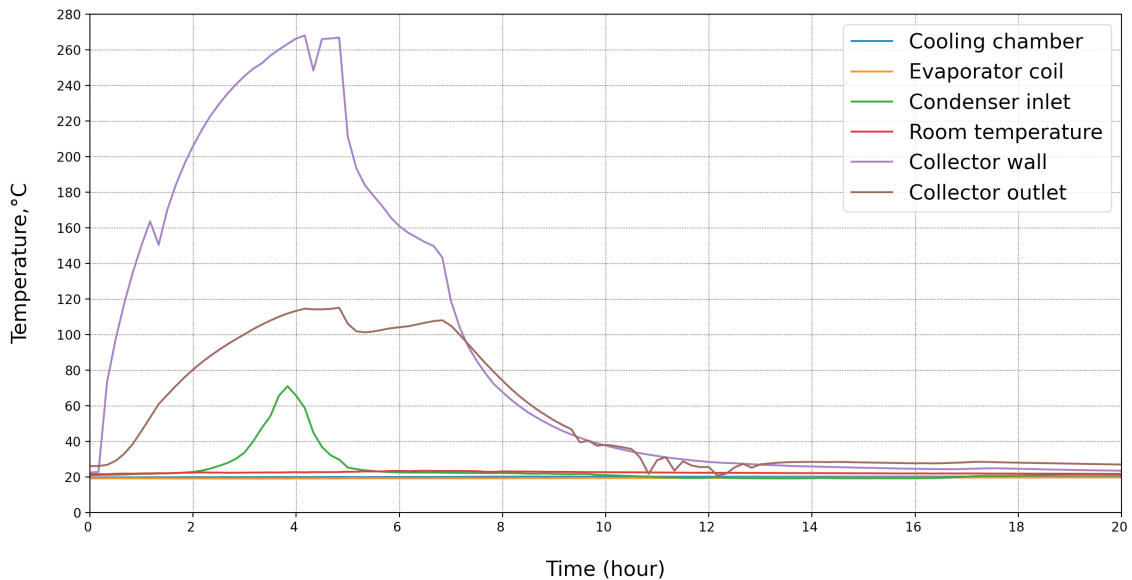
Figure 9.7: Simulation four with insulation at collector outlet

9.1.6 Prototype simulation findings

This system was designed as a prototype to investigate the adsorption process and learn more about how the adsorption pair would react. The problems and issues were investigated deeply to map out the errors and also to find out what worked well. This prototype would then later be changed to make an optimal system where the errors had been fixed. After finishing the preliminary test of the prototype, there were several issues needing addressing and many questions left unanswered. Some very clear trends could be seen from the testing, with the biggest one being regarding temperatures and pressures. The prototype system is characterized by a paucity of thermocouple sensors, with a particular deficiency in the collector where measurements are confined exclusively to the exterior. Three sensors were deployed, each respectively gauging the temperature of the heating cable, the collector's exterior, and the outlet. Elevated heating temperatures were employed owing to the low thermal conductivity of the collector material utilized. It was hypothesized that to achieve the desired internal temperature range of 80-110 °C within the collector, the external surface of the steel pipe would necessitate a significantly higher temperature. The absence of knowledge pertaining to the carbon temperature could precipitate system overheating. Therefore, it is the temperature at the outlet that determines the amount of heat supply added to the collector. This is because the copper pipe conducts heat well and temperatures on the inside and outside were assumed to be relatively similar.

The system operates as a closed entity, thereby necessitating uniform pressure distribution throughout. As the system temperatures escalate, so does the pressure, consequentially impacting the properties of both carbon and methanol. The boiling point of methanol at atmospheric pressure (101,325 KPa) is 64.7 °C. During the prototype tests, the system was subjected to a maximum pressure exceding three bars under the last test, equating to 300 KPa. An elevation in temperature consequently raises the boiling point of methanol, implying that the pressure was excessively high in comparison to the heating temperature. The activated carbon's optimal temperature is 110 °C to utilise the adsorption process in the best way. Any further increase in temperature could potentially instigate the conversion of methanol into alternate gases. Prolonged exposure to such high temperatures may diminish the volume of methanol, thereby limiting the quantity available for the adsorption process.

For each subsequent test run the pressures could be seen increasing. Which in turn leads to less and slower adsorption, as the methanol is dependent on low vacuum pressures to evaporate. For each increase in maximum pressure, the collector would need to cool down to lower temperatures before the evaporation could commence. The working theory behind the increasing pressures is underestimating the carbon temperature. At temperatures above 140 °C the methanol will decompose. however, this process has been reported to start at as low as 120 °C. This decomposition would lead to other compounds and gases being present within the closed system. Among others, dimethyl ether would become present. A substance which is in gas form under ambient temperatures with a boiling point of -25 °C. The presence of this content could be a natural contributor to increased pressures as it contains higher saturated pressures. In addition to increased pressures, it fills the voids in the microporous surface of the carbon and thus decreases the effective volume which methanol can utilize. Consequently reducing the performance of the adsorption process. These findings are in line with the work of Eric Hu [13].

An additional challenge encountered pertains to the limited mass flow transitioning from the collector to the condenser. The system frequently demonstrated a significant mass flow, however, the duration was rather brief. At its peak, the mass flow experienced an elevation for approximately five hours prior to its decline. Maintaining a uniform mass flow throughout the full duration of the desorption phase is pivotal to optimising the adsorption procedure and, as a result, achieving high cooling efficiency. This issue likely constitutes one of several impediments contributing to the subpar performance of the cooling process. As the temperature escalates, the quantity of methanol is released correspondingly. There exists a critical temperature threshold at which no additional methanol remains available for release. This limit is different depending on the type of carbon used. From the papers of henninger et al. a selection of carbon materials can be seen stagnating around 130 °C. Implying that the upper limit for desorption is close to this temperature. However, some samples can be seen increasing beyond this mark, depending on the parameters of evaporation and condenser temperatures as well as pressures [55]. Testing at temperatures beyond the 130 °C

mark could reveal the highest necessary regeneration temperature, but doing so is at the expense of methanol degradation.

Within the condenser configuration, one pertinent factor is the significantly large size of the water bath. This overestimation of condenser water volume remains inconsequential given that the water's temperature persistently mirrors the ambient room temperature. Conversely, the volume of water in the evaporator is of substantial significance. Throughout the prototype trials, the entirety of the evaporator coil was submerged in water. The initial design for the evaporator size did not unfold as anticipated. Two analogous containers for the condenser and evaporator were engineered. As the design stipulated for a marginally smaller evaporator than the condenser, styrofoam plates were positioned at the base. However, upon the introduction of water, buoyancy proved excessively forceful as the evaporator coil floated up in response to the styrofoam plates, subsequently leading to their removal. Even so, the evaporator remained filled with water. An excess volume of water, exceeding the calculated quantity, could yield the inefficiencies observed in the cooling process. The envisioned cooling effect is unlikely to transpire as the expansive volume of water substantially influences the heat transfer properties. The cooling process occurring during the adsorption phase is inadequate relative to the quantity of water at room temperature.

9.2 Adsorption uptake Experiment

After evaluating the first prototype, it became clear that the lack of adsorption data between the activated carbon and methanol was crucial to inherit. Relying on literature data alone, gave a shortcoming in the results. Assessing the system without knowledge of the adsorption at different pressures and temperatures, meant inaccurate calculations but also limited the quality of the data received during testing. To give a better understanding of the system at hand, a secondary system focusing on adsorption characteristics was initialized to gain valuable information regarding the adsorption and desorption quantities. Several adjustments were made to the experimental setup before the final testing could commence. This included adding manometers, weights, and thorough pressure testing with subsequent sealing of leakages. The results presented are therefore taken from which good results could be retrieved.

9.2.1 Preliminary test

In the initial experiment with the adjusted system, the temperature of methanol and carbon was tried kept at a constant level as a workaround for constant pressure. However, as can be seen in **??** this proved harder than initially thought. Around the activated carbon there is employed an ice bath to keep the carbon cool, but even with a temperature gradient of 30°C the carbon continued increasing in temperature during adsorption. The same is seen on the methanol which is also submerged in a water bath. As the Methanol evaporated it absorbed the heat from the surrounding, thus making the water colder by the minute. When being adsorbed by the carbon, this heat was then released which counteracted the cooling from the ice bath. The heat generation from the adsorption was therefore larger than the cooling produced from the ice water. With this being the first attempt, the activated carbon is not yet saturated with any methanol. As a result, the simulation shows a very strong adsorption process.
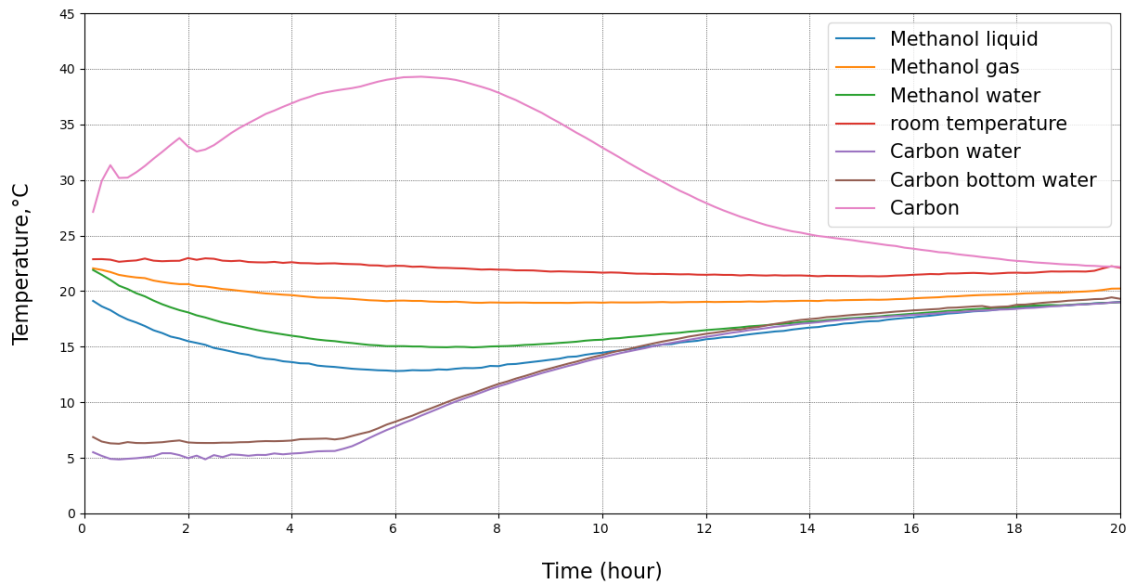

Figure 9.8: Preliminary adsorption test

9.2.2 Simulation one

After several attempts at controlling the adsorbent and adsorbate temperatures, the testing was eventually laid to rest. With the current equipment at hand, controlling the system as initially thought became too difficult. Running the setup without any interference was therefore decided to be a better approach. New carbon was therefore incorporated into the system. Consequently, the system was subjected to another round of vacuum pump operation to establish the desired system pressure. This implies that this simulation lacked a desorption phase.

Figure 9.9 delineates the instantaneous response of the adsorption pair under absolute vacuum conditions. A salient feature observed from the adsorption uptake test is the seamless curve. The temperature of the carbon began to escalate while the methanol simultaneously started to decrease. In the prior test, the carbon was initially placed in a water bath to deter any temperature fluctuations. This strategy, however, proved to be insufficient in maintaining a constant temperature during the adsorption phase. Rather than using cold water, the initial temperature of the water bath was set to ambient, which served as a form of cooling for later desorption phases. As for the methanol, the water bath was removed given its unnecessary function. The cooling process exhibited high efficiency during the initial hours, with a temperature decline of nearly 10 °C. Upon the carbon temperature reaching approximately 34 °C, the cooling process came to a halt. This temperature level remained relatively stable over a significant period before it began to rise nearing the 8-hour mark.
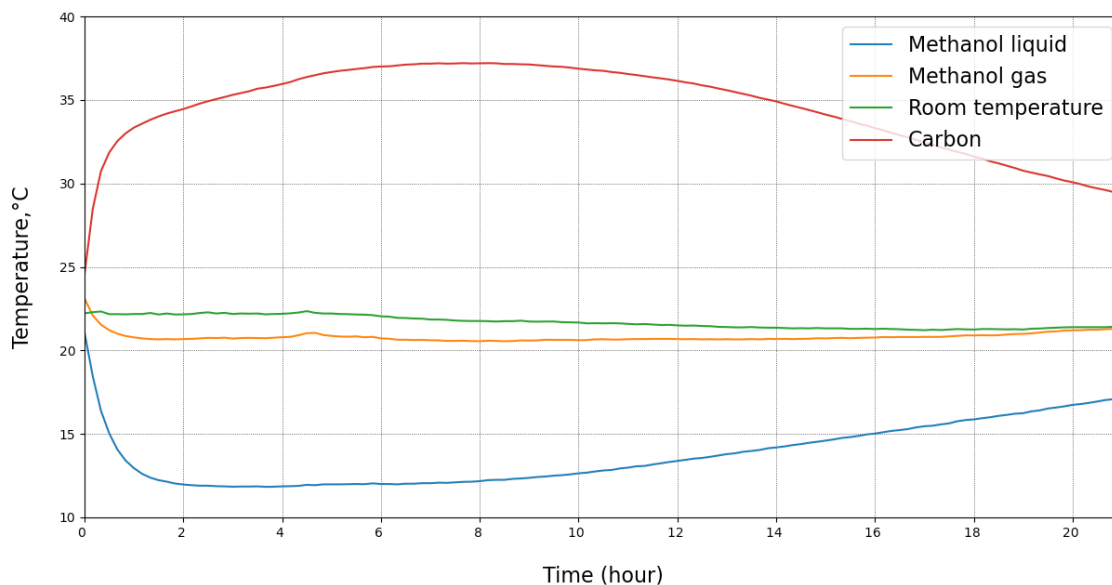
Figure 9.9: Simulation one adsorption uptake

An important aspect in the investigation of the adsorption pair is the adsorption uptake. With the new testing, better weight and pressure measurements were incorporated into the system to yield more accurate results. Figure 9.10 provides a graphical representation of the adsorption phenomenon by comparing the weight of methanol to its pressure at corresponding time intervals. At the onset of the adsorption process, the methanol weight approximated 400 grams, corresponding to a pressure of 60 mbar. The adsorption process exhibits good efficiency initially, resulting in a significant drop in pressure during the first hour, reducing it to 37mbar before it subsequently increases. Over the course of the 21-hour adsorption cycle, the methanol weight has lowered to 225 grams, denoting a total reduction of 175 grams during the first adsorption process. With 800 grams of activated carbon, this yields a maximum adsorption of 0.21875 $kg\ kg^{-1}$
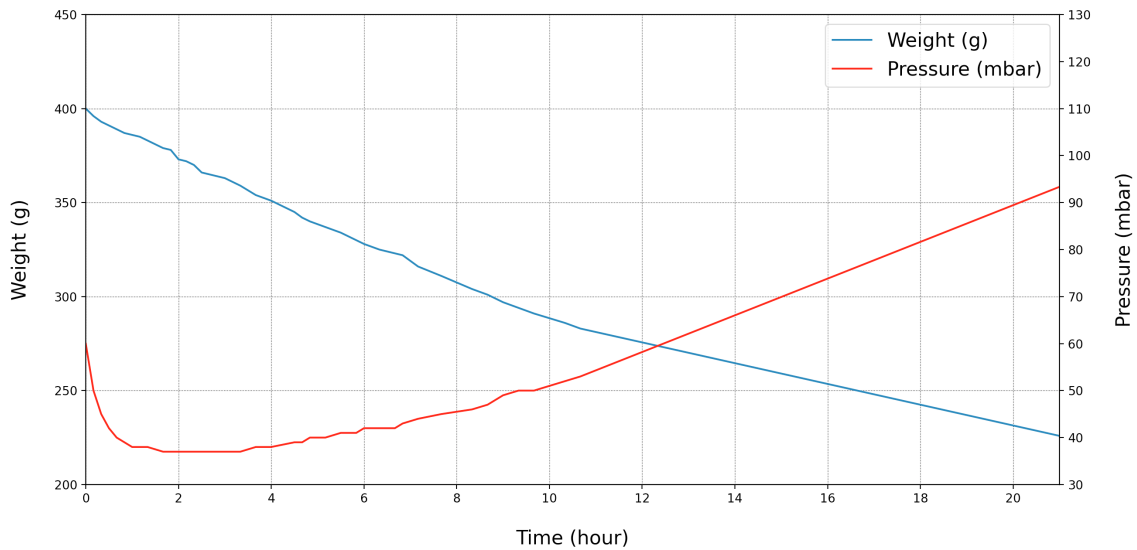
Figure 9.10: Simulation one corresponding weight and pressure graph

9.2.3 Simulation two

The subsequent phase of the adsorption uptake test focused on determining the amount of methanol present during the desorption process, which can be depicted in Figure 9.11. With the challenge of maintaining a stable temperature throughout the heating process, the container was immersed in boiling water. Given that the boiling point of water is 100 °C, this approach facilitates the attainment of consistent heating. The minor variations in temperature observed on the graph can be attributed to supplemental water being added to compensate for evaporative losses. The data indicate that the carbon attains a temperature of 95 °C after 13 hours of boiling. Furthermore, the onset of adsorption is relatively swift upon the reduction of heat. The desorption process is kept going until there is a stagnation in methanol flow, which can be seen with the naked eye through the glass bottles but also in the weight.
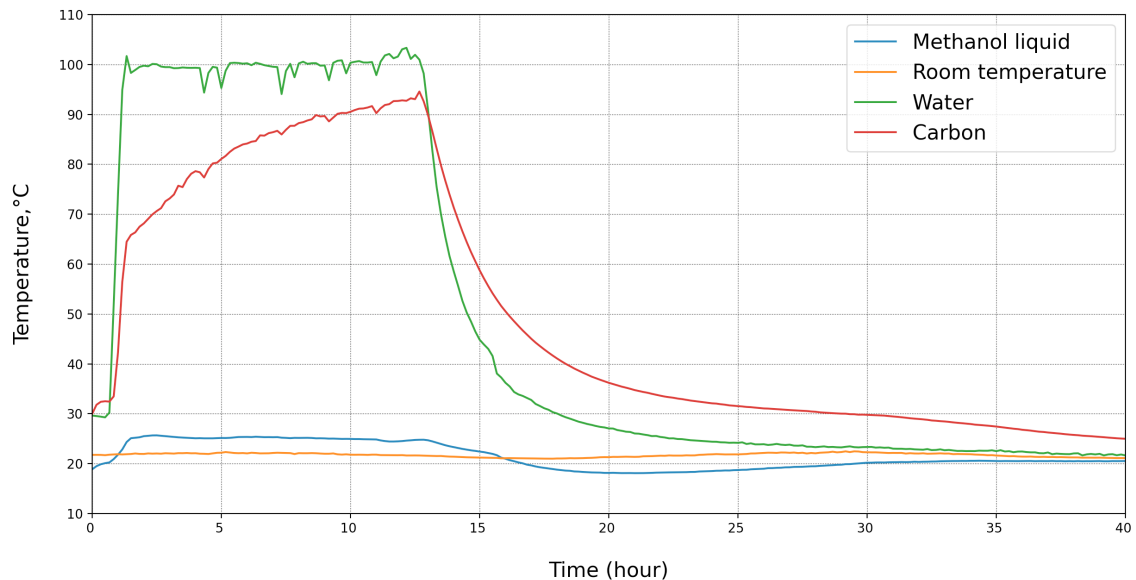
Figure 9.11: Simulation two adsorption uptake

Following the initial adsorption process, the container had approximately 225 grams of methanol remaining before the next desorption phase were to start. Figure 9.12 illustrates the progression of methanol quantity during the desorption and subsequent adsorption phase. Over the course of a 12-hour period, there was an increase of 90 grams in the methanol quantity, culminating in a total of 320 grams post one full cycle. This indicates that not all methanol was desorbed during the inaugural complete cycle, with the original quantity being 400 grams. The corresponding desorption efficiency thus calculates to roughly 51%. Moreover, this plot also reveals information about the ensuing adsorption phase. A manometer, with a maximum limit of 150 mbar, was utilized to monitor the pressure. Given its manual readout, it presented difficulties for nocturnal measurements. Consequently, pressure readings were not recorded until 20 hours into the adsorption process. In addition, the manometer could only be used when the pressure was low. Meaning the desorption period with high temperatures could not be recorded. Finally, by the termination of the adsorption phase, the methanol quantity was confirmed to be 229 grams. This result is in line with the first adsorption period, where the difference could likely be attributed to a measuring uncertainty. Yet a notable difference between the first and second tests is seen regarding pressures. Whereas the first adsorption cycle ends at 95 mbar, the second ends at 114 mbar having increased by 19 mbar. The increased pressure is likely to affect the adsorption as evaporation is highly dependent on low vacuum pressures.
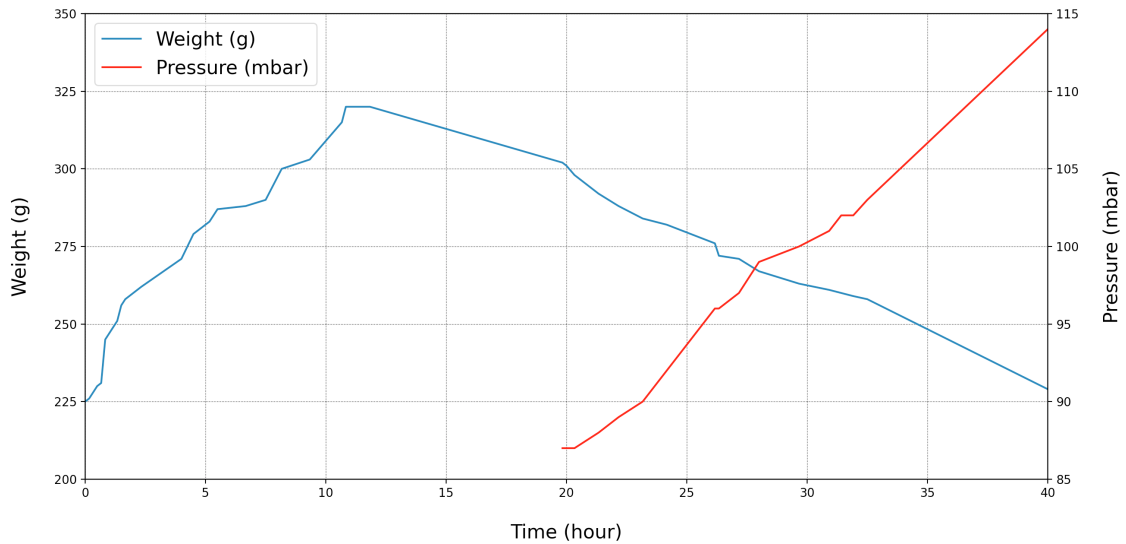

Figure 9.12: Simulation two corresponding weight and pressure graph

9.2.4 Simulation three

The consecutive desorption process is presented in Figure 9.13. For this particular case, oil was substituted with water to gain even higher temperatures. As oil has a higher boiling point than water, it was possible to reach a temperature of almost 130 °C. During desorption the carbon was able to reach a temperature of 115 °C after 12 hours. The justification for going above the threshold of methanol degradation was to find the desorption at high temperatures. The breakdown process takes time, therefore running one cycle at slightly elevated temperatures would not impact the system excessively. In addition, this was the final proper simulation. After cutting the heat to the oil, the system experienced a prolonged cooling interval compared to the water.
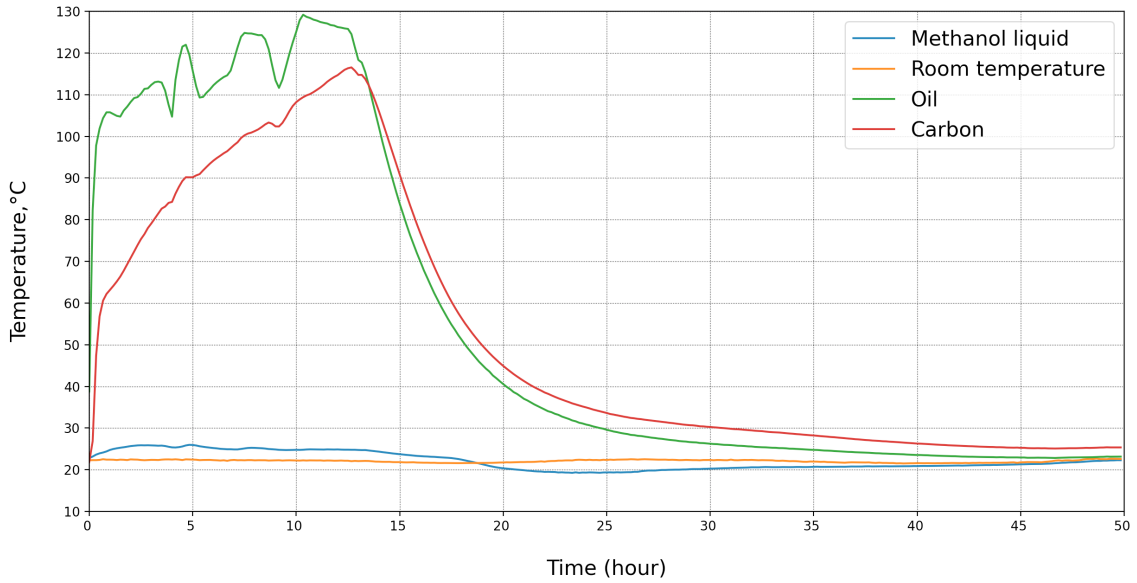
Figure 9.13: Simulation three adsorption uptake

Figure 9.14) displays the methanol weight and corresponding pressures for the given simulation. After a 12-hour heating phase, the quantity of methanol surged from 229 grams to 341 grams, amounting to a total desorption of 112 grams. This implies that the utilization of a higher temperature during desorption results in a more significant desorption of methanol compared to water. With this approach it was possible to increase the desorption, leading to a higher quantity of methanol than what was observed after the preceding desorption test. The figure additionally depicts the subsequent adsorption phase, where the methanol quantity decreased once again, this time down to 245 grams. As there is no mechanism to measure the pressure during nighttime, pressure values are only available for the end of the adsorption phase. At a temperature of 130 °C, the desorption efficiency increased to 64% However, the adsorption phase was not able to evaporate as much methanol. Yet, the pressure curve is highly similar to the previous curve shown in Figure 9.12 which could indicate a faulty weight reading. The adsorption process was kept going for almost two days to make sure all the methanol had desorbed.

Figure 9.14: Simulation three corresponding weight and pressure graph

9.2.5 Final desorption

In order to conclude testing on the secondary system, a final desorption cycle was initiated to ascertain whether all of the methanol could be eliminated from the carbon using higher temperatures. The last recorded temperatures can be observed in Figure 9.15. To facilitate the complete removal of methanol, temperatures were maintained at a high level. During each of the three peak phases, the system experienced a standstill, leading to a rise in temperature. At the conclusion of the cycle, the temperature was intentionally sustained at an extremely high level. Given that the cycle ran for 15 hours, there was insufficient time remaining, as the heating phase required manual operation. By the end of this heating period, nearly all the methanol had been desorbed, leaving only minor traces behind. With a prolonged heating period, it is likely that methanol could be desorbed at a lower temperature, around 160 °C. However, this would entail an extended duration, as desorption appeared to be slow at this stage. Although the test wasn't conducted in a highly analytical manner, the results provide valuable insights into the time required by the system to achieve full desorption.
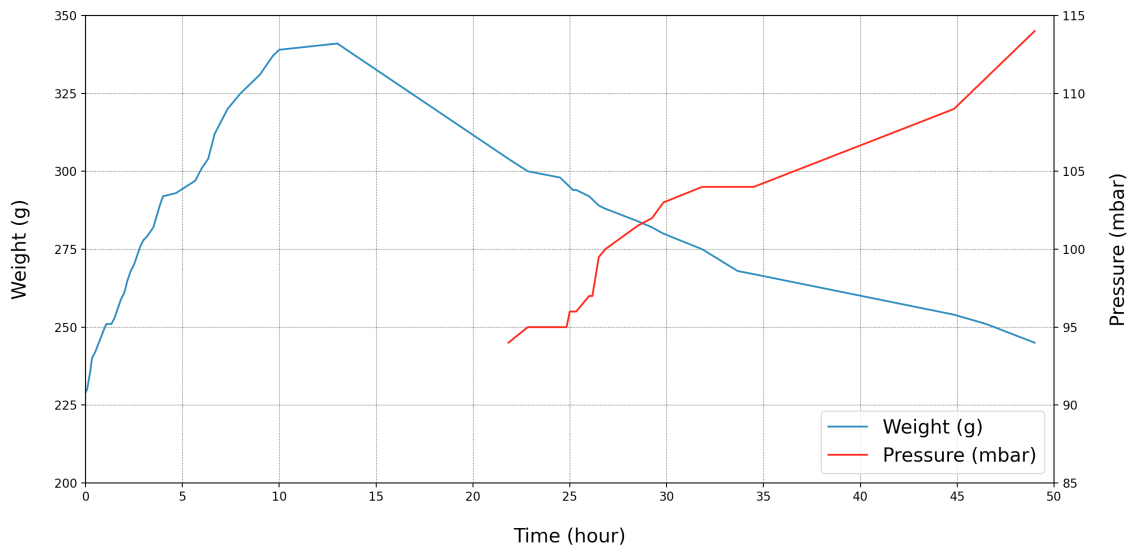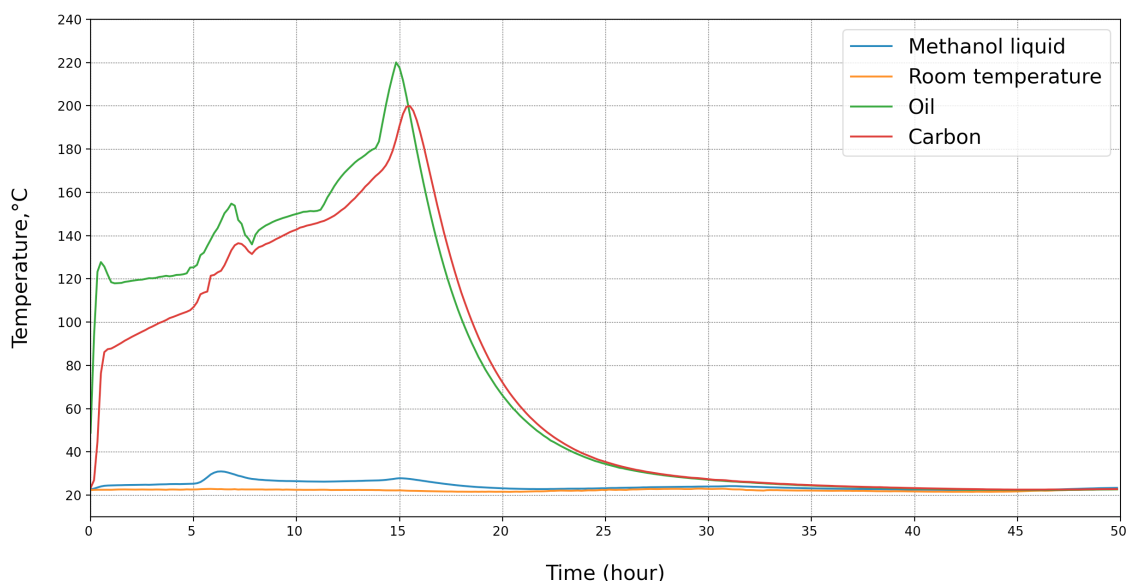

Figure 9.15: Final desorption

9.3 Adsorption uptake findings

In pursuit of generating the most robust dataset, it is critical to maintain a consistent temperature for the carbon. This not only enhances the accuracy of pressure logs but also ensures the reliability of methanol quantity during the adsorption and desorption processes. A feasible method to maintain this temperature constancy involved heating the carbon using water in a pot. By boiling the water, a stable temperature of approximately 100 °C could be achieved. However, the stove used for heating the water offered limited temperature regulation options, posing a challenge during tests requiring lower temperatures. To promote even heat distribution to the carbon, a layer of steel material was placed at the base of the container to elevate it from the plate, thus preventing excessive heating of the bottom section of the carbon compared to the entire bottle. For comparative analysis, it was essential to test the setup under elevated temperature conditions as well. Consequently, the water was substituted with oil, thereby enabling the attainment of higher carbon temperatures due to the oil's higher boiling point.

Upon the completion of these preliminary tests, it was resolved to conduct subsequent experiments without interference. These experiments were divided into two tests with water and the other with oil as the heating medium. With water, it was feasible to sustain a temperature of 100 °C during the desorption phase. The first simulation, however, only delineates a response of the

adsorption pair under absolute vacuum conditions since it was the initial test with new carbon. When comparing the weight of the two simulations, it becomes apparent that the adsorption process unfolds quite linearly. M.Li et al, investigated the experimental study of adsorbent pairs, reported similar findings [19]. The graphs reveal a smooth curve that progressively flattens towards the end, mirroring the patterns observed in our simulations. It is worth noting that the amount of methanol is directly dependent on the energy of adsorbent it accepts. In essence, the more energy the methanol adsorbs, the more effectively the carbon adsorbs the refrigerant. This phenomenon aligns with our observations, though the specifics of the heat input remain elusive.

The first simulation manifested a maximum adsorption of 0.21875 $kg\ kg^{-1}$, corresponding to a reduction of 175 grams of methanol. The second simulation, however, recorded a lesser decrease of 91 grams of methanol, followed by an escalated pressure of 20 mbar when compared with the preceding test. This increase in pressure could potentially come from variations in adsorption duration, or perhaps due to insufficiently low pressure preceding the adsorption process. It is noteworthy that the extended duration of the adsorption phase significantly surpasses the optimal time frame, thereby reinforcing the criticality of uniform methanol distribution within the system. Simulations employing oil as a heating medium exhibit similar trends. Elevated temperature seems to enhance desorption efficiency, as illustrated by the total reduction of 112 grams, implying a desorption efficiency of 64%, superior to that achieved with water. Despite the long adsorption phase, which spanned almost two days, the system failed to evaporate a significant quantity of methanol. The pressure levels observed during the oil simulations had considerable similarity to those noted in the water experiments. It is important to underscore the challenges associated with accurately reading the pressure levels, which introduces potential sources of error. Comparing the analysis of oil and water simulations reveals that despite the temperature increase associated with oil, the carbon cool down period remains unaltered. This finding may substantiate the hypothesis of minor variations in methanol evaporation, irrespective of the heating medium. When regard to desorption, a high temperature of 200 °C has proven to achieve complete desorption of methanol It remains feasible that lower temperatures may achieve this occurrence, however, due to the limited number of simulations conducted, this proposition remains unsubstantiated.

9.4   Isotherm and isobar characteristics

The primary objective of collecting adsorption and desorption data was to establish a simulation script capable of visualizing the adsorption characteristics. The Dubinin-Radushkevich (D-R) equation was employed to generate isobars and isotherms for the studied system. To verify the authenticity and reliability of the applied script, El-Sharkawy et al.'s work was utilized as a reference to reproduce the simulation data [16]. The successful replication can be visualized in Figure 9.16. However, when applying the identical code to our simulation data, several noteworthy differences is important. The primary discrepancy lies in the execution of the experiments. In the findings of El-Sharkawy et al., the temperature of the evaporator and the adsorbent was maintained constant, and uptake was measured at equilibrium. This equilibrium was not achieved in our experiments, as previously discussed. The trials witnessed fluctuations in evaporator temperatures, with the adsorption being recorded during the carbon cooling phase. Furthermore, the measurements were taken as part of an adsorption cycle comprising both adsorption and desorption. As a result, the adsorption was considerably lower than the optimal maximum uptakes, which could have been measured with complete methanol removal. Moreover, due to the manual nature of data logging, some pressure and uptake data at the onset of adsorption were missing, as the event occurred during night hours. Thus, the experiment does not fully align with the intended application of the D-R equation. Nevertheless, despite these limitations, this experiment provides valuable data, which can serve as a foundation for subsequent exploratory endeavors.
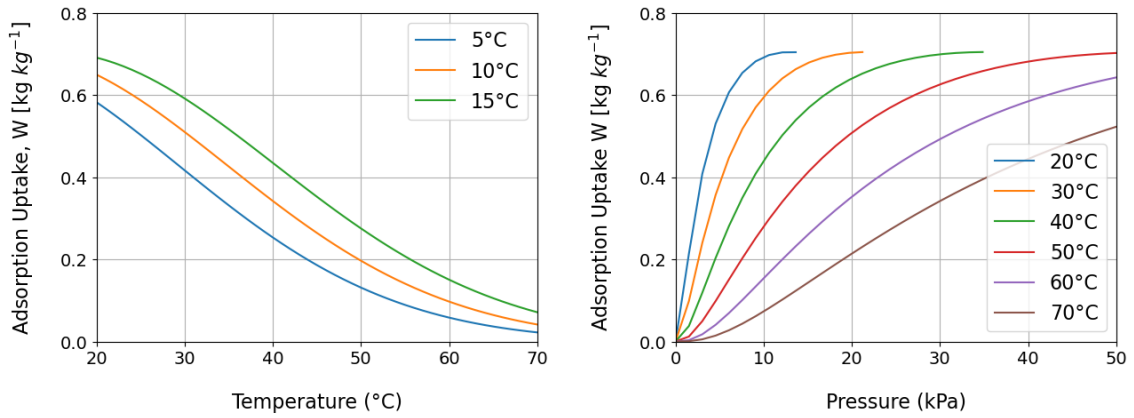
(a) Isobar lines at three different evaporator temperatures

(b) Isotherms for a selection of saturation pressures corresponding to the temperatures given

Figure 9.16: Adsorption characteristics for activated charcoal and methanol replicated from the constants of Sharkawy et.al [16].

The formulation of adsorption attributes commences with the computation of Dubinin-Radushkevich (D-R) constants, specifically W_0 and D. These constants are obtained through a linear approximation of the D-R equation. A visual representation of this approximation is provided in Figure 9.17. As observed from the figure, the fitting process displays an accuracy of 98%, which suggests a commendable outcome. Alternatively, refining the exponent of n may contribute to enhanced fitting accuracy when applying the Dubinin-Astakhov (D-A) equation. The resultant values for W_0 and D are tabulated in Table 9.1, where the experimentally determined data is compared with the findings from El Sharkawy et al.

Table 9.1: Coefficients for D-R equation

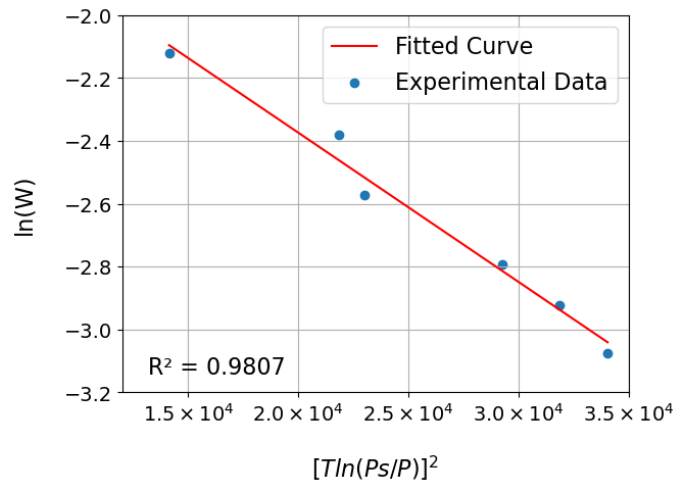|	W_0	D
Experimental data	0.2405	$4.75 * 10^{-5}$
El sharkawy et.al	0.705	$3.012 * 10^{-6}$

Figure 9.17: Linear fitting of the D-R equation

After extracting data from the linear fitting, the adsorption characteristics can be plotted. These isobars and isotherms can be pictured in Figure 9.18. Upon examining the isobar and isotherm graphs in the adsorption system, several noteworthy properties emerge. Initially, an important ob-

72

servation is that the adsorption capacity of the system, referring to the total volume of adsorbate it can accommodate, increases proportionally with pressure. During adsorption, adsorbate molecules transition from a bulk phase, either gas or liquid, to a solid surface, namely the adsorbent. The principal motivator for this process is the interaction between the adsorbate molecules and the adsorbent surface. An increase in the adsorbate's pressure prompts more molecules towards the adsorbent surface, thus providing more opportunities for adsorption to occur. Consequently, more adsorbate molecules can attach to the surface, thereby enhancing the adsorption capacity. However, there exists a certain threshold, beyond which, regardless of further pressure escalation, the adsorption capacity remains static due to the limited number of available adsorption sites on the surface.

Contrastingly, a rise in the system's temperature generally results in a decline in adsorption capacity. This can be attributed to the fact that adsorption is an exothermic process, characterized by the release of heat as the adsorbate binds to the adsorbent. Therefore, the introduction of heat to the system provides the energy necessary for the adsorbate to detach from the adsorbent and return to its original gas or liquid phase. Thus, there exists a disagreement where higher pressures encourage adsorption by directing more adsorbate molecules towards the adsorbent, but higher temperatures induce desorption by supplying the energy needed for the molecules to disengage. This interplay presents a challenge since temperature and pressure often operate in conjunction, necessitating independent regulation of both parameters.

A key element in this context is the need for methanol to be subjected to vacuum pressure in order to facilitate evaporation for adsorption. By reducing the system pressure beneath the vapour pressure of the adsorbate, the latter undergoes a transition from liquid to gas form. Following the methanol's entry into the vapour phase, the driving force behind adsorption is the variance in chemical potential between the vaporous methanol and the methanol adsorbed onto the carbon. As carbon proceeds to adsorb methanol from the vapour phase, the system pressure decreases, which induces further methanol evaporation and subsequent entry into the vapour phase for adsorption. Consequently, the ideal conditions would involve a significantly low pressure to vaporize the methanol, while maintaining relatively high pressures to enhance adsorption. This presents a conundrum as these conditions cannot coexist in an open system. Increased pressure hinders evaporation, whereas decreased pressure limits adsorption. For optimal system performance, it may be beneficial to compartmentalize the system into multiple stages or zones, for instance, one evaporation stage at low pressure and an adsorption stage at higher pressure. However, such a configuration is unattainable in a simplistic adsorption system.
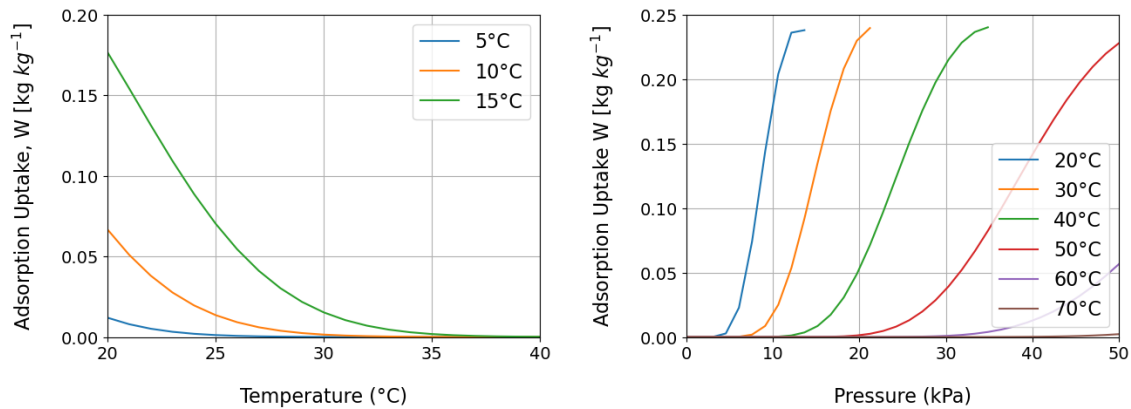
(a) Isobar lines at three different evaporator temperatures.

(b) Isotherms for a selection of saturation pressures corresponding to the temperatures given

Figure 9.18: Adsorption characteristics for experimental data showing isotherms and isobars at various temperatures

9.5 Modified system analysis

Insufficient control over the collector temperatures may have resulted in transformations of methanol. Unstable methanol may lead too an uneven cooling process which can be seen from the reduction in desorption for each successive operation followed by a shorter adsorption. Furthermore, the collector pressure increased which can support the claim of formation of other compounds occupying the voids. Given these challenges with the initial prototype, modifications have been made to the system, including the integration of additional thermocouple sensors within the collector to more accurately monitor the temperatures of both carbon and methanol. The modified system also incorporates further copper piping to facilitate improved methanol distribution. Considering the issues encountered with the collector cores' ability to achieve necessary heat levels, the introduction of more pipes will decrease the distance between the methanol and the heated carbon, consequently promoting more efficient heat distribution. Additionally, the original system's evaporator possessed excessive volume, resulting in a water bath larger than required. Hence, in the modified system, water has been removed to assess its impact on enhancing evaporator measurements. The quantity of methanol has also been reduced, only employing the portion that has undergone desorption. The simulations of the modified system configuration are presented in the subsequent section.

9.5.1 Preliminary tests

Following the new implementation of modifications to the system configurations, particularly in relation to the collector design, the cooling system was once more subjected to testing. Upon the integration of new activated carbon and the decrease in methanol quantity, a pressure test employing nitrogen gas was conducted. In order to ensure the comprehensive removal of nitrogen from the carbon, the collector was subjected to high temperatures. In the context of the revamped configuration, temperature sensors were installed within the collector, thereby enabling the measurement of the center temperature of carbon and methanol. The temperature of the carbon was rapidly elevated to 150 °C, which served to vaporize the nitrogen. The simulation initiates with a center temperature of 115 °C within the collector. The temperature of the activated carbon at this juncture is 71 °C, from which point the cooling process commences. Contrary to preceding trials, the mass flow has ceased entirely. Nonetheless, there persists an unbroken cooling trajectory from this point, extending roughly eight hours into the simulation. The evaporator coil manifests a temperature reading as low as 3 °C at the deepest measurement point after a duration of seven hours.

The evaporator components is shown in detail in Figure 9.19. The data illuminates that the evaporator coil section attains the most significantly reduced temperature, predominantly in the two median coils, specifically Coil 1 top and Coil 2 bottom. The minimum recorded temperature approaches approximately 3.1 °C. The inferior region of the cooling chamber has attained a temperature of approximately 8.7 °C. The graph elucidates the challenge in maintaining a consistent temperature throughout the entire cooling chamber. Exclusively within the cooling chamber, a discrepancy of 4.2 °C is observed between the superior and inferior ends. Paralleled data can be extracted from the evaporator coil, where the most substantial deviation occurs between the top and bottom of Coil 2.
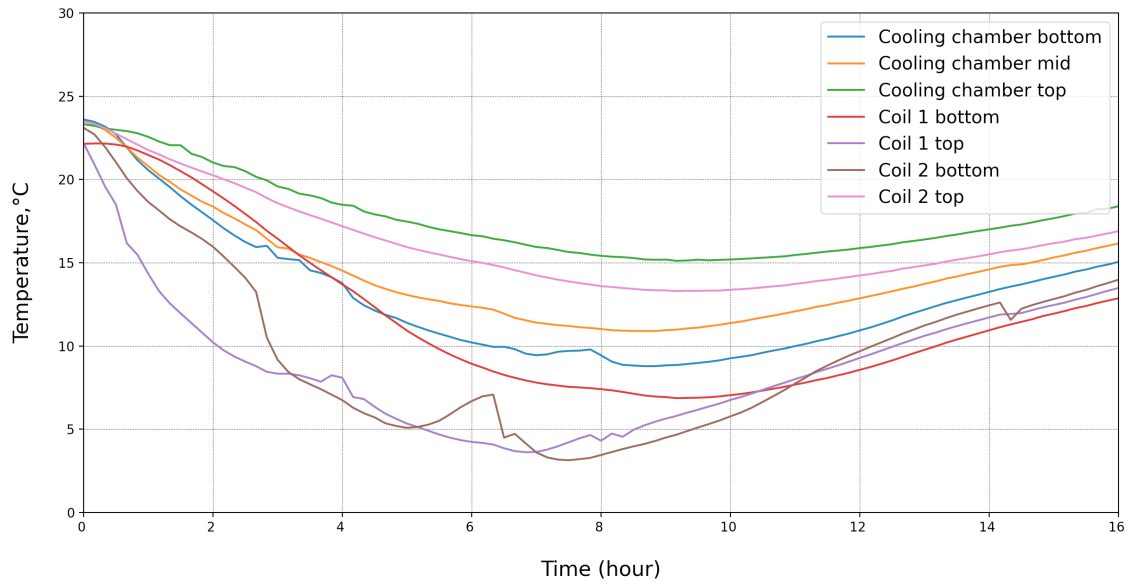
Figure 9.19: Preliminary adsorption test

One of the significant challenges afflicting the cooling system pertains to the difficulty in sustaining a sufficiently low pressure throughout the entire desorption process. This issue is attributable to the inherent correlation between temperature and pressure. As the former increases, the latter escalates which corresponds to an elevated boiling point. If the pressure could be maintained at a consistently low and stable level, this could potentially facilitate a more efficient cooling process. This hypothesis was subjected to testing by the utilization of a vacuum pump throughout the cooling process. This simulation is operating at a temperature of 135 °C. At this juncture, the methanol maintained a temperature of 95 °C and the mass flow reached a maximum of 35 °C. Subsequent to two hours of effective heating, the collector was cooled down. The simulation illustrates that the commencement of the cooling process occurred relatively promptly.

An in-depth examination of the evaporator is delineated in Figure 9.20. This graphical representation illustrates the temperature spectrum of the cooling chamber in conjunction with the temperature measurements from various points on the evaporator coil. As previously mentioned, the cooling process initiates almost instantaneously following the deactivation of the heat source. The most significant decrement occurs in the lower portion of the evaporator coil, where the temperature descends to the freezing point of water. Consequently, the bottom of the cooling chamber attains a temperature of 4.5 °C. This particular temperature range is not only ideal for the formation of ice but also beneficial for the cooling chamber as it establishes an environment conducive for food preservation. After approximately nine hours, the vacuum pump was disengaged, resulting in a subsequent increase in temperature. However, it is not ideal having a continuous operation of a vacuum pump each time the system is active, not only due to practical concerns but also the difficulty in procuring such equipment. Upon disconnecting the pump, the pressure resumes an upward path, consequently stopping the cooling process.
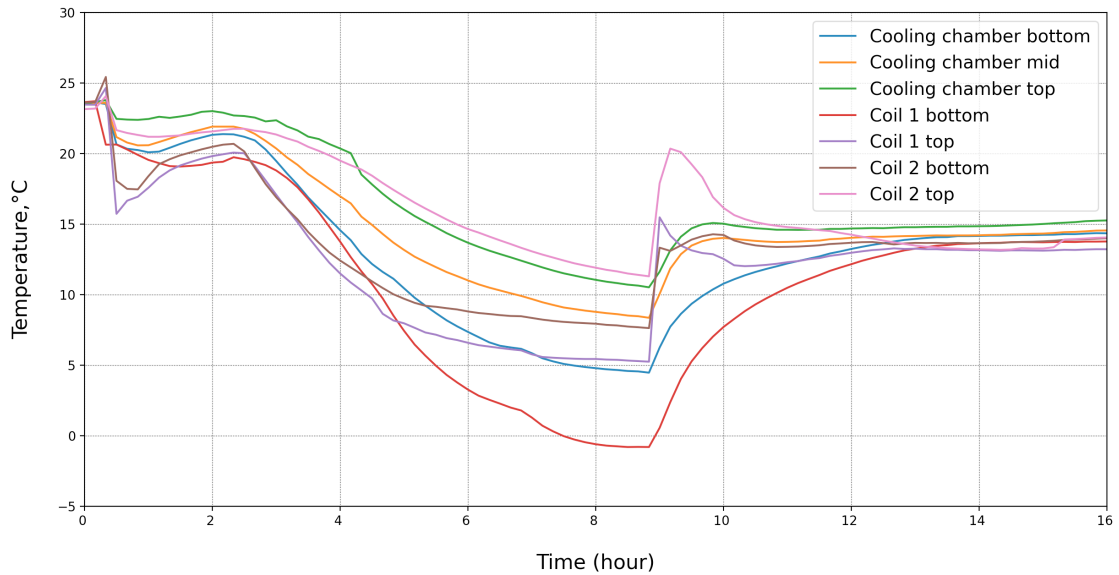
Figure 9.20: Preliminary adsorption test with valves closed

9.5.2 Simulation one

In conducting preliminary tests using reduced methanol quantities, the system was maintained at 110 °C. This was done to ascertain whether lowering the methanol content would have a more significant impact on the cooling effect compared to previous outcomes. As depicted in Figure 9.21, the total duration of heating was approximately nine hours. However, the massflow as indicated by the condenser inlet sensor, lasted approximately eight hours. Getting the carbon temperature at desorption temperature took around an hour, from where it increased steadily towards the target temperature. With a temperature of 110°C the heating process used two hours to reach 100°C and nine hours to finally reach 110°C. The onset and cessation of desorption are recognized by changes in temperature at the condenser inlet, indicative of mass flow changes. The massflow initiation can be identified when the activated carbon reaches approximately 70 °C, increasing steadily until it plateaus at 42 °C. It is notable that the surface temperature of the collector and the internal temperature of the carbon are equivalent, while the center temperature of the collector is considerably lower, suggesting low thermal conductivity towards the centre.

When the temperature between the heating cable and steel wall ΔT is small, so is the temperature gradient. The poor thermal conductivity of the carbon is especially seen in the core temperature marked in green. There is naturally a slower temperature increase on the inside than the outside but as the temperature reaches 70°C the temperature gradient is substantially slower. However, the lower temperature gradient in the core might very well be due to the boiling point of methanol. As the temperature in the system increases, so does the pressure and subsequently also the boiling point of methanol.

Figure 9.21: Simulation one, heating at 110 degrees

The adsorption phase begins as the temperature of the carbon drops to around 70 °C, as discerned from the evaporator coil's readings. Thus, both adsorption and de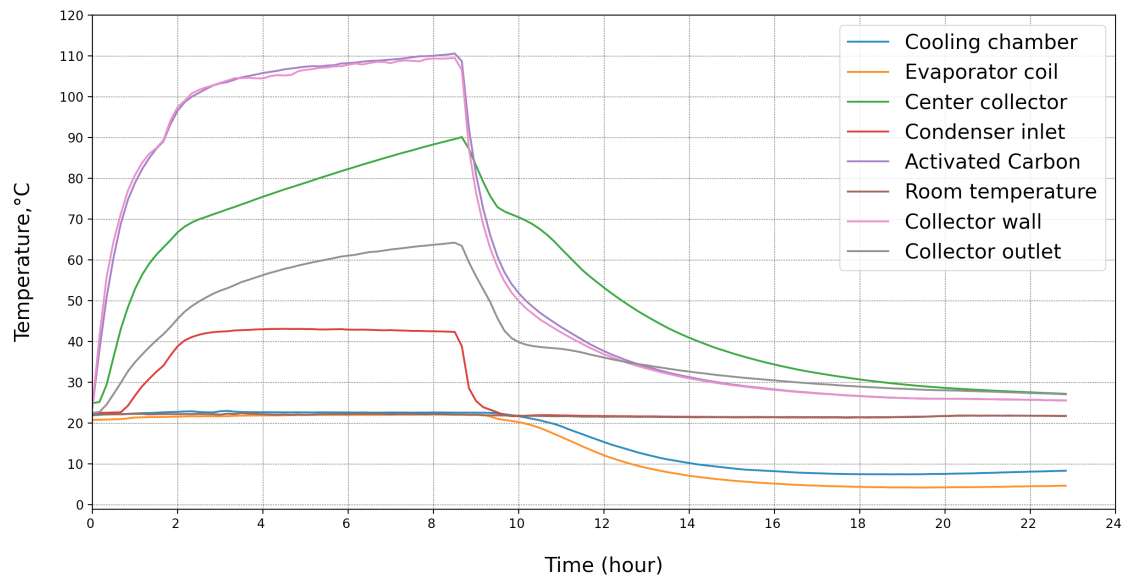sorption processes commence at approximately 70 °C. The adsorption phase persists for about ten hours, during which the minimum temperature registered is 4.2 °C, resulting in a total cycle time of nearly 20 hours. Observing the evaporator alone, several sensors are placed to detect thermal stratification and the location of methanol evaporation. A detailed representation of the evaporator's data is provided in Figure 9.22. Within the cooling chamber, there is a discernible temperature disparity across the chamber. At the end of the adsorption, a temperature difference of four degrees Celsius is recorded between the top and bottom of the chamber. The mid-point sensor provides evidence of a temperature gradient within the chamber.

Regarding the evaporator coils, the observable pattern is likely attributable to diminishing quantities of methanol in the pipes. At the onset of adsorption, methanol positioned at the top of the coil starts evaporating. As the methanol adsorption continues, the evaporation process is eventually confined to the lower sections of the coil. Given that the evaporator is divided into two coils, evaporation commences at the top of each coil and gradually extends downwards. This process likely explains the stagnation observed in the upper coil once the temperature drops below 14 degrees Celsius, followed by a subsequent increase. This pattern is also evident in the bottom section of the upper coil and the top of the lower coil. Despite an early stagnation the upper coil resumes its temperature decrease As the system cools down, with the cooling process localized at the bottom of the container. Irregularities in methanol distribution can be discerned from the graph, particularly in the lower coil, which exhibits a longer cooling production duration than the upper coil. Methanol regenerated in the system is distributed to both coils through a T-pipe, which could potentially lead to uneven distribution.
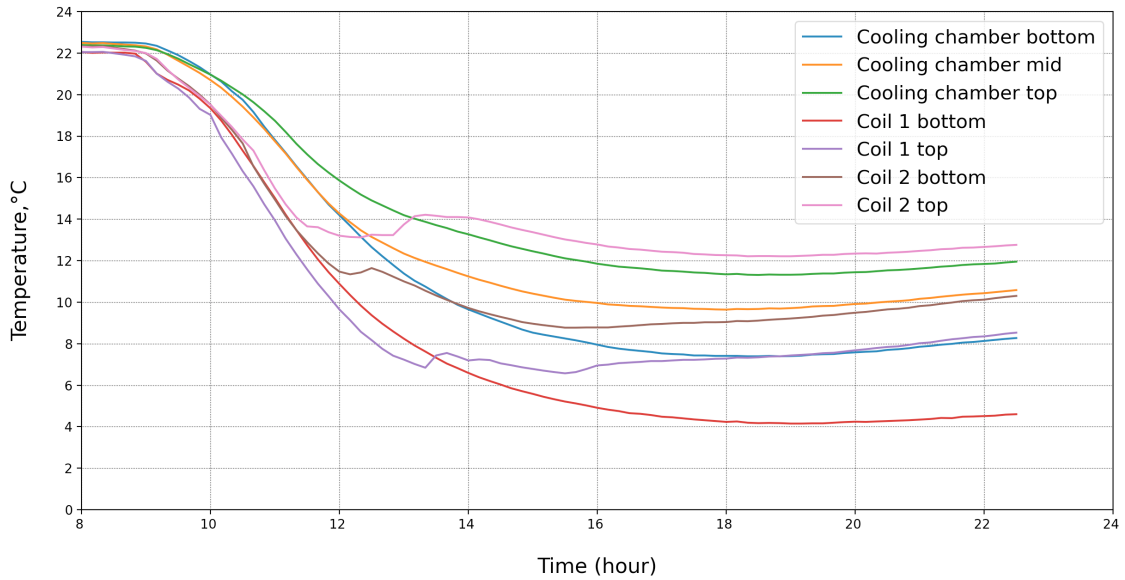
Figure 9.22: Adsorption curve for the evaporator during simulation one

9.5.3 Simulation two

Figure 9.23 shows the adsorption curve for heating at 110 °C. For this particularly case, the valves are closed from the start, which means that the valve between the collector and condenser is closed, as well as the valve between condenser and evaporator. Consequently, significant mass flow was not observed until 2.5 hours into the desorption phase. This is due to the valve being closed at this point. Upon opening the valve on the collector side, the mass flow experienced an immediate increase at a temperature of 47 °C. However, the system did not manage to hold this flow for long, witnessing a sharp decline after a 20-minute duration. The heating was stopped after 7 hours and the evaporator valve was subsequently opened once the collector temperature fell below 50 °C. The cooling process commenced after the system had been running for 10 hours and reached a bottom of 8.3 °C.
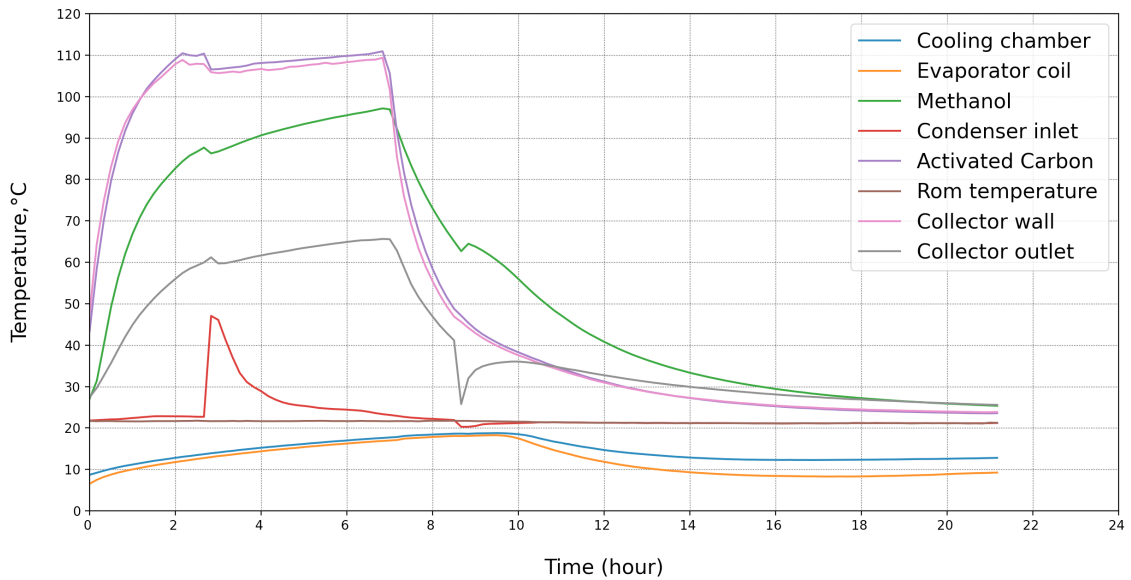
Figure 9.23: Simulation two, heating at 110 degrees with valves closed

9.5.4 Simulation three

Figure 9.24 presents the complete cycle with the collector subjected to heating at 95 °C. It is compelling to observe the differences in the cooling process under the influence of varying collector temperatures. The central section of the collector, containing the methanol, achieves a temperature of 85 °C. In alignment with numerous tests, a persistent challenge lies in maintaining the mass flow, which was only sustained for the initial three hours. Nevertheless, the desorption process proceeded without interruption, despite the absence of flow. Following eight hours, the heat supply was discontinued and the adsorption process was initiated as soon as the collector outlet reached a state of stagnation, approximately ten hours into the cycle. From this juncture onwards, cooling was observed and it reached a temperature of 12 °C around the 16-hour mark.
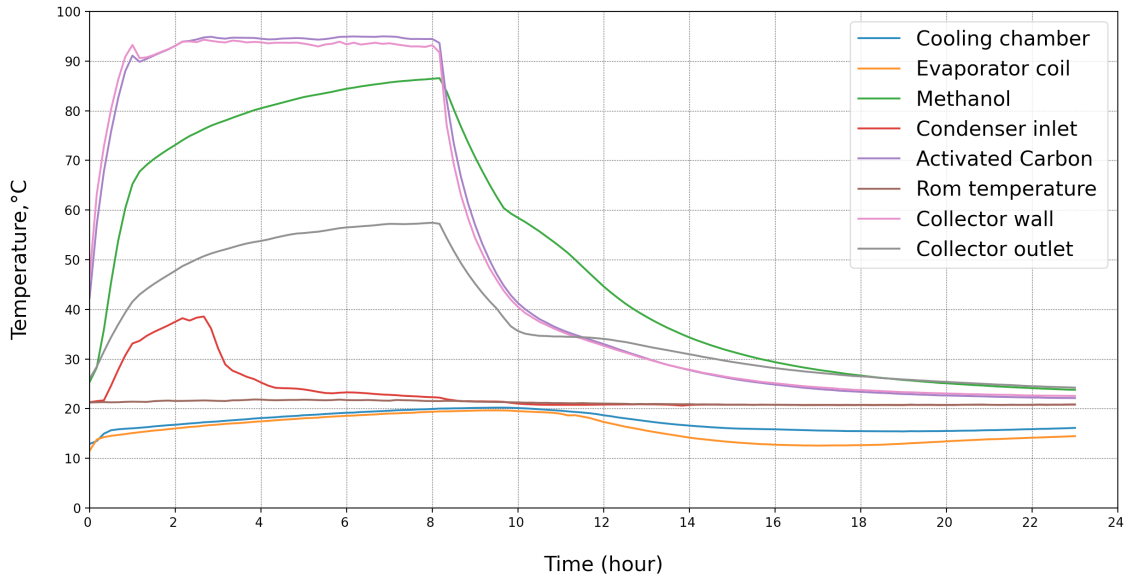
Figure 9.24: Simulation three, heating at 90 degrees

9.5.5 Simulation four

The impact on the cooling process from terminating the heat supply when the mass flow stops is depicted in Figure 9.25. The previous test had disappointing outcomes as the mass flow stopped relatively early despite the heat supply lasted for considerable duration. The collector temperature decreased rapidly after 5 hours when the heat was switched off. However, the figure displays a marginal temperature decline in the evaporator. An intriguing aspect of these dynamics could be the change in system pressure. There is a manometer situated at the outlet from the collector and another positioned just before the inlet to the evaporator which measures the pressure. Unfortunately, these pressure measurements are not automatic, necessitating manual data reading. For the remaining simulations, the pressure was registered.
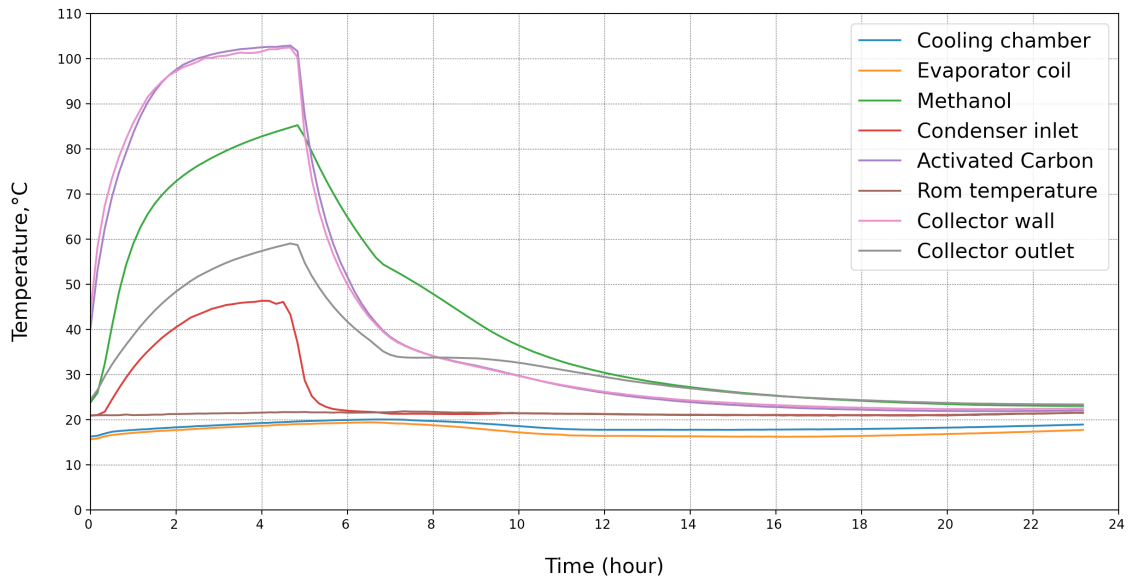
Figure 9.25: Simulation four, heating at 100 degrees

9.5.6 Simulation five

In the subsequent test, the pressure readings were recorded to analyze the variation in pressure both during the desorption phase and the cooling process. This simulation was executed with a collector temperature set at 110 °C. Figure 9.26 depicts the simulation where the desorption has lasted for a duration of eight hours, with mass flow present during the initial six hours. The rate of cooling achieved reached a bottom temperature of 14 °C after 17 hours. Figure 9.27 presents the corresponding pressure measurements. For the initial cycle, the pressure was first recorded after a span of 4.5 hours. Typically, pressure escalates as long as there is mass flow from the collector to the condenser. Nonetheless, a decrease is observed. This can be attributed to the infrequency of pressure readings, as there were few measurements taken between the first point at 4.5 hours and the 8-hour mark. The steep decline is a consequence of interpolation, which stipulate a pressure drop where it normally would have been elevated.
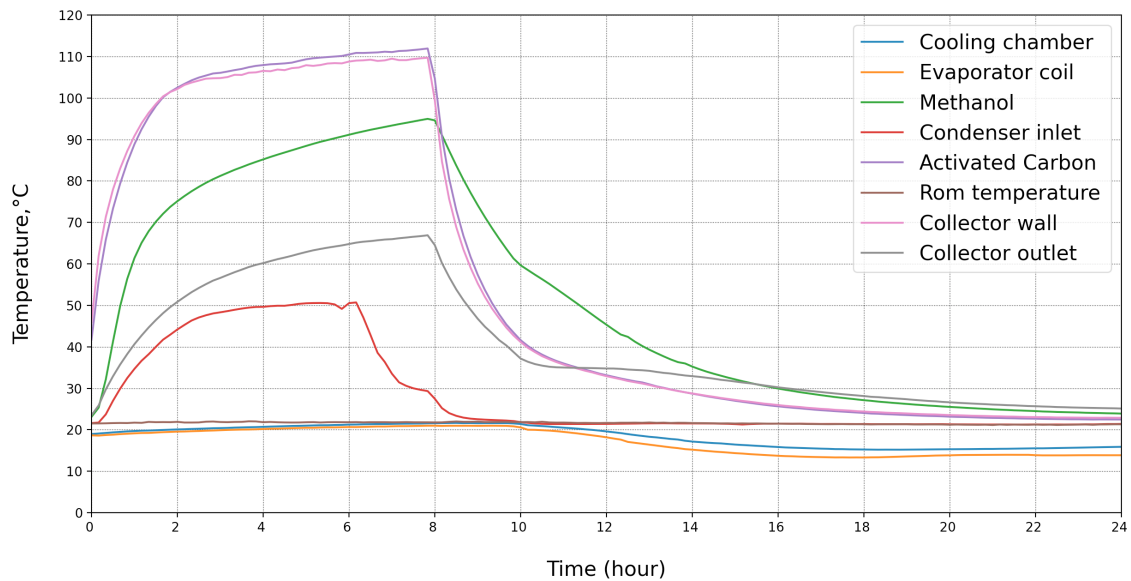
Figure 9.26: Simulation five, heating at 110 degrees
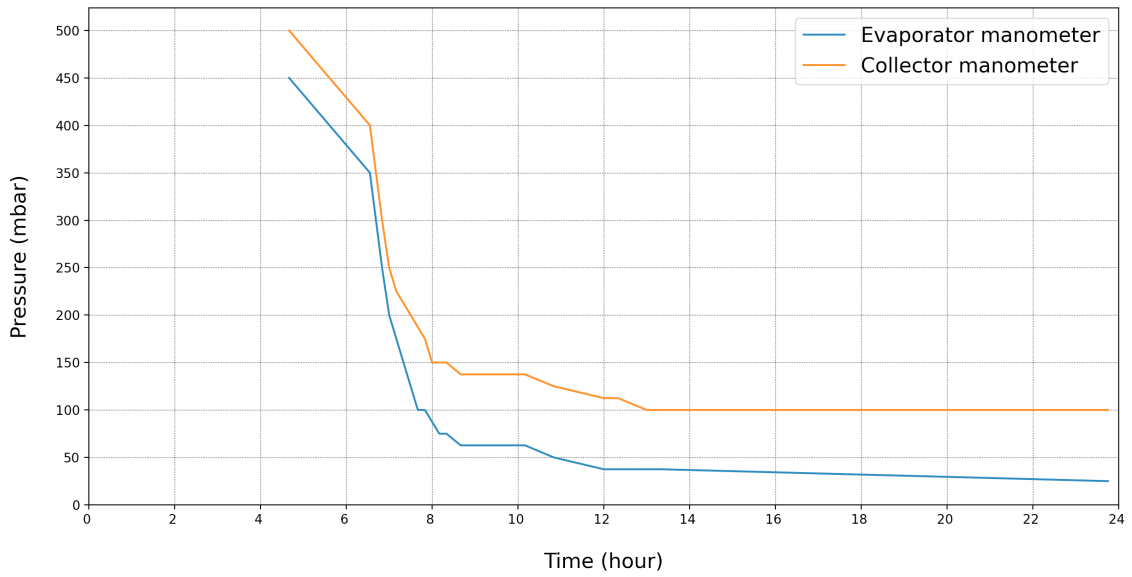
Figure 9.27: Pressure curve for simulation five

9.5.7 Simulation six

Figure 9.28 also undergoes heating at a temperature of 110 degrees, with corresponding pressure measurements shown in Figure 9.29. The desorption lasts for eight hours with an almost equally long mass flow resulting in a temperature of 8 °C in the evaporator. Despite the heating occurring at similar temperatures for simulation five and six, distinct pressure patterns are observed within the system. The maximum pressure is registered in the collector at 425 mbar, whereas in Figure 9.27, the pressure reaches 500 mbar under identical heating conditions. This event may arise due to the duration of mass flow, as it is evident that pressure decreases in both simulations when the flow into the condenser diminishes. The question is why this occasion occurs, whether the massflow decreases since the pressure cannot be maintained at the desired level anymore, or if the pressure decreases since there is no more methanol to desorb.
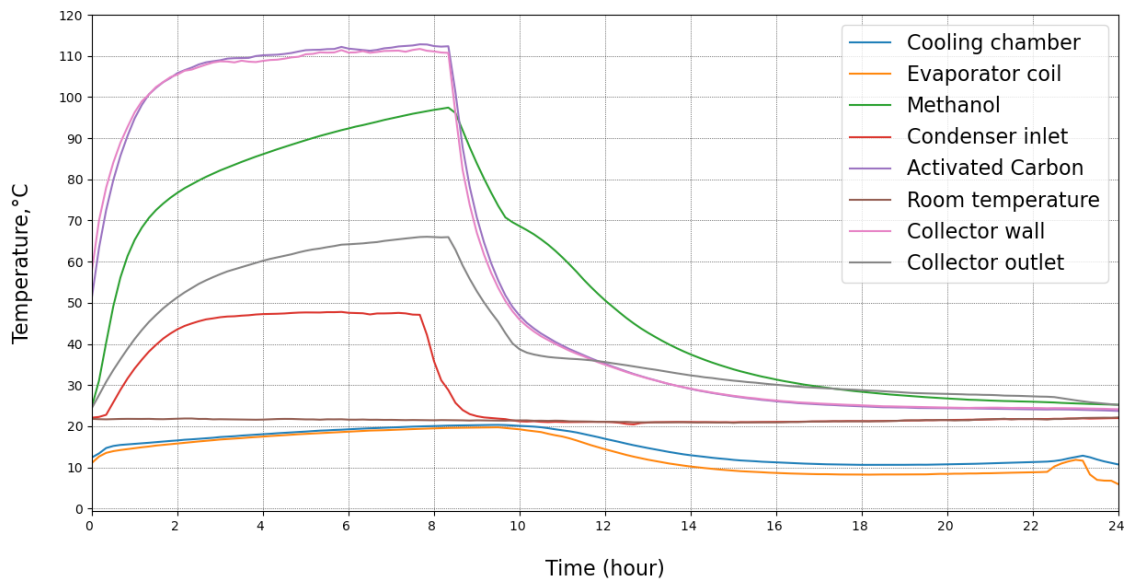
Figure 9.28: Simulation six, heating at 110 degrees
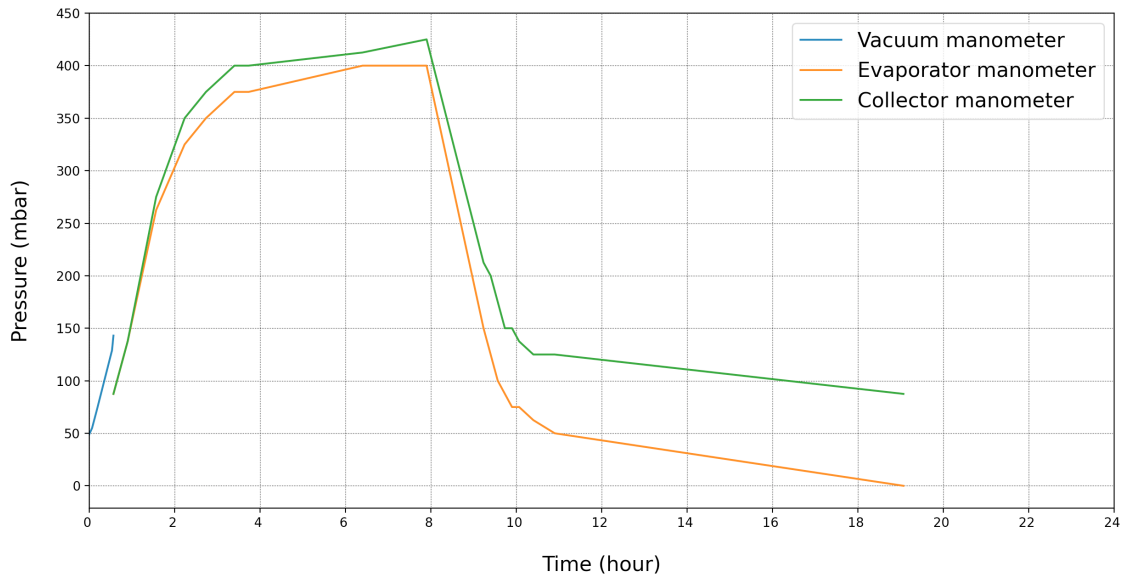
Figure 9.29: Pressure curve for simulation six

9.5.8 Simulation seven

Following a few days of cooling, an additional simulation was undertaken to corroborate the hypo-
thesis pertaining to escalated pressure. This refers to the scenario where the pressure increases if
the cooling process is not entirely finalized prior to the recommencement of desorption. The given
simulation demonstrates the heating of carbon to 120 °C, which might be perceived as marginally
high based on prior knowledge. However, provided the methanol does not surpass 120 °C, this
method is considered adequate. As indicated in Figure 9.30, it takes approximately four hours for
the carbon temperature to attain 120 °C. Interestingly, the collector outlet and carbon maintain
consistent temperature throughout the entire process. Furthermore, the mass flow persists for an
duration of 11 hours before exhibiting a decline. The heating process continues for another two
hours before being discontinued. Subsequently, every component of the system undergoes a de-
crease. The cooling phase for the collector commences 60 minutes after, followed by the initiation
of the cooling process in the evaporator. The plotted data reveals a remarkable temperature re-
duction in the evaporator coil, which precisely reaches a minimum of 0.73 °C. In accordance with
the previous pressure measurements, a decrease in pressure corresponds with a decrease in mass
flow for this case as well. In this particular test, where the system was allowed to reach absolute
vacuum, a lower pressure was attained despite the higher collector temperatures. This finding
underscores the criticality of fully evacuating the methanol from the evaporator before initiating
a new desorption cycle, in order to achieve optimal performance.
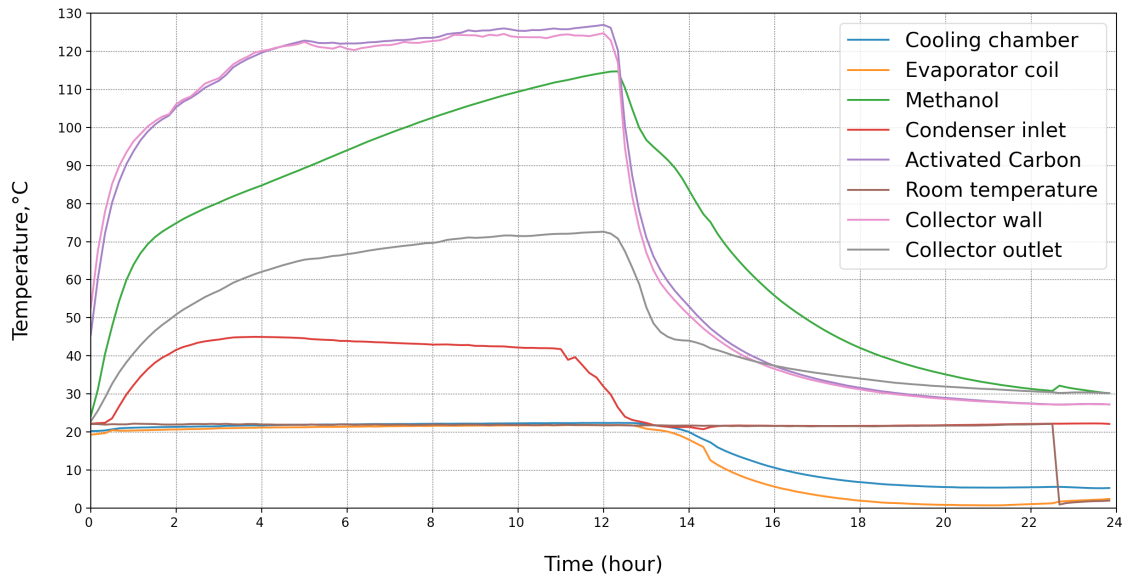
Figure 9.30: Simulation seven, heating at 120 degrees

The most favorable outcomes are attained when the evaporator temperature is set at 20 degrees, corresponding to an approximate saturation pressure of 127 mbar. On revisiting Figure 9.31, it becomes apparent that the initiation of the adsorption process is equal with this pressure layer. A similar pattern emerges in Figure 9.27, where the adsorption phase is noted to take place within the 120-130 mbar ambit. The limited availability of pressure data introduces an additional level of insecurity to the simulation analysis. Nonetheless, it is feasible to examine simulations that were less effective, wherein adsorption failed to manifest. The unifying attribute in these instances is the exceedingly low evaporator temperatures at the start of the simulation. This indicates that the system must attain substantially lower pressures for the cooling process to be activated, suggesting that a truncated adsorption period could result in a sub-optimal cooling process.
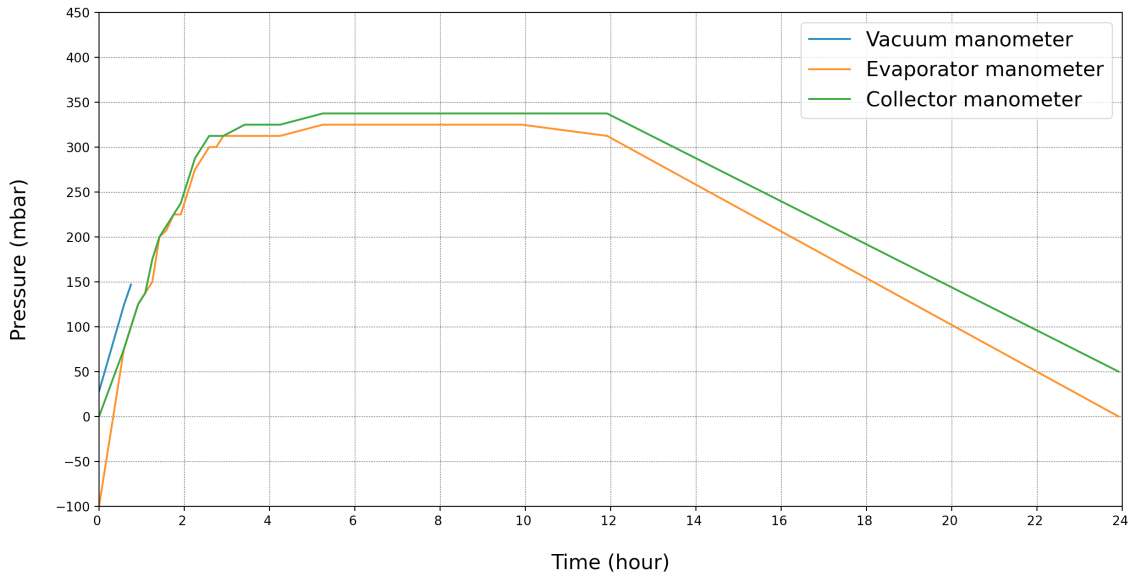
Figure 9.31: Pressure curve for simulation seven

In the evaporator, the location of the actual cooling process, is provided in Figure 9.32. The segment exhibiting the lowest temperature is the measurment at Coil 1 bottom, positioned closest to the base. This particular area records a temperature almost 5 °C lower than the next coldest

segment, the bottom of the cooling chamber. Idealistically, a more uniform temperature distribution would be anticipated throughout the cooling process. Although most parts of the evaporator do exhibit consistent temperature readings, the irregularity could be attributed to the adsorption process occurring predominantly within the bottom coil. It stands to reason that the gravitational force would facilitate the methanol liquid to flow to the system's lowest point, which, in this case, is the bottom of the coil.
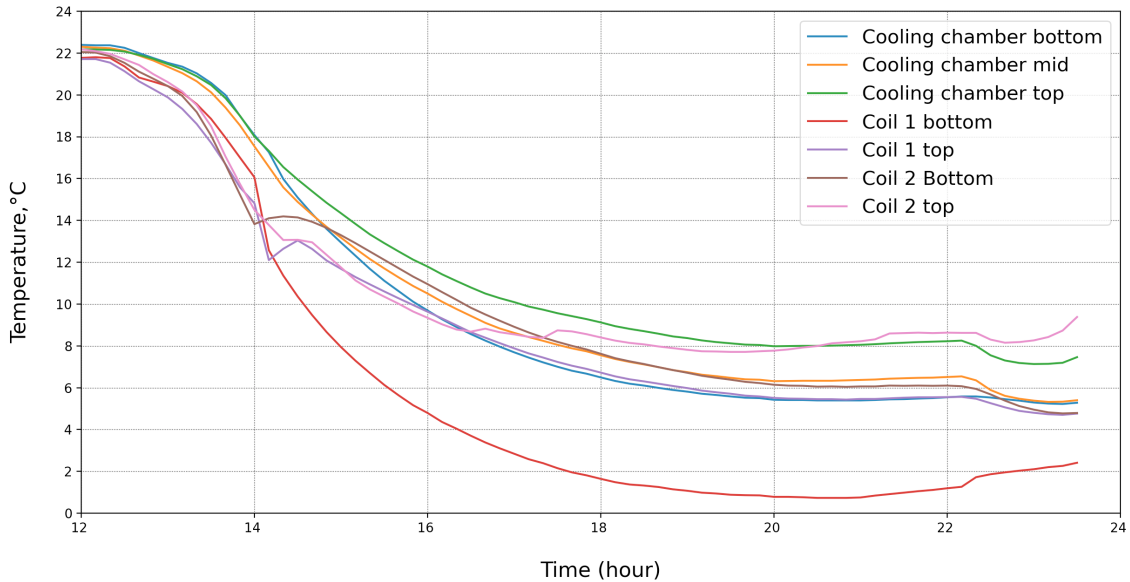
Figure 9.32: Adsorption curve for the evaporator during simulation seven

9.5.9 System pressure characteristics

The observation of pressure variations within the manometers for the collector and evaporator, respectively, raises intriguing queries. Notably, as a closed system, the pressure within the system should theoretically maintain uniformity throughout. However, distinct pressure readings are reported between different tests, even when conducted under identical temperature conditions. This discrepancy could potentially be attributed to incomplete adsorption of methanol prior to the desorption phase, thereby inhibiting the system from reaching absolute vacuum before the subsequent test. This theory is supported by vacuum pump trials between tests, where difficulties in attaining sufficiently low pressure potentially indicate methanol leftovers within the evaporator. A close study of pressure measurements from two different tests illustrates discernible differences. An examination of Figure 9.29 demonstrates that over a span of eight hours, with a carbon temperature maintained at 110 °C, the pressure escalates from an initial 50 mbar to a peak of 425 mbar. This escalation coincides with the cooling process ending at a temperature of 8 degrees Celsius. In contrast, Figure 9.31 presents a scenario where the carbon temperature is set at 120 °C, with the pressure commencing at absolute vacuum and achieving a pressure of 330 mbar. When comparing these two simulations, it is noteworthy that a lower pressure is achieved even in the presence of a higher temperature. The experiment conducted at 120 °C benefited from an extended cooldown period of three days, leading to complete adsorption of methanol within the evaporator. This observation indicates that exposing the system to a higher temperature while maintaining a lower initial pressure results in enhanced cooling efficiency.

The significance of evaporator temperature within the cooling process initiation has been emphasized in the work of Vingelsgård [1]. There are mainly two pressure levels in the system that are particularly noteworthy, specifically, those in the condenser and the evaporator. Given that the condenser comprises a sizable water bath, the saturation pressure remains constant due to the stability of the temperature. On the contrary, the evaporator exhibits a range of temperatures, as elaborated previously. Consequently, the evaporator temperature governs the saturation pressure, indicating that an elevation in temperature would lead to a corresponding rise in the saturation pressure of methanol. Figure 9.33 illustrates the saturation pressure of methanol at varying temperatures, clarifying that an increase in temperature may expedite the adsorption process.
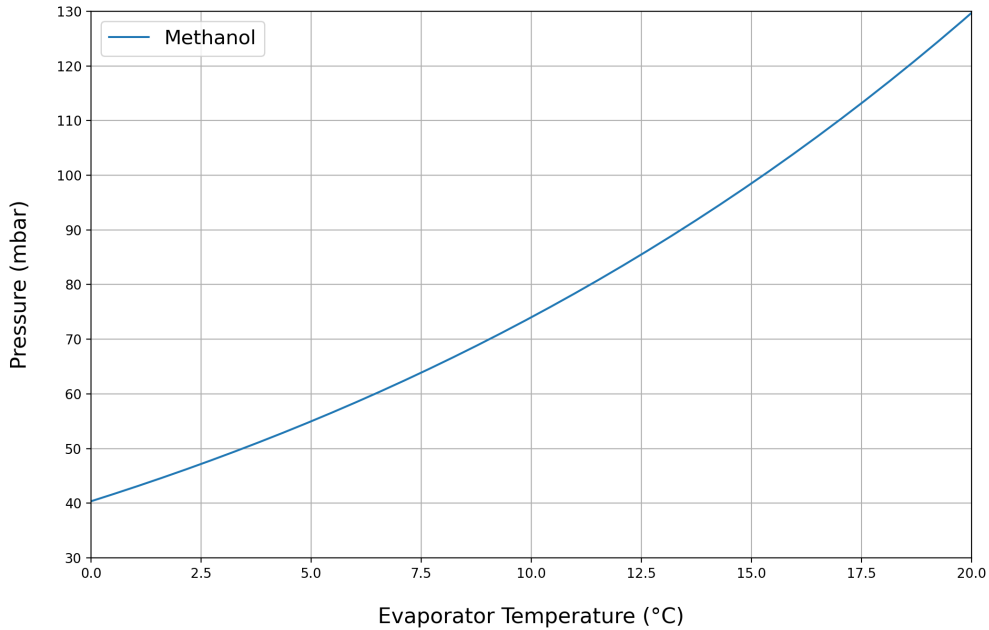
Figure 9.33: Saturation pressure diagram for different temperatures for methanol

Optimal results are observed when the evaporator temperature stands at 20 °C, corresponding to a pressure of approximately 127 mbar, as depicted in the graph. El-sharkawy et al, has investigated this situation and observed that the uptake and cycle performance of the system decreases with lower evaporator temperature. Revisiting Figure 9.31, it is evident that the onset of the adsorption process aligns with this pressure level. Similarly, in Figure 9.27, where the adsorption phase was observed to occur in the vicinity of the 120-130 mbar range. The lack of pressure data adds a layer of complexity to the comparison of other outcomes. However, it is plausible to investigate less successful simulations where adsorption has not been triggered. The unifying factor in these scenarios is the exceedingly low evaporator temperatures at the commencement of the simulation. This signifies that the system must reach significantly lower pressures to initiate the cooling process, implying that a shorter adsorption duration could lead to an ineffective cooling process. [16]

9.6 Modified system simulation findings

The revised system design has incorporated several critical modifications. Firstly, the introduction of thermocouple sensors within the collector is a substantial change that allows for precise monitoring of both carbon and methanol temperatures at the collector's center point. Under the original prototype structure, the system was primarily regulated through a single measurement point at the collector outlet. Given copper's notable thermal conductivity, there was a presumption of uniform internal and external temperatures. However, the applicability of the methanol temperature as a universal standard has been brought into question. Given the substantial dimensions of the collector, it might have been more pertinent to utilize the carbon temperature as the fundamental parameter for the conducted temperature simulations. Unfortunately, due to the logistical challenges posed by the prototype simulations, methanol temperature was instead selected as the operational baseline. A comparative analysis of the outlet temperature in the modified configuration system with the methanol temperature at the collector's center yields intriguing insights. During an eight hour simulation at 120 °C, the thermocouple sensor positioned at the collector outlet recorded a temperature of 110 °C, whereas the corresponding collector outlet temperature was only 71 °C. This represents a significant discrepancy of nearly 40 °C, suggesting that inferring the internal methanol temperature solely from the outlet temperature can lead to inaccurate conclusions.

As an illustrative case, considering the third prototype simulation, wherein the collector outlet temperature neared 115 °C. When compared with the outcomes from the upgraded configuration system, this translates to an excessively high methanol temperature of 150 °C, which is highly undesirable. According to Goyal et al, the operator desorption temperature for methanol is below 120 °C [38]. Deviations significantly above this benchmark could cause the transformation of methanol into other gases, thereby jeopardizing the system's integrity. More alarmingly, such temperature anomalies could weaken the cooling process altogether.

The reconfiguration of the internal copper pipes within the collector constitutes another significant alteration. Instead of a singular pipe, the system now integrates five interconnected pipes. The design maintains the original pipe but supplements it with four smaller identical pipes. The prototype's original pipe was engineered with slits/slices, with the outer wall of the copper pipe featuring 10 cm long and 1 mm wide apertures to facilitate the flow of methanol. To inhibit the descent of carbon into the pipe while still ensuring free flow of methanol, a mesh netting was wrapped around it. This particular method was also adopted for the additional copper pipes incorporated in the redefined configuration. While this slice procedure is an efficient means of promoting free methanol flow, the prototype's structure manifested an excessive amount of carbon situated between the heated outer pipe and the internal copper pipe. This layer of carbon potentially causes a substantial temperature disparity, with the carbon proximate to the wall being exposed to higher temperatures than that near the copper pipe. To address this issue, the revised configuration accommodates additional copper pipes in closer proximity to the outer wall. This modification potentially augments the efficiency of the desorption period, given that the carbon closest to the copper pipe attains higher temperatures at identical levels due to the reduced distance between the heating element at the outer pipe and the methanol.

Additionally the water in the evaporator is removed due to the oversized volume. Since the water amount ended up being larger than determined in the calculation, this has possibly led to it being more difficult to cool down the water because the amount of methanol in the adsorption process is too small compared to the water. After the water was removed, the evaporator has resulted in much lower temperatures in both the coil and cooling chamber.

Another significant observation pertains to the consistent diminution of adsorption with each successive test undertaken. Notably, the duration of the mass flow from the collector to the condenser's inlet proves to be a challenge over an extended period. Initial tests indicate that the mass flow persisted throughout the process. However, with each subsequent test, despite the system operating at a consistent temperature, the duration of mass flow showed a declining trend. This circumstance can be contextualized by insights garnered from initial tests. Upon the introduction of new carbon into the system, it has entirely unoccupied pore spaces. In the absence of heat input, under absolute vacuum conditions, methanol added to the system ascends towards the collector to be adsorbed

into these pores. When the desorption process commences, which involves the addition of heat, the pores liberate the adsorbed methanol, but not all of it. The requisite of substantially higher temperatures for complete release introduces an issue, given the potential detrimental effects on methanol at these temperatures. The phenomenon of incomplete methanol release from the carbon constrains the system's ability to adsorb an equivalent volume of methanol during the subsequent adsorption phase. The principle that adsorption volume cannot exceed desorption volume results in diminished cooling. This likely elucidates why the most efficacious simulations typically occur during the first simulation after the introduction of new carbon into the system.[56]

A possible extension of the previous issue could be linked to the pressure related complications intrinsic to the system. Each successive test results in a truncated desorption phase, attributable to diminished methanol content in the system. The correlation between less methanol to desorb and expedited carbon heating is notable. A potential problem could happen if the initiation of the desorption occurs prior to the completion of the adsorption process. Evidence for this is provided by the preliminary use of the vacuum pump before conducting the tests. If the evaporator is devoid of methanol, the system pressure rapidly plummets to a vacuum state when the pump is employed. Even though it occasionally appears as though all the methanol has been adsorbed, the crux of the issue may reside in the fact that the system, as a whole, has not had sufficient time to cool down to ambient temperature fully. A probable cascading effect might explain this scenario, given the established absence of any leakage within the system. It is observed that with each subsequent test undertaken, the pressure is marginally elevated compared to the preceding test. Consequently, tests conducted in succession yield different pressures at an identical collector temperature.

The exploration of methanol's saturation pressure, as conducted in Section 9.5.9, provides potential explanations for the observed scenario. The evaporator temperature serves as a factor for the pressure at which the adsorption process commences. It appears that the tests with a higher initial evaporator temperature tend to instigate the adsorption process at elevated pressures. This observation is substantiated by Figure 9.30, which reflects a simulation-free interval of three days. Prior to the desorption process, the evaporator temperature was recorded at 20 °, and following the adsorption a significant drop to 0.73 °was observed.

10 Implications and recommendations

This section engages with a selection of further noteworthy considerations that have emerged during the course of the research. It primarily focuses on the cooling effect observed during pressure testing and delineates the principal limitations associated with the system's operation. Additionally, proposed changes are discussed to improve the system's efficiency.

10.1 Cooling effect with only carbon and nitrogen

A situation that may have led to problems is the pressure testing before the system startup. Pressure testing is a crucial part of the preliminary work to ensure that the system is tight. A leak will contribute to poorer results and most likely destroy the entire test. A major uncertainty that was not taken into account beforehand was the properties of nitrogen used during pressure testing. It turns out later that nitrogen has relatively similar properties to methanol. This has led to the possibility of nitrogen being taken up by the carbon during the pressure test, which has led to the pore spaces being partially filled with nitrogen. Henninger et al, has investigated the surface and pore characteristics of nitrogen together with activated carbon as an adsorption pair [55]. The data has compared both the total nitrogen and methanol micropore volume during the highest adsorption point. One can see from Table 10.1 that the total accessible pore volume measured from the nitrogen adsorption is pretty similar with the values obtained during methanol adsorption. This indicates that the theory can be strengthened and that nitrogen occupies part of the pore volume which the methanol will mainly utilize. Solving this problem can be done by heating the carbon to over 150°C to ensure that the hydrogen evaporates before the methanol is added to the system. By not doing this procedure have probably contributed to a weaker cooling process.

Table 10.1: Parameters for the DA equation from methanol and nitrogen [55]

	Methanol				Nitrogen		
	W_0	E	n	b	W_0	E	n
G32-H	0.482	19.22	2.59	0.00406	0.469	6.486	1.7
Norit R 1 Extra	0.519	17.38	2.27	0.00449	0.530	6.161	1.4
Rutgers CG1-3	0.535	14.26	1.80	0.00547	0.545	5.059	1.2
Norit RX 3 Extra	0.551	16.89	2.06	0.00462	0.576	6.119	1.2
CarboTech C40/1	0.633	12.46	1.85	0.00626	0.695	4.366	1.1
CarboTech A35/1	0.786	11.72	1.76	0.00666	0.772	4.119	1.2

10.2 Main challenges

When running the experiments, both the main full-scale setup and the smaller test rig, there are very clear issues that arise. The main difficulty with using methanol as a refrigerant is its very high sensitivity to pressure. Due to the vapour pressure being in a vacuum, the methanol needs extremely low pressures to function. This can be attained with a vacuum pump. However, getting sufficient vacuum is very time-consuming and can be difficult. Especially since the pores of the carbon are filled with gases which can need heat treatment to be released. Even small amounts of air or gases can prevent the system from reaching a good functioning vacuum. While achieving vacuum is one issue, maintaining it is another one. For example, when filling methanol into the system, there needs to be a well-executed filling process to prevent air bubbles from entering the system. The construction also needs to be very airtight and able to hold a vacuum as small fractions of leakages will prevent the system to operate well. Putting such a system in a difficult environment like Tanzania makes it very vulnerable as access to maintenance and repairs are low in the areas where the intended use is.

Another key element to assess when using this kind of system is the crucial need for accurate data. Knowing the exact amount of methanol has proved to be very important as too much methanol decreases the cooling capacity. Also knowing how the system responds under different operating conditions is a significant detail. The ramifications to obtain the necessary data are based on sophisticated equipment. It is therefore not something to go easy on. While knowing the amount of methanol corresponding to the amount of carbon is difficult enough on its own, there is furthermore essential to dimension the rest of the system components based on accurate parameters. By underdimensioning the evaporator there will not be a sufficiently cooled volume to keep the cooling chamber cold. But by overdimensioning it, the system never reaches the set point temperature. It is therefore a very thin line to balance. The dimensioning of system components is additionally dependent on the mass flow of the methanol which is a function of time. Decreasing or increasing the expected desorption time by one hour has a major impact on the calculated parameters. Knowing the exact mass flow is also difficult as the methanol condensates in small drops. Making a thorough thermodynamic calculation is therefore a challenging feat.

Lastly, the system is designed to function in accordance with 24-hour cycles, aligning with the solar irradiation paths. This results in a consistent operational window. However, this consistency could impose limitations on the system's performance. Current data illustrates adsorption and desorption durations that exceed the stipulated time frame. The system experiences both desorption periods that extend beyond a typical solar day and adsorption periods that surpass the duration of the evening and night. Despite these extensions, the system's functionality remains suboptimal, implying that performance under realistic conditions could be considerably poorer. As previously discussed, system performance degrades over time as the number of cycles increases. Several factors may contribute to this degradation, one potential cause being escalating pressure. The adsorption uptake experiment also reveals that adsorption takes significantly longer than anticipated. Additionally, because the methanol adsorbs at a very slow rate, the cooling production is not observable. This suggests that, even when adsorption is assumed to have concluded in the primary setup due to stagnant evaporator temperatures, there could still be a substantial amount of methanol remaining to be adsorbed.

10.3   Proposed changes

Upon analyzing the current operational functionality of the system, several significant issues were identified, offering opportunities for enhancement and optimization. Primarily, the hindrance was observed in the aspect of heat transfer within the collector. The current design utilizes a large-diameter construction to accommodate the carbon quantity, thereby necessitating an extended heating period. Moreover, the system also requires an elongated cooling time. From these observations, it becomes readily apparent that revising the collector's structure to be more elongated and slimmer could result in an improved heat transfer rate. An optimal configuration might require a significant departure from the current design. The existing collector was primarily designed to accommodate a heating cable and was chosen for its simplistic design and expedited assembly process. However, given the insights from our study, it is plausible to assume that a system comprised of multiple smaller pipes might deliver superior heat transfer efficiency. Increasing the number of pipes will result in more metal being available for heat distribution to the carbon. Additionally, a greater proportion of carbon would be in direct contact with the metal, effectively increasing the surface area exposed to the heating source. This modification would also shorten the distance that heat needs to travel to the pipe's center. Therefore, such an arrangement could potentially reduce both desorption and adsorption times.

In the existing setup, there has observed desorption times of up to ten hours, which pose challenges in replicating with solar radiation. Although sunlight may be available for up to twelve hours on a typical day, solar intensity is not consistently high throughout this period. The duration of adequate heating may be limited to only six to eight hours, given the reduced solar radiation at the beginning and end of the day. Consequently, achieving desorption times of ten hours at maximum effect can be difficult outside of laboratory conditions. Therefore, any reduction in desorption times would prove beneficial to the cooling output. Furthermore, it is also critical to minimize adsorption times. From the secondary setup, adsorption times can span between 10-20 hours as

the weight continues to decrease for a significantly longer period than initially anticipated. In a context where solar cycles dictate the initiation and termination of operational cycles, adsorption is constrained to a limited functional window.

A proposed modification to the collector design is presented in Figure 10.1. This perspective view from above, with a cross-sectional slice at the mid-plane to expose the internal structure, illustrates several key changes. The revised design comprises multiple copper pipes to facilitate better heat transfer, each filled with activated carbon and interconnected in parallel to the same inlet/outlet. These pipes, serving as containers for the carbon, are enclosed within an insulated, glass-covered box to enhance and maintain the heat within the pipes, thereby ensuring a more consistent temperature, particularly during sudden shifts in solar irradiance such as cloud cover. In addition, the pipes could be stacked vertically, thereby maximizing the use of available space for accommodating a larger quantity of activated carbon. An operational mechanism would be necessary to control the opening and closing of the box during adsorption and desorption phases, thereby enhancing the system's overall efficiency and time management. To further increase efficiency and facilitate better methanol dispersion, the pipes could be designed to have connections at both ends. This feature would also enable separate inlet and outlet capabilities if necessary. The outlined solution will likely yield better results than the current setup, but will could also possibly need another heat source to operate in the lab. Using an artificial sun is a better approach to this new system solution but also to replicate more accurate operating conditions.
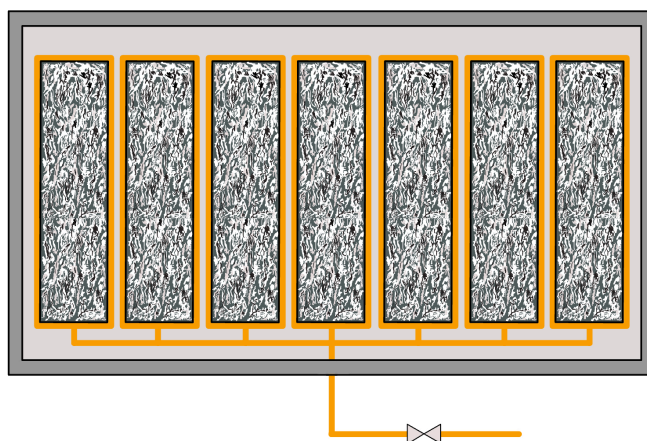

Figure 10.1: New collector

The second critical modification concerns the system's evaporator and cooling chamber. Currently, an excess of methanol is observed relative to the quantity of activated carbon. This results in an oversized evaporator chamber and subsequent cooling coils. While the present cooling production allows the evaporator to attain acceptable temperatures within the tank and cooling chamber, this is feasible only when air is used, leading to rapid loss of coolness. Originally, the system was designed to be filled with water, aiming to leverage it as a thermal energy storage for more effective cold preservation. However, the existing cooling capacity proved insufficient to cool the water volume within the container. It is suggested that a smaller water container, fewer evaporating coils, and less methanol could significantly enhance system performance. Instead of accommodating 3.3 liters of methanol, an amount closer to 1.5 liters seems more appropriate. Notably, during the first adsorption cycle with fresh carbon, adsorption rates exceed those in subsequent cycles. It is not possible to desorb all methanol between cycles without risking methanol decomposition. Therefore, a slightly greater amount of methanol should be introduced into the system than what corresponds to the expected adsorption capacity at given parameters. This can be determined by taking into account the maximum adsorption capacity, and then subtracting the desorption that occurs at a particular temperature and pressure.

Parallel to the need for a downsized evaporator, a similar requirement is seen for the condenser. The water tank and associated condenser coil were initially designed to accommodate a considerably shorter desorption duration with higher mass flow. Consequently, none of the experimental trials evidenced a substantial temperature rise in the condenser water. While this does not present a problem, as the cooling of methanol to ambient temperature is indeed beneficial. It indicates that the current design is excessively large. Therefore, a reduction in size could yield beneficial impacts, both spatially and in terms of material cost. A more advantageous solution is envisioned in the form of a smaller container with a condenser coil of increased pitch. Considering there were some problems with methanol clogging in the pipe, this revision could enhance the overall efficiency of the system, rendering it more compact and cost-effective.

A further beneficial modification might involve the implementation of a circular system facilitated by valve regulation. The current arrangement does not fully leverage the potential utility of valves. As currently configured, the collector valve can be closed off to expedite desorption at a higher pressure and subsequently opened to the condenser upon reaching condenser pressure. Once the system achieves full desorption, the collector valve is closed again. As the system cools, the evaporator valve can be opened, followed by the re-opening of the collector valve. This method of valve regulation ensures that the warm methanol from the condenser is retained until the adsorption process commences, thereby preventing the unnecessary warming of the evaporator. As the evaporator and collector valves open, the adsorption process initiates immediately, optimizing cooling retention.

While this might shorten the heating duration and effectively preserve evaporator cooling, there are potentially more efficient designs. A bypass installed from the evaporator back to the collector, as depicted in Figure 10.2, could introduce greater driving forces into the system. The same valve regulation could be employed until the onset of adsorption. At this point, instead of opening the collector valve when the evaporator valve is to be opened, the bypass valve post-evaporator would be opened instead. Consequently, the collector would be positioned in a low-pressure zone, theoretically facilitating the accelerated flow of methanol through the evaporator, resulting in enhanced evaporation. This modification could potentially expedite both desorption and adsorption processes within the system.
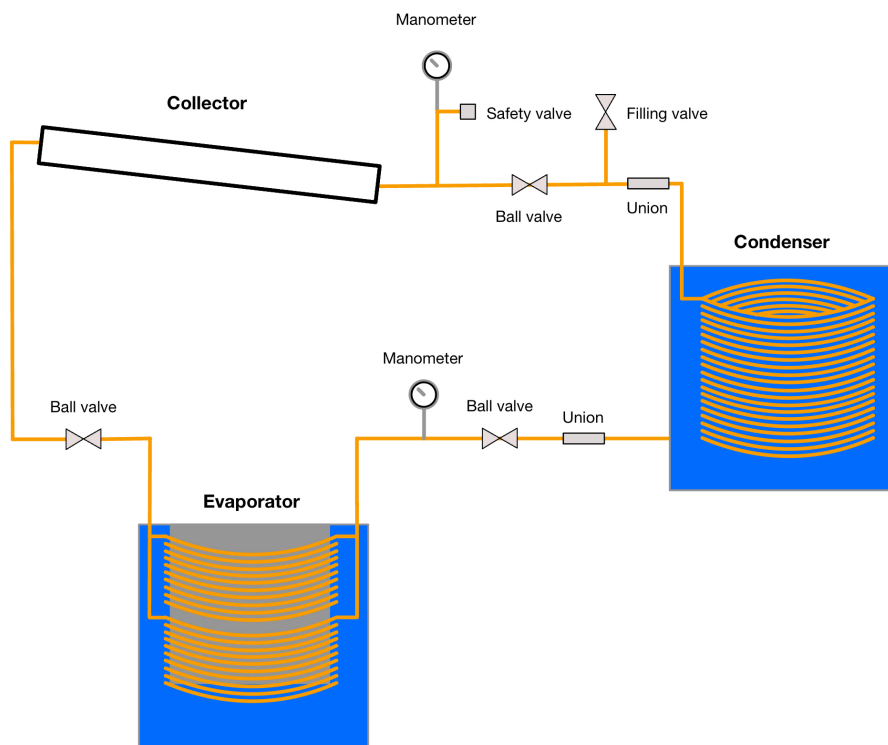
Figure 10.2: By pass

Finally, and perhaps most crucially, one could consider modifying the adsorption pair combination. The utilization of methanol presents significant challenges related to pressure sensitivity. Its high reactivity to pressure variations makes methanol ill-suited for a straightforward adsorption cycle. In operational conditions where durability is key, methanol presents numerous problems that need to be addressed before it can be potentially used. If a system leak occurs, the adsorption process would immediately halt. Restoring the system is not a simple task either, as it would necessitate a vacuum pump. As such, it may be worthwhile to explore a system using activated carbon and ammonia as an alternative. Despite studies showing methanol's superiority over ammonia [25], ammonia's lower boiling point of -34°C makes it far more manageable since there is no need for a vacuum to run the system. This could result in a more robust system that is more suited to the challenging conditions in Tanzania, where the system will be exposed to intense solar radiation and hard working conditions. [51]

11   Conclusion

In conclusion, this master's thesis represents a significant journey in the exploration of adsorption cooling systems. The research process began with a comprehensive literature review, which involved a meticulous assessment of several potential working pairs. The objective was to identify the most suitable adsorption pair and system configuration for the specific climate conditions in Tanzania. Factors such as the ability to operate below zero degrees, low desorption temperatures, and high latent heat of evaporation were considered in this assessment. The literature review led to the selection of the activated carbon and methanol pair. This choice was not arbitrary but was the result of careful consideration of the unique properties of this pair. The decision was based on the understanding that it would provide the desired cooling effect while being suitable for the environmental conditions in Tanzania. This phase of the research was critical in setting the stage for the experimental phase of the study. However, the journey from literature review to experiment was fraught with challenges. One of the most significant obstacles was the sensitivity of methanol to pressure. As the pressure of the system increased, the adsorption of methanol weakened due to its low vapour pressure. This phenomenon made methanol a challenging substance to work with, and maintaining vacuum conditions proved to be a complex task. This finding underscores the inherent difficulties in using methanol as a refrigerant and highlights the need for future research.

The design of the collector was another critical aspect that the study brought to light. The results obtained underscored the importance of heat transfer and methanol dispersion in the design process. However, the current design failed to achieve the desired results, indicating a need for significant improvements in future iterations. This finding suggests that the design of the collector is not just a structural or mechanical consideration, but a key determinant of the overall system efficiency. In the course of the study, the importance of understanding the adsorption uptake between methanol and carbon became evident. This relationship is a vital piece of the puzzle in designing an effective system. However, the current study was unable to fully explore this relationship, indicating a gap in the research that future studies will need to address. The research process also highlighted the need for better measuring equipment in the prototype. The study identified the potential benefits of automated logging of pressure and mass transfer recording. However, the lack of such equipment in the current prototype significantly hampered the accuracy of the data and the reliability of the insights into the system's performance.

Towards the end of the study, the potential of using other adsorption pairs due to their preferable operating pressure was suggested. This opens up new avenues for future research and could potentially lead to the development of more efficient and robust adsorption-based cooling systems. However, this remains a theoretical proposition at this stage, with no experimental data to support it. In light of these findings, it is clear that while the study aimed to advance understanding of adsorption and its applications in cooling systems, it fell short in several areas. The quest to fully harness the potential of adsorption in cooling systems, and to realize the full potential of methanol as a refrigerant in the specific context of Tanzania's climate conditions, remains a distant goal. The findings and recommendations of this thesis, while providing some direction, underscore the significant challenges that lie ahead in this field. The journey, though marked by hurdles, has also been filled with valuable insights that set the stage for future research.

Bibliography

[1] Erling Vingelsgård. 'Design og simulering av soldrevet adsorpsjonsbasert ismaskin'. eng. Accepted: 2019-10-12T14:01:15Z. MA thesis. NTNU, 2019. URL: https://ntnuopen.ntnu.no/ntnu-xmlui/handle/11250/2621753 (visited on 08/06/2023).

[2] Edna Makule, Noel Dimoso and Savvas A. Tassou. 'Precooling and Cold Storage Methods for Fruits and Vegetables in Sub-Saharan Africa—A Review'. en. In: *Horticulturae* 8.9 (Sept. 2022). Number: 9 Publisher: Multidisciplinary Digital Publishing Institute, p. 776. ISSN: 2311-7524. DOI: 10.3390/horticulturae8090776. URL: https://www.mdpi.com/2311-7524/8/9/776 (visited on 10/06/2023).

[3] Julian Parfitt, Mark Barthel and Sarah Macnaughton. 'Food waste within food supply chains: quantification and potential for change to 2050'. In: *Philosophical Transactions of the Royal Society B: Biological Sciences* 365.1554 (Sept. 2010). Publisher: Royal Society, pp. 3065–3081. DOI: 10.1098/rstb.2010.0126. URL: https://royalsocietypublishing.org/doi/10.1098/rstb.2010.0126 (visited on 11/06/2023).

[4] Anne Marie Thow et al. 'How can health, agriculture and economic policy actors work together to enhance the external food environment for fruit and vegetables? A qualitative policy analysis in India'. en. In: *Food Policy* 77 (May 2018), pp. 143–151. ISSN: 0306-9192. DOI: 10.1016/j.foodpol.2018.04.012. URL: https://www.sciencedirect.com/science/article/pii/S0306919217304372 (visited on 11/06/2023).

[5] Valeria Palomba and Andrea Frazzica. 'Recent advancements in sorption technology for solar thermal energy storage applications'. en. In: *Solar Energy*. Thermal Energy Storage for Solar Applications 192 (Nov. 2019), pp. 69–105. ISSN: 0038-092X. DOI: 10.1016/j.solener.2018.06.102. URL: https://www.sciencedirect.com/science/article/pii/S0038092X18306546 (visited on 21/10/2022).

[6] Ahmed A. Askalany et al. 'An overview on adsorption pairs for cooling'. en. In: *Renewable and Sustainable Energy Reviews* 19 (Mar. 2013), pp. 565–572. ISSN: 1364-0321. DOI: 10.1016/j.rser.2012.11.037. URL: https://www.sciencedirect.com/science/article/pii/S1364032112006491 (visited on 18/10/2022).

[7] Nagham Aljamali, Radhiyah Khdur and Intisar Alfatlawi. 'Physical and Chemical Adsorption and its Applications'. In: 7 (Dec. 2021), pp. 1–8. DOI: 10.37628/IJTCK.

[8] Manoj Tapare. *#Difference between Physical Adsorption & Chemical Adsorption. #Physical Adsorption #Adsorption.* Mar. 2021. URL: https://www.youtube.com/watch?v=yE9wM0tLMiw (visited on 10/11/2022).

[9] Anupama Sapkota. *Absorption vs Adsorption- Definition, 10 Differences, Examples.* en-US. Jan. 2022. URL: https://thebiologynotes.com/absorption-vs-adsorption/ (visited on 22/09/2022).

[10] M.A. Alghoul et al. 'Review of materials for adsorption refrigeration technology'. In: *Anti-Corrosion Methods and Materials* 54.4 (Jan. 2007). Publisher: Emerald Group Publishing Limited, pp. 225–229. ISSN: 0003-5599. DOI: 10.1108/00035590710762366. URL: https://doi.org/10.1108/00035590710762366 (visited on 27/09/2022).

[11] *What is activated carbon?* en-US. URL: https://www.carbotecnia.info/learning-center/activated-carbon-theory/what-is-activated-carbon/?lang=en (visited on 16/11/2022).

[12] N. C. Srivastava and I. W. Eames. 'A review of adsorbents and adsorbates in solid–vapour adsorption heat pump systems'. en. In: *Applied Thermal Engineering* 18.9-10 (1998), p. 707. ISSN: 1359-4311. URL: https://www.academia.edu/28265978/A_review_of_adsorbents_and_adsorbates_in_solid_vapour_adsorption_heat_pump_systems (visited on 16/11/2022).

[13] Eric J Hu. 'A study of thermal decomposition of methanol in solar powered adsorption refrigeration systems'. en. In: *Solar Energy* 62.5 (May 1998), pp. 325–329. ISSN: 0038-092X. DOI: 10.1016/S0038-092X(98)00012-7. URL: https://www.sciencedirect.com/science/article/pii/S0038092X98000127 (visited on 07/05/2023).

[14]   L. W. Wang, R. Z. Wang and R. G. Oliveira. 'A review on adsorption working pairs for refrigeration'. en. In: *Renewable and Sustainable Energy Reviews* 13.3 (Apr. 2009), pp. 518–534. ISSN: 1364-0321. DOI: 10.1016/j.rser.2007.12.002. URL: https://www.sciencedirect.com/science/article/pii/S1364032108000038 (visited on 17/11/2022).

[15]   M. Pons and J. J. Guilleminot. 'Design of an Experimental Solar-Powered, Solid-Adsorption Ice Maker'. In: *Journal of Solar Energy Engineering* 108.4 (Nov. 1986), pp. 332–337. ISSN: 0199-6231. DOI: 10.1115/1.3268115. URL: https://doi.org/10.1115/1.3268115 (visited on 18/11/2022).

[16]   I. I. El-Sharkawy et al. 'Study on adsorption of methanol onto carbon based adsorbents'. en. In: *International Journal of Refrigeration* 32.7 (Nov. 2009), pp. 1579–1586. ISSN: 0140-7007. DOI: 10.1016/j.ijrefrig.2009.06.011. URL: https://www.sciencedirect.com/science/article/pii/S014070070900156X (visited on 17/11/2022).

[17]   Mohamed M. Younes et al. 'A review on adsorbent-adsorbate pairs for cooling applications'. en. In: *Applied Thermal Engineering* 114 (Mar. 2017), pp. 394–414. ISSN: 1359-4311. DOI: 10.1016/j.applthermaleng.2016.11.138. URL: https://www.sciencedirect.com/science/article/pii/S1359431116334809 (visited on 19/12/2022).

[18]   L. W Wang et al. 'Study of the performance of activated carbon–methanol adsorption systems concerning heat and mass transfer'. en. In: *Applied Thermal Engineering* 23.13 (Sept. 2003), pp. 1605–1617. ISSN: 1359-4311. DOI: 10.1016/S1359-4311(03)00104-2. URL: https://www.sciencedirect.com/science/article/pii/S1359431103001042 (visited on 18/11/2022).

[19]   M. Li et al. 'Experimental study on adsorbent of activated carbon with refrigerant of methanol and ethanol for solar ice maker'. en. In: *Renewable Energy* 29.15 (Dec. 2004), pp. 2235–2244. ISSN: 0960-1481. DOI: 10.1016/j.renene.2004.04.006. URL: https://www.sciencedirect.com/science/article/pii/S0960148104001703 (visited on 08/12/2022).

[20]   B. B. Saha et al. 'Study on an activated carbon fiber–ethanol adsorption chiller: Part II – performance evaluation'. en. In: *International Journal of Refrigeration* 30.1 (Jan. 2007), pp. 96–102. ISSN: 0140-7007. DOI: 10.1016/j.ijrefrig.2006.08.005. URL: https://www.sciencedirect.com/science/article/pii/S0140700706001794 (visited on 08/12/2022).

[21]   B. B. Saha et al. 'Study on an activated carbon fiber–ethanol adsorption chiller: Part I – system description and modelling'. en. In: *International Journal of Refrigeration* 30.1 (Jan. 2007), pp. 86–95. ISSN: 0140-7007. DOI: 10.1016/j.ijrefrig.2006.08.004. URL: https://www.sciencedirect.com/science/article/pii/S0140700706001800 (visited on 08/12/2022).

[22]   I. I. El-Sharkawy et al. 'Experimental investigation of activated carbon fibers/ethanol pairs for adsorption cooling system application'. en. In: *Applied Thermal Engineering* 26.8 (June 2006), pp. 859–865. ISSN: 1359-4311. DOI: 10.1016/j.applthermaleng.2005.10.010. URL: https://www.sciencedirect.com/science/article/pii/S1359431105003170 (visited on 08/12/2022).

[23]   Ibrahim I. El-Sharkawy et al. 'A study on the kinetics of ethanol-activated carbon fiber: Theory and experiments'. en. In: *International Journal of Heat and Mass Transfer* 49.17 (Aug. 2006), pp. 3104–3110. ISSN: 0017-9310. DOI: 10.1016/j.ijheatmasstransfer.2006.02.029. URL: https://www.sciencedirect.com/science/article/pii/S0017931006001256 (visited on 08/12/2022).

[24]   I. I. El-Sharkawy et al. 'Experimental investigation on activated carbon–ethanol pair for solar powered adsorption cooling applications'. en. In: *International Journal of Refrigeration* 31.8 (Dec. 2008), pp. 1407–1413. ISSN: 0140-7007. DOI: 10.1016/j.ijrefrig.2008.03.012. URL: https://www.sciencedirect.com/science/article/pii/S0140700708000674 (visited on 08/12/2022).

[25]   R. E. Critoph. 'Activated carbon adsorption cycles for refrigeration and heat pumping'. en. In: *Carbon*. Proceedings of the Conference on Porosity and Carbon materials: Measurements and applications 27.1 (Jan. 1989), pp. 63–70. ISSN: 0008-6223. DOI: 10.1016/0008-6223(89)90157-7. URL: https://www.sciencedirect.com/science/article/pii/0008622389901577 (visited on 18/11/2022).

[26]   R. E. Critoph. 'Forced convection enhancement of adsorption cycles'. en. In: *Heat Recovery Systems and CHP* 14.4 (July 1994), pp. 343–350. ISSN: 0890-4332. DOI: 10.1016/0890-4332(94)90038-8. URL: https://www.sciencedirect.com/science/article/pii/0890433294900388 (visited on 08/12/2022).

[27] R. E. Critoph. 'Forced convection adsorption cycles'. en. In: *Applied Thermal Engineering* 18.9 (Sept. 1998), pp. 799–807. ISSN: 1359-4311. DOI: 10.1016/S1359-4311(97)00110-5. URL: https://www.sciencedirect.com/science/article/pii/S1359431197001105 (visited on 08/12/2022).

[28] Z. Tamainot-Telto et al. 'Carbon–ammonia pairs for adsorption refrigeration applications: ice making, air conditioning and heat pumping'. en. In: *International Journal of Refrigeration* 32.6 (Sept. 2009), pp. 1212–1229. ISSN: 0140-7007. DOI: 10.1016/j.ijrefrig.2009.01.008. URL: https://www.sciencedirect.com/science/article/pii/S0140700709000061 (visited on 16/11/2022).

[29] Akiyoshi Sakoda and Motoyuki Suzuki. 'Fundamental study on solar powered adsorption cooling system.' en. In: *JOURNAL OF CHEMICAL ENGINEERING OF JAPAN* 17.1 (1984), pp. 52–57. ISSN: 0021-9592, 1881-1299. DOI: 10.1252/jcej.17.52. URL: http://www.jstage.jst.go.jp/article/jcej1968/17/1/17_1_52/_article (visited on 08/12/2022).

[30] Elisa C. Boelman, Bidyut B. Saha and Takao Kashiwagi. 'Experimental investigation of a silica gel-water adsorption refrigeration cycle - the influence of operating conditions on cooling output and COP: Proceedings of the 1995 ASHRAE Annual Meeting'. In: *ASHRAE Transactions* 101.Pt 2 (Dec. 1995), pp. 358–366. ISSN: 0001-2505. URL: http://www.scopus.com/inward/record.url?scp=0029514579&partnerID=8YFLogxK (visited on 08/12/2022).

[31] Bidyut B. Saha, Elisa C. Boelman and Takao Kashiwagi. 'Computer simulation of a silica gel-water adsorption refrigeration cycle - the influence of operating conditions on cooling output and COP: Proceedings of the 1995 ASHRAE Annual Meeting'. In: *ASHRAE Transactions* 101.Pt 2 (Dec. 1995), pp. 348–357. ISSN: 0001-2505. URL: http://www.scopus.com/inward/record.url?scp=0029545777&partnerID=8YFLogxK (visited on 08/12/2022).

[32] Bidyut B. Saha, Atsushi Akisawa and Takao Kashiwagi. 'Silica gel water advanced adsorption refrigeration cycle'. en. In: *Energy* 22.4 (Apr. 1997), pp. 437–447. ISSN: 0360-5442. DOI: 10.1016/S0360-5442(96)00102-8. URL: https://www.sciencedirect.com/science/article/pii/S0360544296001028 (visited on 08/12/2022).

[33] B. B. Saha et al. 'Performance evaluation of a low-temperature waste heat driven multi-bed adsorption chiller'. en. In: *International Journal of Multiphase Flow* 29.8 (Aug. 2003), pp. 1249–1263. ISSN: 0301-9322. DOI: 10.1016/S0301-9322(03)00103-4. URL: https://www.sciencedirect.com/science/article/pii/S0301932203001034 (visited on 08/12/2022).

[34] H. T. Chua et al. 'Modeling the performance of two-bed, sillica gel-water adsorption chillers'. en. In: *International Journal of Refrigeration* 22.3 (May 1999), pp. 194–204. ISSN: 0140-7007. DOI: 10.1016/S0140-7007(98)00063-2. URL: https://www.sciencedirect.com/science/article/pii/S0140700798000632 (visited on 08/12/2022).

[35] H. T. Chua et al. 'Multi-bed regenerative adsorption chiller — improving the utilization of waste heat and reducing the chilled water outlet temperature fluctuation'. en. In: *International Journal of Refrigeration* 24.2 (Mar. 2001), pp. 124–136. ISSN: 0140-7007. DOI: 10.1016/S0140-7007(99)00078-X. URL: https://www.sciencedirect.com/science/article/pii/S014070079900078X (visited on 08/12/2022).

[36] B. Choudhury, P. K. Chatterjee and J. P. Sarkar. 'Review paper on solar-powered air-conditioning through adsorption route'. en. In: *Renewable and Sustainable Energy Reviews* 14.8 (Oct. 2010), pp. 2189–2195. ISSN: 1364-0321. DOI: 10.1016/j.rser.2010.03.025. URL: https://www.sciencedirect.com/science/article/pii/S1364032110000870 (visited on 09/12/2022).

[37] İsmail Solmuş et al. 'Adsorption properties of a natural zeolite–water pair for use in adsorption cooling cycles'. en. In: *Applied Energy* 87.6 (June 2010), pp. 2062–2067. ISSN: 0306-2619. DOI: 10.1016/j.apenergy.2009.11.027. URL: https://www.sciencedirect.com/science/article/pii/S0306261909005145 (visited on 09/12/2022).

[38] Parash Goyal et al. 'Adsorption refrigeration technology – An overview of theory and its solar energy applications'. en. In: *Renewable and Sustainable Energy Reviews* 53 (Jan. 2016), pp. 1389–1410. ISSN: 1364-0321. DOI: 10.1016/j.rser.2015.09.027. URL: https://www.sciencedirect.com/science/article/pii/S1364032115009971 (visited on 18/12/2022).

[39] T. F. Qu, R. Z. Wang and W. Wang. 'Study on heat and mass recovery in adsorption refrigeration cycles'. en. In: *Applied Thermal Engineering* 21.4 (Mar. 2001), pp. 439–452. ISSN: 1359-4311. DOI: 10.1016/S1359-4311(00)00050-8. URL: https://www.sciencedirect.com/science/article/pii/S1359431100000508 (visited on 14/12/2022).

[40] R. Z Wang. 'Performance improvement of adsorption cooling by heat and mass recovery operation'. en. In: *International Journal of Refrigeration* 24.7 (July 2001), pp. 602–611. ISSN: 0140-7007. DOI: 10.1016/S0140-7007(01)00004-4. URL: https://www.sciencedirect.com/science/article/pii/S0140700701000044 (visited on 15/12/2022).

[41] R. Z Wang et al. 'Performance researches and improvements on heat regenerative adsorption refrigerator and heat pump'. en. In: *Energy Conversion and Management* 42.2 (Jan. 2001), pp. 233–249. ISSN: 0196-8904. DOI: 10.1016/S0196-8904(99)00189-2. URL: https://www.sciencedirect.com/science/article/pii/S0196890499001892 (visited on 05/12/2022).

[42] Wassila Chekirou, Nahman Boukheit and Ahcene Karaali. 'Heat recovery process in an adsorption refrigeration machine'. en. In: *International Journal of Hydrogen Energy*. Special Issue on 17th International Conference on Emerging Nuclear Energy Systems (ICENES'2015), 4-8 October 2015, Istanbul, Turkey 41.17 (May 2016), pp. 7146–7157. ISSN: 0360-3199. DOI: 10.1016/j.ijhydene.2016.02.070. URL: https://www.sciencedirect.com/science/article/pii/S0360319915314737 (visited on 14/12/2022).

[43] Quanwen Pan et al. 'A novel adsorption heat pump cycle: Cascaded mass recovery cycle'. en. In: *International Journal of Refrigeration* 95 (Nov. 2018), pp. 21–27. ISSN: 0140-7007. DOI: 10.1016/j.ijrefrig.2018.08.004. URL: https://www.sciencedirect.com/science/article/pii/S0140700718303001 (visited on 10/12/2022).

[44] M. Pons and F. Poyelle. 'Adsorptive machines with advanced cycles for heat pumping or cooling applications: Cycles á adsorption pour pompes á chaleur ou machines frigor: figues'. en. In: *International Journal of Refrigeration* 22.1 (Jan. 1999), pp. 27–37. ISSN: 0140-7007. DOI: 10.1016/S0140-7007(97)00042-X. URL: https://www.sciencedirect.com/science/article/pii/S014070079700042X (visited on 15/12/2022).

[45] D. C. Wang et al. 'A review on adsorption refrigeration technology and adsorption deterioration in physical adsorption systems'. en. In: *Renewable and Sustainable Energy Reviews* 14.1 (Jan. 2010), pp. 344–353. ISSN: 1364-0321. DOI: 10.1016/j.rser.2009.08.001. URL: https://www.sciencedirect.com/science/article/pii/S1364032109001890 (visited on 10/12/2022).

[46] L. W Wang et al. 'Experimental study of a solidified activated carbon-methanol adsorption ice maker'. en. In: *Applied Thermal Engineering* 23.12 (Aug. 2003), pp. 1453–1462. ISSN: 1359-4311. DOI: 10.1016/S1359-4311(03)00103-0. URL: https://www.sciencedirect.com/science/article/pii/S1359431103001030 (visited on 18/11/2022).

[47] Akira Akahira et al. 'Mass recovery adsorption refrigeration cycle—improving cooling capacity'. en. In: *International Journal of Refrigeration* 27.3 (May 2004), pp. 225–234. ISSN: 0140-7007. DOI: 10.1016/j.ijrefrig.2003.10.004. URL: https://www.sciencedirect.com/science/article/pii/S0140700703001671 (visited on 09/12/2022).

[48] Akira Akahira et al. 'Experimental investigation of mass recovery adsorption refrigeration cycle'. en. In: *International Journal of Refrigeration* 28.4 (June 2005), pp. 565–572. ISSN: 0140-7007. DOI: 10.1016/j.ijrefrig.2004.10.001. URL: https://www.sciencedirect.com/science/article/pii/S0140700704002166 (visited on 15/12/2022).

[49] Bartosz Zajaczkowski. 'Optimizing performance of a three-bed adsorption chiller using new cycle time allocation and mass recovery'. en. In: *Applied Thermal Engineering* 100 (May 2016), pp. 744–752. ISSN: 1359-4311. DOI: 10.1016/j.applthermaleng.2016.02.066. URL: https://www.sciencedirect.com/science/article/pii/S1359431116302095 (visited on 15/12/2022).

[50] Z. S. Lu and R. Z. Wang. 'Performance improvement by mass-heat recovery of an innovative adsorption air-conditioner driven by 50–80 °C hot water'. en. In: *Applied Thermal Engineering* 55.1 (June 2013), pp. 113–120. ISSN: 1359-4311. DOI: 10.1016/j.applthermaleng.2013.03.001. URL: https://www.sciencedirect.com/science/article/pii/S1359431113001518 (visited on 13/12/2022).

[51] Michael John. 'Development of adsorption refrigeration system for off grid application'. en. In: *2022* (2022), pp. 81–86.

[52]   Zoya. *Post harvest Technologies for Fruits and Vegetables by Hosahalli Ramaswamy pdf free download - BooksFree*. en-US. Section: Agriculture. Jan. 2023. URL: https://www.booksfree.org/post-harvest-technologies-for-fruits-and-vegetables-by-hosahalli-ramaswamy-pdf-free-download/ (visited on 17/04/2023).

[53]   Rebecca Brill. *How Much Do Solar Panels Cost?* en-US. Section: Solar. Nov. 2022. URL: https://www.forbes.com/home-improvement/solar/cost-of-solar-panels/ (visited on 17/12/2022).

[54]   *Solcellepanel 280Watt, PARTIVARE*. nb. URL: https://www.sparelys.no/solcellepanel-280watt (visited on 17/12/2022).

[55]   S.K. Henninger et al. 'Evaluation of methanol adsorption on activated carbons for thermally driven chillers part I: Thermophysical characterisation'. en. In: *International Journal of Refrigeration* 35.3 (May 2012), pp. 543–553. ISSN: 01407007. DOI: 10.1016/j.ijrefrig.2011.10.004. URL: https://linkinghub.elsevier.com/retrieve/pii/S0140700711002489 (visited on 24/04/2023).

[56]   S. K. Henninger et al. 'Evaluation of methanol adsorption on activated carbons for thermally driven chillers part I: Thermophysical characterisation'. en. In: *International Journal of Refrigeration*. Refrigeration and Heat Pumping with Sorption Processes 35.3 (May 2012), pp. 543–553. ISSN: 0140-7007. DOI: 10.1016/j.ijrefrig.2011.10.004. URL: https://www.sciencedirect.com/science/article/pii/S0140700711002489 (visited on 17/11/2022).